ABSTRACT

CROSBY, LYNN MARIE. Studies on Mechanisms of Potassium Bromate-Induced Mesothelial Carcinogenesis in the Male F344 Rat. (Under the direction of R.B. Leidy & A.B. DeAngelo.)

Potassium bromate ($KBrO_3$) is a drinking water disinfection by-product and may represent a health hazard if found to be carcinogenic for humans, as was determined in rats (DeAngelo *et al*., 1998; Hayashi *et al*., 1986; Kurokawa, 1985; Kurokawa *et al*., 1985; Kurokawa *et al*., 1986a; Kurokawa *et al*., 1982; Kurokawa *et al*., 1983a; Kurokawa *et al*., 1987a; Kurokawa *et al*., 1983b; Kurokawa *et al*., 1986b; Ohno *et al*., 1982; Onodera *et al*., 1985). The purpose of this research was to determine the mechanism of toxicity. The peritoneal mesothelium is a (rat) target organ of potassium bromate carcinogenicity, but has not been studied due to the inherent difficulties of working with this one cell layer-thick tissue. Data from a two-year bioassay were used to more precisely map the location of origin, revealing that these tumors in the male F344 rat originate on the mesorchium of the tunica vaginalis testis, the mesosplenium, or at a point in between. An *in vitro* cell culture system was developed to study the mechanism of toxicity. It was demonstrated that $KBrO_3$ caused cell cycle arrest and markedly increased the number of apoptotic cells. $KBrO_3$ is a powerful oxidant and glutathione (GSH) is the major cellular antioxidant. Therefore, GSH-related responses were studied revealing mesothelial cells contained substantially less GSH than a human hepatocellular carcinoma cell line (Hep-G2). Studies employing GSH ester or N-acetyl cysteine (a GSH precursor) pre-treatment demonstrated abatement of toxicity in mesothelial, but not Hep-G2, cells. Experiments carried out to determine the chemical or enzymatic nature of the reaction between GSH and $KBrO_3$ revealed differences between the reaction kinetics of

the unbuffered and buffered chemical and cell-free/cell lysate reactions, probably due to reaction pH. Both chemical and cellular reactions exhibited a similar first step reaction between GSH and $KBrO_3$; thus, enzyme participation is probably not required. Experiments using diethylmaleate, which depletes GSH by a reaction involving $KBrO_3$, showed that GSH depletion greatly enhanced $KBrO_3$ toxicity, indicating GSH glutathione S-transferase, buthionine sulfoximine (which prevents synthesis of GSH) and was protective. This does not support the hypothesis that the reaction of $KBrO_3$ and GSH itself produces a radical/reactive species that oxidatively damages lipids, proteins and DNA. Rather, depletion of GSH likely precedes oxidative damage. Gene expression studies demonstrated that peritoneal mesothelial cells displayed expression changes in a discrete set of genes, including oxidative stress-responsive genes, after treatment with $KBrO_3$ for four or 12 hours. Mesothelial cells severely damaged by five days $KBrO_3$ treatment recovered from complete cell cycle arrest after four weeks and exhibited explosive growth, focus formation and altered morphology. The redox imbalance created by GSH depletion appears to mediate increased expression of known oxidative stress responsive genes (e.g., HO-1,GADD45, GADD153, QR), activation of transcription factors (AP-1 and NFκB) and down-regulation of cell cycle initiating cyclins (and up-regulation of the CDK inhibitor $p21^{waf1/cip1}$) in $KBrO_3$–mediated toxicity. These alterations may permit cell survival, as observed after severe toxicity, and may be accompanied by transforming mutations or clastogenic changes. Taken together, these data suggest that mesothelial cells represent a population susceptible to $KBrO_3$-mediated toxicity *in vitro*, and suggest that tissue susceptibility *in vivo* plays a role in the nascence of mesotheliomas in the male F344 rat.

Studies on Mechanisms of Potassium Bromate-Induced Mesothelial Carcinogenesis in the Male F344 Rat

by

Lynn M. Crosby

A thesis submitted to the Graduate Faculty of

North Carolina State University

in partial fulfillment of the

requirements for the Degree of

Ph.D.

TOXICOLOGY

Raleigh

2000

APPROVED BY:

C.W. Qualls, Jr.	R.C. Smart
Sharon A. Meyer	Richard J. Miller
Ross Leidy	A.B. DeAngelo, Ph.D.
Co-Chair of Advisory Committee	Co-Chair of Advisory Committee

Dedication

I dedicate this work to my husband, Kevin, who has in every way contributed to this work, and to my daughter, Sam, who grew up right along side of it.

Personal Biography

I was born in St. Paul, Minnesota in February, 1960. I never considered science as a life's work until I studied the history of science in 1984. It was at this point that I became amazed and fascinated by the breadth of knowledge that had been accumulated by my forebears, which I was not aware of and did not understand. Since that time, my interest gradually grew, and in 1987, at the age of 27, I undertook studies in biochemistry at Old Dominion University, Norfolk, Virginia, because I wanted to be one of Paul De Kruif's "Microbe Hunters". A kindly professor there told me it would be good training. Graduating Magna Cum Laude in December, 1990, I then went to work as a chemist, while continuing graduate studies part-time. A dream was fulfilled when I came to Raleigh in 1994 to study toxicology at the Ph.D. level under one of my heroes, Dr. Ernest Hodgson, and the rest of the Toxicology faculty. Thus ends the dream, and begins the reality.

Acknowledgements

This work was supported by an NIEHS Training Grant through the Department of Toxicology, a GAANN Fellowship through the Department of Education, The GlaxoWellcome Company, and anUS EPA/NC State University Cooperative Training Grant Fellowship. I also wish to thank several persons who assisted in this work in various ways, viz.; Gina Benavides, Roger Brown, Bill Benson, Tracy Brainard, Nik Liv, Lawrence Yoon, Mike George, Tanya Moore, Gary Hatch, Bob Chapin, Ron Laetham and the members of the committee.

The ideas presented herein in no way reflect the policies or opinions of the US EPA.

Table of Contents

List of Tables

List of Figures

Chapter 1. Potassium Bromate: Historical Context, Uses and Focus on Carcinogenesis.

INTRODUCTION

Although always an interesting ototoxin of the same genre as gentamycin (Kurokawa, 1985; Matsumoto, 1973), since 1982, when Kurokawa, et al. (1982) first described the carcinogenic properties of potassium bromate in rats, interest has grown steadily regarding the chronic toxicity of this compound. Potassium bromate is used as a dough conditioner in bread-making and as a food additive to preserve freshness (IARC, 1986). Concentrations of potassium bromate are found at less than 50 mg/kg in bread dough and are completely converted to potassium bromide during baking, thus do not present a hazard of bromate formation or toxicity (IARC, 1986). Its use as a fish paste additive in Japan has been curtailed, since it has been found that non-heat-treated potassium bromate has carcinogenic properties, at least in rats, mice and hamsters (Kurokawa *et al*., 1990). Beauticians no longer employ potassium bromate as a cold wave neutralizer due to the dangers of accidental or intentional poisoning (IARC, 1986).

Bromate anion is formed as a byproduct during drinking (and waste-) water disinfection (Kurokawa *et al*., 1990). Potassium bromate forms via a hydroxyl radical-mediated mechanism during both chlorination and ozonation, although in greater amounts during the latter (von Gunten and Holgne, 1994). Ozone first efficiently transforms bromide into hypobromous acid and hypobromite. Then, approximately 23% of the latter reacts to form bromate. The extent of bromate formation is greater in those waters containing a proportionally greater amount of either natural or artificial bromine/bromide. Therefore, more bromate is produced from naturally

brackish waters, and also downstream from soda production, potassium and coal mining, where bromide enters as point-source runoff (von Gunten and Holgne, 1994).

Concern has arisen that exposure to potassium bromate-containing drinking waters may present an excess risk of cancer (Kurokawa *et al*., 1990). The excess lifetime risk of cancer for a 70 kg human being is one in 10^5 upon ingestion of 2 L/day of water containing 3 ug/L of potassium bromate. At issue is whether the general public can drink substantial amounts of treated water over many decades without an elevated risk of the development of cancer(s).

Chronic studies performed to date (Table 1) do not show that female rats, mice, or hamsters are vulnerable to carcinogenesis in the same manner as males, although high doses (500 ppm) do reduce survival time markedly in either sex. The argument can be made, however, in reviewing these data (Table 1) that more studies using female animals would put this conclusion on firmer footing. Potassium bromate does induced an increased incidence of renal neoplasms in male mice, a neoplasm which is rare in this species. As regards the toxicity of potassium bromate in male rats, the contribution of α_{2U} globulin to the renal pathology must be addressed, due to the presence of eosinophilic droplets in the proximal tubule epithelium (DeAngelo *et al*., 1998; Kurokawa *et al*., 1990). No data are available concerning mechanisms of carcinogenesis in the other two target organs, the thyroid and peritoneal mesothelia, in any species. Thus, while it would appear that the mechanism(s) of potassium bromate-induced mesotheloma may be a rat-specific phenomenon, and not of concern in the context of human health, in order to resolve this issue, more basic toxicological studies are needed. Data identifying the mechanism(s) as applicable to humans as well as rodents would justify the regulation of this substance in drinking water as necessary to protect public health.

PHYSICAL PROPERTIES AND CHEMISTRY

Potassium bromate is a white solid (powder or crystalline) with a melting point of 350 °C (approx.) and a decomposition temperature of 370 °C. It has a density of 3.27 g/cm^3 (@ 17.5 °C), and is very soluble in water and slightly soluble in alcohol (Lewis, 1991). It has a molecular weight of 167.01 g/mol and the molecular formula BrO_3K. It is otherwise known as "bromic acid, potassium salt". The molecular shape is most likely a trigonal pyramid (Cotton *et al*., 1987), with the three oxygen atoms each at a vertex fanning away from the bromine atom and the potassium cation loosely bound to the bromine atom at an orientation of approximately 180° from the negatively charged bromate anion (Fig. 1).

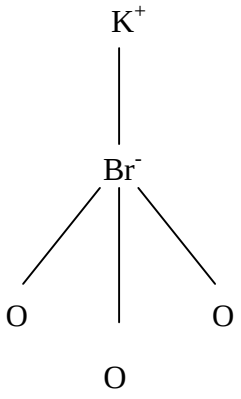

Fig. 1. Probable Structure of the Potassium Bromate Molecule

Potassium bromate is an ionic compound with extremely unequal sharing of electrons between bromine and potassium. Most of the charge resides with bromine. Each oxygen atom shares its six electrons with two from bromine (per oxygen). Bromine has 7 electrons and completes its octet with one from potassium (Patnaik, 1992)

Potassium bromate is a strong oxidizer, reacting in water as follows:

$KBrO_3 + 3\ H_2O + 6e^- \Rightarrow K^+ + Br^- + 6\ OH^-$ $E = {}^+0.61$ V Equ'n. 1.

Or in an acidic environment as follows:

$6\ H^+ + KBrO_3 + 5e^- \Rightarrow K^+ + ½\ Br_2\ (g,l,s) + 3\ H_2O$ $E = {}^+1.52$ V Equ'n. 2.

The positive value of the electronegative potential for these reactions indicates oxidizing strength. Therefore, $KBrO_3$ is a stronger ozidizer in acid than at neutral pH.

It reacts with strong acids, such as gastric acid, to produce hydrogen bromate, an irritant. On heating, it decomposes explosively, producing oxygen. It also reacts violently with other substances of an organic, combustible, or otherwise oxidizable nature. The reaction with hydrides of calcium or strontium with bromates causes explosion; mixing with concentrated mineral acids, lead acetate, or phosphonium iodide results in ignition; and the reaction of finely divided bromates with finely divided metals, phosphorus, sulfur, or metal sulfides may be explosive if heat or friction is applied (Patnaik, 1992). Heating to decomposition produces toxic fumes of Br^- and K_2O.

ACUTE, SUB-ACUTE, AND LONG-TERM TOXICITY

Table 1 summarizes studies reported to date concerning the toxicity of $KBrO_3$ *in vivo*. Notably, in subacute studies, very high doses were used for the studies in drinking water, and the rest of the studies listed were carried out using bread made from flour treated with $KBrO_3$, or flour treated with $KBrO_3$, which would have yielded Br^- during baking, so that animals were not exposed to $KBrO_3$. Chronic drinking water studies have not found any mesotheliomas in female rats (either treated or control), but did find renal, thyroid and peritoneal mesothelial cancers at significant levels in treated male rats.

STUDIES ON THE INITIATING AND PROMOTING ACTIVITIES OF POTASSIUM BROMATE: KIDNEY AND LIVER TUMORIGENESIS

The potent initiator of carcinogenesis, N-ethyl-N-hydroxyethylnitrosamine (EHEN) was used to test the promoting capability of potassium bromate in male F344 rats (Kurokawa *et al*., 1983b). Rats were given EHEN orally for 2 weeks followed by potassium bromate (500 ppm) orally for 24 weeks. The numbers of dysplastic foci and renal cell tumors at microscopic examination were elevated significantly in those groups given EHEN + $KBrO_3$ compared to those given EHEN alone. No other significant changes were observed in either the kidney or the liver.

An initiation-promotion experiment was performed on rats using diethylnitrosamine (DEN) as a single i.p. injection (200 mg/kg) and then feeding potassium bromate in the diet at 4000 ppm for 6 weeks. At week 3 a partial hepatectomy was performed. No liver tumor promoting activity was observed by this test (Kurokawa *et al*., 1986a).

Kurokawa, et al.(1983b) tested the promoting ability of potassium bromate in the male F344 kidney using the EHEN protocol mentioned above, with the specific aim of establishing a promotional threshold for potassium bromate. It was found that for animals given 15 to 30 ppm potassium bromate, the numbers of dysplastic foci increased dose-dependently. The related compound, KBr (potassium bromide) was tested similarly, but did not exhibit promoting capacity by this assay. In the potassium bromate study, lesion size/dose were not correlated.

Umemura, et al. (1993) tested the cell proliferation effects of potassium bromate, sodium bromate, and potassium bromide in the kidney of male/female F344 rats at concentrations of 500, 500, and 1750 ppm, respectively, for 2, 4, and 8 weeks. Increased numbers of hyaline droplets observed in treated animals were positively stained for α_{2u}-globulin in male rats. Increases in cell

proliferation were evident for all three time points in male rats treated with sodium-, or potassium-bromate but not potassium bromide, and not in female rats. Since it is known that the kidney is a site of tumorigenesis in the female rat as well (Kurokawa *et al*., 1982), but that the time to tumor is greater on average than in the male, the authors hypothesize that the participation of α_{2u}-globulin in the process of carcinogenicity was possible. It may act as an additive effector, and that the longer time required to produce tumors in females may account for the lack of positive proliferation data in this study. It is significant from this study that sodium bromate ($NaBrO_3$) behaved in the same manner as potassium bromate ($KBrO_3$). We are led to conclude, as do the authors, that indeed bromate is responsible for the carcinogenic effects of this compound.

Two-Stage and Complete Carcinogenesis in Mouse Skin.

Groups of female Sencar mice were administered 7, 12-dimethylbenz[*a*]anthracene topically followed by either potassium bromate (40mg/mL), 12-O-tetradecanoylphorbol-13-acetate (TPA), or acetone for a period of 51 additional weeks. A separate group was given only potassium bromate (40 mg/mL), without any prior initiation. Potassium bromate failed to exhibit any promotion or initiation- type effects (Kurokawa *et al*., 1984).

Two-Stage Whole Body Carcinogenesis in the Rat.

The chemical, methylnitrosurea (MNU), is an initiator used to assess the promotional activity of compounds in nervous, hematopoietic and gastrointestinal tract tissues. Kurokawa (Kurokawa *et al*., 1990) used this system to test potassium bromate by giving male F344 rats four i.p. injections of MNU for 2 weeks followed by 500 ppm potassium bromate orally for 24

weeks. High tumor incidences, including mesotheliomas, were observed; however, no promoting effect was seen.

Two-Stage Forestomach Carcinogenesis in Mice.

Kurokawa (unpublished observations cited by Kurokawa *et al*., 1990) administered a single i.g. dose of dimethylbenzanthracene (DMBA) to male C57Bl mice, followed by 500 ppm potassium bromate orally for 26 weeks. This study proved negative for promotional activity.

Two-Stage Esophageal Carcinogenesis in Rat.

Using dibutylnitrosamine (DBN), Kurokawa (unpublished, *vide supra*) administered an initiating dose orally, followed by 500 ppm potassium bromate orally for 32 additional weeks. No increased growth of neoplasms occurred in potassium bromate-promoted groups vs. those in controls.

Mutagenicity.

Table 2 summarizes the results of assays performed in various laboratories to date with respect to the mutagenic properties of potassium bromate. Strains TA102 and TA104 represent oxidative-stress sensitive strains of *S. typhimurium*, thus may better measure mutagenicity due to potassium bromate. The results listed indicate that, although not capable of causing mutational events in every strain tested, potassium bromate possesses positive mutagenic properties in certain strains. Potassium bromate was shown to be a complete carcinogen in rats (Kurokawa *et al*., 1982).

Chromosome Aberration Tests, Micronucleus Test, Silkworm Test.

Potassium bromate has been determined to be clastogenic in chromosome aberration assays. Chinese hamster lung cells treated with 0.0625-0.25 mg/mL (0.4-1.6 mM) potassium bromate showed 10-100% structural aberrations in chromosomes (Ishidate, 1987; Ishidate *et al*., 1981; Ishidate and Yoshikawa, 1980; Kawachi *et al*., 1980) in the absence of exogenous metabolic activation. The dose producing aberrations in 20% of these cells was 0.071 mg/mL (0.425 mM). Chinese hamster DON-6 cells also showed chromatid breaks upon dosing with 0.5 mM (0.0835 mg/mL) potassium bromate (Kurokawa *et al*., 1986b). Heat-treated or non-heat-treated potassium bromate was administered to male Long-Evans rats either i.p. or orally, producing significant increases in abnormal metaphases at 18 hours in bone marrow cells of the non-heat-treated potassium bromate treated animals only (Matsushima *et al*., 1986), by both the oral and i.p. routes. Others (Ishidate, 1987; Kurokawa *et al*., 1987a) found that the related compound, KBr, was positive in chromosome aberration assays (e.g., gaps, breaks, exchanges) at doses of 4 mg/mL (24 mM) or greater. This test (i.e., KBr) is essentially equivalent to that of giving heat-treated $KBrO_3$, (because heat treatment of $KBrO_3$ causes it to decompose to KBr) except that the amount administered was much greater (4 mg/mL vs. 0.0835 mg/mL = 0.5 mM).

In an assay of the ddY strain, male mice administered potassium bromate by i.p. and oral routes, (25, 100 mg/kg), an increased number of micronucleated polychromatic erythrocytes were observed (Hayashi *et al*., 1986). Later, these results were confirmed in female ddY mice as well (Kurokawa *et al*., 1987b). By contrast, potassium bromide and 39 other natural and synthetic food additives tested did not induce such changes. Kasai, et al. (1987) found that in two strains of mice, ddY and a mutagen-sensitive strain, potassium bromate produced greater amounts of micronuclei in the sensitive strain.

A silkworm mutagenicity test of potassium bromate revealed no evidence of genotoxic activity (Kawachi *et al*., 1980).

ABSORPTION, DISTRIBUTION & ELIMINATION

Intragastric administration of $KBrO_3$ (50 mg/kg, male Wistar rats), was performed, and organs examined for the presence of $KBrO_3$ (IARC, 1986). Approximately 30% of $KBrO_3$ was detected in the urine after 24 hours as bromate ion (basically unchanged except for the loss of the potassium ion). Levels of Br^- were elevated in plasma, RBC, kidney, pancreas, stomach, small intestine, and urine. Due to technical limitations, little information can be drawn from these studies (i.e. redistribution cannot be ruled out or inferred), and loss of analyte during the extractive process may have occurred. Most of the bromate was found in urine and feces, while most bromide was found in plasma, followed in order by erythrocytes, spleen, stomach, kidney, small intestine, liver, pancreas and feces. (Control amounts of Br^- are not given.) Thus, it appears that, upon gastric administration, most of $KBrO_3$ is absorbed via the gastrointestinal tract into the circulatory system, becoming, by inference, transformed at the rate of about 70% into bromide, but remaining essentially contained within these tissues, by about 24 hours. It appears that the kidney handles most of the excretory function of this compound, and, as a result, the kidney, GI tract, and blood systems are the most probable sites of susceptibility. The role of local blood flow in susceptibility of the peritoneal mesothelium, especially splenic mesothelium and tunica vaginalis mesothelium, and thyroid to $KBrO_3$ remains to be determined. Notably absent from this experiment was the measurement of $KBrO_3$ in the thyroid gland.

Interestingly, no bromate was detected in the urine of rats given less than 2.5 mg/kg, while a dose-dependent bromate excretion product was detected at all doses above 5 mg/kg. It

appears that a threshold exists for the excretion of parent compound, and what becomes of bromate concentrations of <2.5 mg/kg is a mystery, if accurately detectable at that level. There may be cellular mechanisms that effectively sequester, or metabolize, bromate up to this amount. There may be specific sequestration in specific target tissues (thyroid?).

Clearly, at doses of >5 mg/kg, bromate is present in the kidney tubules, and may exert its toxic effects in that location, as histologically observed in several *in vivo* studies (DeAngelo *et al*., 1998; Kurokawa *et al*., 1982).

Studies measuring the degradative capabilities of various tissues on $KBrO_3$ *in vitro* are of interest to determine cellular mechanisms capable of metabolizing or detoxifying bromate (IARC, 1986). Rat tissue homogenates were tested for their ability to degrade the parent compound, $KBrO_3$, when incubated at 37^{o}C for three minutes, with or without heat treatment at 100 ^{o}C. The products of these reactions remain to be determined. It was found that the kidney, liver, spleen, stomach, small intestine and RBC and gastric juice were able to effectively degrade $KBrO_3$, compared to plasma and (human) saliva. Kidney, liver and RBC were, in fact, most effective. The heat-treatment was designed to inactivate any enzyme systems that might be present. High molecular weight fractions of the liver showing degradative ability, lost this ability when heated. Low molecular weight fractions, on the other hand (containing GSH and other SH compounds), did not lose their degradative capacity on heating. This rationale proved true for the other degradative tissues (see above) as well. Sulfhydryl-containing compounds such as glutathione, ergothioneine, and cysteine were investigated, and found to be able to degrade bromate very effectively, *in vitro*, in the series glutathione > cysteine > ergothioneine, at concentrations to 20 ppm within 20 minutes (Odashima, 1980). In fact, a near-perfect stoichiometric relationship exists between glutathione concentration and bromide production,

and bromate disappearance. Therefore, given that bromide concentrations increase in certain tissues upon treatment of the animal with $KBrO_3$ and that these tissues possess a non-heat-labile bromate degradative capacity, (which includes sulfhydryl compounds), it is likely that the principal activity results from glutathione or other related compounds.

POSSIBLE MECHANISMS OF CARCINOGENICITY

Among the possible explanations for $KBrO_3$ carcinogenicity are lipid peroxidation (with or without concomitant DNA damage), and redox switch effects such as cell signaling changes, which may effect transcription factors (via changes in signal transduction), and subsequent gene expression changes prompting proliferation/preventing apoptosis/altering senescence patterns. All of these possibilities have a common theme, viz.: that radicals in the cell (sometimes referred to as "free radicals") fundamentally alter the way in which a cell functions without killing it. These changes result in a transformed cell – a cancerous nidus.

Oxygen Radical Theory

Less than five percent of all cellular oxygen consumed in a healthy cellular respiration form radical species (Fridovich, 1978), principally via superoxide generation in mitochondria. Cellular superoxide generation may also be augmented by oxidative xenobiotics such as $KBrO_3$. The mitochondrial electron transport system (ETS) contributes to radical generation as well. Superoxide anion ($O_2^{-\cdot}$) formed by the electron transport system or in the cytosol may be dismutated, spontaneously or through the catalytic action of either Mn (mitochondrial) or Cu/Zn (cytoplasmic) superoxide dismutases (SOD1 and 2 respectively), to yield hydrogen peroxide. Susequently, hydrogen peroxide (H_2O_2), may be converted to water and molecular oxygen by catalase or glutathione peroxidase (GSH dependent reaction of the GSH redox cycle), or undergo

disproportionation to OH^- and $OH^{\cdot}$. Latter reaction is catalyzed by Fe^{2+} (the "Fenton reaction") and can lead to severe radical damage to proteins, lipid, and carbohydrates.

Light, heat, chemical energy (i.e. reactive species) or radioactivity can lead to the formation of free radicals (henceforth referred to as 'radicals') within the cell. Such radicals include singlet-state oxygen (O_2^1) or hydrogen peroxide which may form radicals. The half-life of hydrogen peroxide is long enough to react at considerable distances from its site of generation. Many excellent reviews of radical chemistry exist (Bensasson *et al*., 1993; Packer and Cadenas, 1998; Scandalios, 1997), and from these, we will examine suggested mechanisms involving radical and/or reactive species generation by $KBrO_3$.

$KBrO_3$ (Equation 1, p. 18) is capable of accepting six electrons making it a very strong oxidizing agent and electrophile, even at neutral pH. Thus, $KBrO_3$ is theoretically capable of oxidizing the following molecules within the cell:

1) proteins (esp. sulfhydryl-containing)
2) carbohydrates
3) nucleic acids
4) lipids
5) uncomplexed/free metal ions

In fact, $KBrO_3$ has been observed to cause lipid peroxidation (Sai *et al*., 1991), and formation of 8-OH-deoxyguanosine adducts (8-OHG) (Kasai *et al*., 1987) *in vivo* in the rat kidney. Furthermore, phase II metabolic detoxification reactions involving $KBrO_3$ may produce reactive oxygen species (ROS) that damage macromolecules or change gene expression by eliciting alterations in either transcription factor activation and/or signal transduction mechanisms (Suzuki

et al., 1997). Error-prone DNA repair may be initiated after 8-OHG formation, or base adduct formation. The evidence for each of these possibilities is examined below.

Oxidation of proteins/non-protein sulfhydryls. In general, the redox status of the cell is determined by the level of oxidation of its constituent molecules (i.e., proteins, lipids, carbohydrates and nucleic acids). The cellular redox balance is tipped toward a highly reducing environment, because of the paradox of aerobic life. That is, oxygen, itself a diradical (but a stable one, and a weaker oxidant than superoxide or hydroxyl radicals) is essential for life to all aerobic organisms, but will oxidize biomolecules. The oxidation of sulfhydryl species in the cell causes the spontaneous formation of disulfide bonds (sometimes referred to as "bridges"), resulting in protein misfolding or aggregation and oxidation of GSH to GSSG. The latter must be reduced by glutathione reductase and NADPH in order for it to act as a required cofactor in vital enzymatic reactions and to maintain other molecules in a reduced state. Together with oxidative metabolism and key antioxidants (thioredoxin, vitamins E and C, SOD, catalase, Se-dependent GSH peroxidase and thioredoxin hydroperoxidase), GSH forms the cellular redox buffering system (Packer and Cadenas, 1998). Evidence exists for the oxidation of GSH to GSSG by $KBrO_3$ (Tanaka *et al*., 1984). $KBrO_3$ is degraded stoichiometrically by GSH to Br^-, as mentioned previously, and cysteine and ergothioneine were also found to exhibit degradative ability for $KBrO_3$ (Kurokawa *et al*., 1990).

Formation of Specific DNA Adducts.

Targeting of guanosine residues forming 8-OH deoxyguanosine adducts.

The oxidizing systems GSH/Fe^{3+}/O_2, ADP/Fe^{2+}/H_2O_2 (generating $OH^{\cdot}$), singlet oxygen, or oxidized methyl linolenate/phosphatidylcholine/methyl arachidonate liposomes (in the presence of metal ions Cu^{2+} or Fe^{3+}) have all been shown to induce the formation of 8-OHG in cell-free systems (Devasagayam *et al*., 1991; Floyd *et al*., 1986b; Park and Floyd, 1992; Park and Floyd, 1994; Park and Floyd, 1997). Among the oxidative stress inducers known to produce 8-OHG are aging (rat), smoking (humans), x-rays (mice, *in vivo*) and administration of tetradecanylphorbolacetate (TPA) (human granulocytes, *in vitro*) (Floyd *et al*., 1986a; Fraga *et al*., 1990; Kasai *et al*., 1986; Loft *et al*., 1992). $KBrO_3$ has also been observed to induce 8-OHG under cell free conditions, *in vitro*, and *in vivo* after oral, i.p. or gavage treatments of male F344 rats in kidney, but not liver tissues (Ballmaier and Epe, 1995; Kasai *et al*., 1987; Sai *et al*., 1991; Sai *et al*., 1992; Umemura *et al*., 1995). The formation of 8-OHG has implications for mutagenicity due to mispairing during repair.

Targeting of Ha-ras gene.

Kamiya, et al. (1992) found that by inserting 8-OHG into a c-Ha-*ras* proto-oncogene, which was then transfected into mammalian cells, focus formation could be increased. Sequencing revealed random mutations (G→T, G→A, G→C) at the modified site and also at the adjacent 5' G (G→A and G→T). Thus, formation of 8-OHG results in mis-insertion of any of the three remaining nucleotides in a random fashion and correlates with the induction of focus formation. During DNA replication, α-polymerase miscodes the replicated strand at 8-OHG sites (Kuchino *et al*., 1987), producing a defective daughter strand. A glycosylase has been identified (8-oxoguanine/8-hydroxyguanine DNA glycosylase (Tchou *et al*., 1991)) that specifically cleaves

double-stranded templates containing single 8-OHG residues opposite dG, dC or dT, both 3' and 5' of the 8-OHG. In the event of imperfect/non-existent repair, the mis-coded base will be transcribed into an aberrant mRNA and ultimately a defective protein. The defective protein may have altered function such that cellular mechanisms of growth control and differentiation are disturbed. Another possibility is that the mutated base will result in altered binding of transcription factors or transcription factor complexes to the DNA, leading to the dysregulation of transcription of the gene. Regulatory element mutations are especially damaging because there are no mechanisms in place to detect and correct such dysregulation, as there are for aberrant proteins. The loss of regulatory elements may result in proliferation of a damaged cell or the failure by the cell to execute programmed cell death after exposure to oxidative stress.

Lipid Peroxidation.

Arachidonic acid (AA).

During the normal production of prostaglandins, thromboxane A2 and prostacyclins from AA, oxygen is a co-factor that, together with cyclooxygenase (COX), converts AA to prostaglandin G2 (PGG2) (Klaasen, 1996). PGG2 is a peroxidated fatty acid, which must be reduced by a peroxidase to prostaglandin H2 (PGH2) before it can be converted to the endproducts named above. If the oxygens from $KBrO_3$ were substitutable for O_2 during PGG2 production and the remaining atoms participated in the peroxidase reaction (as xenobiotics have been found to do, becoming oxidized in the process), an increase in the transcription of mRNA for necessary components to the pathway might be observed. A change in the prostaglandin profile may occur, as has been observed during oxidative stress(Scandalios, 1997).

Other lipids.

The peroxidation of membrane lipids is followed by their excision by phospholipase A2 (PLA2) (de Paulet *et al*., 1990). The peroxidated lipids are then enzymatically converted to the corresponding alcohols by GST. GSH is a required cofactor for this pathway. Increased lipid peroxidation could thus stimulate increased production of PLA2/GST through increased transcription by redox-regulated pathways (Klaassen, 1996; Scandalios, 1997). GSH synthetic enzymes (γ-glutamylcysteinyl synthetase, γ-GCS and glutathione synthetase, GS and possibly γ-glutamyl transpeptidase, γ-GGT) may also be produced in larger amounts (Klaassen, 1996).

Generation of radicals.

Via direct membrane peroxidation.

The electrophile $KBrO_3$ may be reductively dehalogenated, creating an oxygen radical species that may peroxidate membrane lipids, creating unstable hydroperoxides/lipid hydroperoxide radicals (also referred to as "homolytic bond fission", "reductive fission") (Klaassen, 1996). A chain reaction of radical formation may result in amplification of peroxidative damage until a radical scavenging molecule (ascorbate, α-tocopherol, etc.) is encountered (chain termination) (Bensasson *et al*., 1993).

Via increased "leakage" from the electron transport system.

Under normal circumstances, < 5% of cellular oxygen is converted to radical species during oxidative phosphorylation (*vide supra*). Although a minor contributor to oxidative stress, leakage from the ETS is noteworthy because xenobiotics/other molecules in proximity may pick

up an electron and thus propagate a chain reaction, and stimulation of the ETS by certain xenobiotics can increase the rate of production of ROS (Scandalios, 1997).

During the production of arachidonic acid (AA).

Co-oxidation of xenobiotics (X) during the conversion of AA to PGG2 (see above) has been observed to produce either an oxidized xenobiotic (XO) or two xenobiotic radicals plus water ($2X^{\cdot} + H_2O$) (Klaassen, 1996).

Via phase I reactions.

Cytochrome P450 reductase generates superoxide radicals by donating an electron to redox cyclers such as paraquat (Klaassen, 1996). The superoxide radical can generate hydroxyl radicals, which are more reactive and more dangerous (Bensasson *et al*., 1993; Scandalios, 1997).

RNA/DNA radical species.

Evidence for the generation of DNA radicals exists from radiation studies. ROS also are capable of generating direct DNA damage (Bensasson *et al*., 1993; Scandalios, 1997). The hydroxyl radical causes base modifications, abasic sites, DNA strand breaks and cross-links (Scandalios, 1997). The formation of radical DNA species through indirect oxidation may be expected to occur since ROS and free radicals will propagate to other nearby molecules.

Changes in regulation of Oxidative Stress Response Genes: The "Redox Switch" Transcription factors (NFκB, AP-1), p53 activation, signal transduction activation. Shifting the redox balance within the cell has many consequences, a few of which are beginning to be understood (Foletta *et al*., 1998; Lu, 1999; Mansur, 1998; Sun and Oberley, 1996; Wang and Ohnishi, 1997). Membrane receptors such as receptor tyrosine kinases, have been found to be redox sensitive,

and can be activated by direct oxidation or by peroxidation in the adjacent plasmalemma (Suzuki *et al*., 1997). Autophosphorylation follows, initiating a signal transduction cascade either through the MAP Kinase pathway (which is still being elucidated fully) or through PKC activation and resultant signals mediated via calcium efflux from intracellular stores.

An important molecule, p53, is known to contain 10 cysteine residues at its DNA-binding interface (Mansur, 1998). Studies have indicated that oxidation of these residues inactivates p53, however, conflicting cell-free and *in vitro* results throw doubt on this conclusion (Sun and Oberley, 1996). Opposite results have been obtained concerning the ability of transcription factors to bind DNA in an oxidized vs. reduced environment. Under cell-free conditions, the requirement is for an oxidized environment, but *in vitro* experiments have demonstrated that a highly reducing peri-nucleic acid environment results in transcription factor activation. Once activated, p53 has been shown to induce $p21^{waf1/cip1}$ expression (Mansur, 1998; Sun and Oberley, 1996; Wang and Ohnishi, 1997), followed by *c-fos* and *c-jun* expression, the components of the transcription factor, AP-1. Binding sites for AP-1 are found in several "oxidative stress responsive" genes, viz.; heme oxygenase 1 (HO-1) (Choi and Alam, 1996), GST Ya (Daniel, 1993), quinone reductase (QR, NQO1, DT diaphorase, NMOR1) (Bergelson *et al*., 1994) and ferritin heavy chain (FH) (Tsuji *et al*., 1998). H_2O_2 has been observed to induce NF-κB activation (Sun and Oberley, 1996), and this transcription factor binds to promoter regions of HO-1, QR, and iNOS, initiating increased mRNA expression of antioxidant response factors (Feuillard, 1997; Patten and DeLong, 1999; Saura *et al*., 1999; Schiaffonati and Tiberio, 1997; Vos and al., 1999). These gene products have been demonstrated to play roles in antioxidant defense (Scandalios, 1997). HO-1, for instance, is the rate-limiting enzyme in the catabolism of oxidized heme proteins, especially hemoglobin, leading (via biliverdin) to bilirubin formation

(Choi and Alam, 1996). Bilirubin is a radical species scavenger, and byproducts of this breakdown are carbon monoxide (CO), a co-activator of guanylyl cyclase, and Fe^{3+}. Thus, signal transduction alteration can occur as a result of oxidative stress, and may have profound consequences for cell health (Suzuki, et al. 1997). Transcriptional activation may lead to aberrant increases in growth factor production and autocrine growth loop(s), tumor impaired suppressor function or overexpressed oncogenes, all of which have as their end result loss of growth control by the cell.

Alteration of cell proliferation. Increased cell proliferation through growth factor activation is known to precede focus formation and tumorigenesis for certain carcinogens, when coupled with loss of senescence (Klaasen, 1996). Increased mitotic index, nucleic acid incorporation of tritiated thymidine and/or bromodeoxyuridine (BrdU) have been employed to quantitate this phenomenon.

Alteration of apoptotic pathways. A decrease in the apoptotic index due to upregulation of mRNA expression of the gene bcl-2 (which acts to prevent apoptosis), downregulation of gene expression for pro-apoptotic mRNA's bax, bad, and/or bcl-X would result in increased damaged cell survival, and mutation fixation. TNFα, FasL, iNOS and APO are other pro-apoptotic signalling molecules that might be downregulated in the presence of carcinogenic substances (Jehn and Osborne, 1997).

Formation of Toxic Cysteine Conjugate. It is postulated that $KBrO_3$ may form a cysteine S conjugate through the action of cysteine conjugate β lyase (Klaasen, 1996), an enzyme found in high concentration in the kidney. First, a GSH conjugate would be formed between GSH and $KBrO_3$. Then γ-GT would act on the conjugate, forming an aminosulfonic acid, which would then be enzymatically transformed by cysteinyl glycinase to the cysteine S conjugate. The

cysteine S conjugate would then be converted by cysteine S conjugate β lyase (if present) to NH_3, pyruvate and HSO_3^-/H_2SO_4. The end result would be pH change, corrosion and necrosis.

TARGET ORGAN SPECIFICITY: KIDNEY, THYROID AND MESOTHELIUM

$KBrO_3$ specifically targets the kidney, thyroid and peritoneal mesothelium in the F344 rat. Although the kidney has been thoroughly investigated with regard to the mechanisms of toxicity of $KBrO_3$, neither the thyroid nor the mesothelium have been examined.

THE KIDNEY MODEL: A PARADIGM FOR THE MESOTHELIUM?

The excellent work of Y. Kurokawa et al. (Kurokawa *et al*., 1985; Kurokawa *et al*., 1990; Kurokawa *et al*., 1987b; Kurokawa *et al*., 1986b) yielded a model upon which to pattern studies of the mesothelium. In this model, lipid peroxidation and formation of 8-OHG adducts are postulated to result in genetic mutations and, along with α_{2U} globulin, contributes to cell proliferation (in the male rat). The existence of these model studies begs the question of whether these tissues (kidney, mesothelium) are identical in their biologic responses to $KBrO_3$, with a common mechanism of toxicity.

IMPORTANCE/IMPACT OF THIS STUDY

Mechanistic data are now being incorporated into the justification process for development of regulations (USEPA, 1998). Therefore, data demonstrating that $KBrO_3$ operates through a specific mechanism (or mechanisms) in rats (or other species) that are not relevent in humans can be used to support higher maximum tolerable limits for $KBrO_3$ concentration in municipal drinking water, or reduced/eliminated testing requirements for the same. Alternatively, if the mechanism of carcinogenicity is seen to be possible in humans, rats may be used as a sentinel

species for determination of the lowest acceptable concentration of $KBrO_3$ in finished drinking water, at a known rate of ingestion over time. Furthermore, if gene expression studies of $KBrO_3$ exposures of rats/human *in vitro* cultures yield similar results to those from rat *in vivo* exposures, a new model for the identification of limits for this carcinogen, and possibly others, may exist. Such a tool would be powerful because of 1) improved speed, 2) elimination of need for live animal testing, 3) reduced cost and 4) versatility.

RESEARCH HYPOTHESES

The research hypotheses addressed examine mechanisms of toxicity on three levels. Each level places the question in sharper focus, in effect looking at the problem from macroscopic, microscopic, and molecular levels.

Tissue level

1) Mesotheliomas observed in the male F344 rat are located in specific site(s) on the tunica vaginalis testis.

It was investigated whether more tumors arose in specific site(s) with greater frequency than others in order to better understand the physiologic forces which may have a role in tumor development.

Biochemical level

2) Glutathione is mechanistically involved in $KBrO_3$-induced toxicity.

The data from kidney-based studies indicate that biochemically, GSH plays a pivotal role in $KBrO_3$-induced toxicity, with most reports implying that it is protective. I studied the responses of mesothelial cells *in vitro*, by means of a tissue-culture system I developed, toward the augmentation and depletion of GSH prior to treatment with $KBrO_3$.

Molecular level

3) $KBrO_3$ induces specific oxidative stress-characteristic gene expression changes indicative of a) lipid, b) protein, and c) DNA damage to the cell *in vitro*.

To date, no information is available as to whether a specific oxidative stress pattern of gene expression is observed with $KBrO_3$ treatment in any system. I examined the effects at the mRNA expression level of $KBrO_3$ treatment of target mesothelial, and non-target hepatocellular carcinoma cell cultures *in vitro*.

References

Ballmaier, D. and Epe, B. (1995). Oxidative DNA damage induced by potassium bromate under cell-free conditions and in mammalian cells. *Carcinogenesis* **16,** 335-342.

Bensasson, R. V., Land, E. J. and Truscott, T. G. (1993). Excited States and Free Radicals in Biology and Medicine; Contributions from Flash Photolysis and Pulse Radiolysis, pp. 431. Oxford: Oxford Science Publications.

Bergelson, S., Pinkus, R. and Daniel, V. (1994). Quinone Reductase. *Oncogene* **9,** 565-571.

Choi, A. M. K. and Alam, J. (1996). Heme Oxygenase-1: Function, Regulation and Implication of a Novel Stress-inducible Protein in Oxidant-induced Lung Injury. *Am. J. respir. Cell Mol. Biol.* **15,** 9-19.

Cotton, F. A., Wilkinson, G. and Gaus, P. L. (1987). Basic Inorganic Chemistry, 2nd Edition. New York: John Wiley & Sons.

Daniel, V. (1993). Glutathione S-Transferases: Gene Structure and Regulation of Expression. *Critical Reviews in Biochemistry and Molecular Biology* **28,** 173-207.

de Paulet, C., Douste-Blazy, L. and Paoletti, R. (1990). Free Radicals, Lipoproteins, and Membrane Lipids. In *Life Sciences (Series A), Volume 189,* vol. 189 (ed. A. C. de Paulet), pp. 403. New York: Plenum Press w/ NATO Scientific Affairs Division.

DeAngelo, A., George, M., Kilburn, S., Moore, T. and Wolf, D. (1998). Carcinogenicity of Potassium Bromate Administered in the Drinking Water to Male B6C3F1 Mice and F344/N Rats. *Toxicol. Pathol.* **26,** 724-729.

Devasagayam, T. P. A., Steenken, S., Obendorf, M. S. W., Schulz, W. A. and Sies, H. (1991). Formation of 8-Hydroxy(deoxy)guanosine and Generation of Strand Breaks at Guanine Residues in DNA by Singlet Oxygen. *Biochemistry* **30,** 6283-6289.

Feuillard, J. (1997). Nuclear Rel-A and c-Rel protein complexes are differentially distributed within human thymocytes. *J. Immunol.* **158,** 2585-2591.

Fisher, N., Hutchinson, J., Hardy, J., Ginocchio, A. and Waite, V. (1979). Long-term toxicity and carcinogenicity studies of the bread improver potassium bromate. 1. Studies in rats. *Food Cosmet. Toxicol.* **17,** 33-39.

Floyd, R. A., Watson, J. J., Harris, J., West, M. and Wong, P. K. (1986a). Formation of 8-Hydroxydeoxyguanosine, Hydroxyl Free Radical Adduct of DNA in Granulocytes Exposed to the Tumor Promoter, Tetradeconylphorbolacetate. *Biochem. Biophys. Res. Comm.* **137,** 841-846.

Floyd, R. A., Watson, J. J., Wong, P. K., Altmiller, D. H. and Rickard, R. C. (1986b). Hydroxyl Free Radical Adduct of Deoxyguanosine: Sensitive Detection and Mechanisms of Formation. *Free Rad. Res. Comms.* **1,** 163-172.

Foletta, V. C., Segal, D. H. and Cohen, D. R. (1998). Transcriptional regulation in the immune system: all roads lead to AP-1. *J. Leukocyte Biol.* **63,** 139-152.

Fraga, C. G., Shigenaga, M. K., Park, J., Degan, P. and Ames, B. N. (1990). Oxidative damage to DNA during aging: 8-Hydroxy-2'-deoxyguanosine in rat organ DNA and urine. *Proc. Natl. Acad. Sci.* **87,** 4533-4537.

Fridovich, I. (1978). Superoxide radicals, superoxide dismutases and the aerobic lifestyle. *Photochem. Photobiol.* **28,** 733-41.

Ginocchio, A., Waite, V., Hardy, J., Fisher, N., Hutchinson, J. and Berry, R. (1979). Long-term toxicity and carcinogenicity studies of the bread improver potassium bromate. 2. Studies in mice. *Food Cosmet. Toxicol.* **17,** 41-47.

Hayashi, Y., Kurokawa, Y., Maekawa, A. and Takahashi, M. (1986). Strategy of long-term animal testing for quantitative evaluation of chemical carcinogenicity. In *New Concepts and developments in Toxicology* (ed. P. L. Chambers, Gehring, P. and Sakai, F.), pp. 383-391. New York: Elsevier Science Publishers.

IARC. (1986). Some Naturally Occurring and Synthetic Food Components, Furocoumarins and Ultraviolet Radiation. *IARC Monographs on the Evaluation of the Carcinogenic Risk of Chemicals to Humans* **40,** 207-220.

Ishidate, M. (1987). Data Book of Chromosomal Aberration Tests In Vitro, revised edition., pp. 334. Tokyo: L.I.C. Inc.

Ishidate, M., Sofuni, T. and Yoshikawa, K. (1981). Chromosomal aberration tests in vitro as a primary screening tool for environmental mutagens and/or carcinogens. *Gann Monogr. Cancer Res.* **27,** 95-108.

Ishidate, M., Sofuni, T., Yoshikawa, K., Hayashi, M., Nohmi, T., Sawada, M. and Matsuoka, A. (1984). Primary mutagenicity screening of food additives currently used in Japan. *Food Chem. Toxicol.* **22,** 623-636.

Ishidate, M. and Yoshikawa, K. (1980). Chromosome aberration tests with Chinese hamster cells in vitro with and without metabolic activation - a comparative study on mutagens and carcinogens. *Arch. Toxicol.* **Suppl. 4,** 41-44.

Ishidate, M., Yoskikawa, K. and Sofuni, T. (1982). Studies on the mutagenicity of potassium bromate and other oxidizing chemicals. In *Proceedings of the 41st Annual Meeting of the Japanese Cancer Association*.

Jehn, B. M. and Osborne, B. A. (1997). Gene regulation associated with apoptosis. *Crit. Rev. Eurkary. Gene Expr.* **8,** 179-193.

Kamiya, H., Miura, K., Ishikawa, H., Inoue, H., Nishimura, S. and Ohtsuka, E. (1992). c-Ha-ras Containing 8-Hydroxyguanine at Codon 12 Induces Point Mutations at the Modified and Adjacent Positions. *Cancer Res.* **52,** 3483-3485.

Kasai, H., Crain, P. F., Kuchino, Y., Nishimura, S., Ootsuyama, A. and Tanooka, H. (1986). Formation of 8-hydroxyguanine moiety in cellular DNA by agents producing oxygen radicals and evidence for its repair. *Carcinogenesis* **7,** 1849-1851.

Kasai, H., Nishimura, S., Kurokawa, Y. and Hayashi, Y. (1987). Oral administration of the renal carcinogen, potassium bromate, specifically produces 8-hydroxydeoxyguanosine in rat target organ DNA. *Carcinogenesis* **8,** 1959-1961.

Kawachi, T., Yahagi, T., Kada, T., Tazima, Y., Jr., M. I., Sasaki, M. and Sugiyama, T. (1980). Cooperative programme on short-term assays for carcinogenicity in Japan. In *Molecular and Cellular Aspects of Carcinogen Screening Tests*, vol. IARC Scientific Publications No. 27 (ed. R. Montesano, H. Bartsch and L. Tomatis), pp. 330-333. Lyon, France: International Agency for Research on Cancer.

Klaassen, C. D. (1996). Casarett and Doull's Toxicology: The Basic Science of Poisons, pp. 1111. New York, NY: McGraw-Hill.

Kuchino, Y., Mori, F., Kasai, H., Inoue, H., Iwai, S., Miura, K., Ohtsuka, E. and Nishimura, S. (1987). Misreading of DNA templates containing 8-hydroxydeoxyguanosine at the modified base and at adjacent residues. *Nature* **327,** 77-79.

Kurokawa, Y. (1985). Overview on the toxicity and carcinogenicity of potassium bromate (in Japanese). *Kosankinbyo Kenkyuzasshi* **37,** 139-149.

Kurokawa, Y., Aoki, K., Imazawa, T., Hayashi, Y., Matsushima, Y. and Takamura, N. (1985). Dose-related enhancing effect of potassium bromate on renal tumorigenesis in rats initiated with N-ethyl-N-hydroxyethylnitrosamine. *Jpn. J. cancer Res. (Gann)* **76,** 583-589.

Kurokawa, Y., Aoki, S., Matsushima, Y., Takamura, N., Imazawa, T. and Hayashi, Y. (1986a). Dose-response studies on the carcinogenicity of potassium bromate in F344 rats after long-term oral administration. *J. Natl. Cancer Inst.* **77,** 977-982.

Kurokawa, Y., Hayashi, Y., Maekawa, A., Takahashi, M. and Kokubo, T. (1982). Induction of renal cell tumors in F344 rats by oral administration of potassium bromate, a food additive. *Gann* **73,** 335-338.

Kurokawa, Y., Hayashi, Y., Maekawa, A., Takahashi, M., Kokubo, T. and Odashima, S. (1983a). Carcinogenicity of Potassium Bromate Administered Orally to F344 Rats. *J. Nat'l. Cancer Inst.* **71,** 965-971.

Kurokawa, Y., Maekawa, A., Takahashi, M. and Hayashi, Y. (1990). Toxicity and Carcinogenicity of Potassium Bromate - A New Renal Carcinogen. *Env. Hlth. Persp.* **87,** 309-335.

Kurokawa, Y., Matsushima, Y., Takamura, N., Imazawa, T. and Hayashi, Y. (1987a). Relationship between the Duration of Treatment and the Incidence of Renal Cell Tumors in Male F344 Rats Administered Potassium Bromate. *Jpn. J. Cancer Res. (Gann)* **78,** 358-364.

Kurokawa, Y., Takahashi, M., Kokubo, T., Ohno, Y. and Hayashi, Y. (1983b). Enhancement by potassium bromate of renal tumorigenesis initiated by n-ethyl-N-hydroxyethylnitrosamine in F-344 rats. *Gann* **74,** 607-610.

Kurokawa, Y., Takamura, N., Matsuoka, C., Imazawa, T., Matsushima, Y., Onodera, H. and Hayashi, Y. (1987b). Comparative studies on lipid peroxidation in the kidney of rats, mice and hamsters and on the effect of cysteine, glutathione and diethyl maleate treatment on mortality and nephrotoxicity after administration of potassium bromate. *J. Am. Coll. Toxicol.* **6,** 489-501.

Kurokawa, Y., Takamura, N., Matsushima, Y., Imazawa, T. and Hayashi, Y. (1984). Studies on the promoting and complete carcinogenic activities of some oxidizing chemicals in skin carcinogenesis. *Cancer Lett.* **24,** 299-304.

Kurokawa, Y., Takayama, S., Konishi, Y., Hiasa, Y., Asahina, S., Takahashi, M., Maekawa, A. and Hayashi, Y. (1986b). Long-term in vivo carcinogenicity test of potassium bromate, sodium hypochlorite and sodium chlorite conducted in Japan. *Environmental Health Perspect.* **69,** 221-235.

Levin, D. E., Hollstein, M. C., Christman, M. F., Schwiers, E. A. and Ames, B. N. (1982). A new Salmonella tester strain (TA102) with A:T base pairs at the site of mutation detects oxidative mutagens. *Proc. Natl. Acad. Sci. USA* **79,** 7445-7449.

Lewis, R. J., Sr. (1991). Hazardous Chemicals Desk Reference, 2nd Edition. New York: Van Nostrand Reinhold.

Loft, S., Vistisen, K., Ewertz, M., Tjonneland, A., Overvad, K. and Poulsen, H. E. (1992). Oxidative DNA damage estimated by 8-hydroxydeoxyguanosine excretion in humans: influence of smoking, gender and body mass index. *Carcinogenesis* **13,** 2241-2247.

Lu, S. c. (1999). Regulation of hepatic glutathione synthesis: current concepts and controversies. *FASEB J.* **13,** 1169-1183.

Mansur, C. P. (1998). The Regulation and Function of the p53 Tumor Suppressor. In *Advances in Dermatology*, vol. 13, pp. 121-165: Mosby-Year Book, Inc.

Matsumoto, I. (1973). Clinical and experimental studies on ototoxicity of bromate (in Japanese). *Otol. Fukuoka* **19,** 220-236.

Matsushima, Y., Takamura, N., Imazawa, T., Kurokawa, Y. and Hayashi, Y. (1986). Lack of carcinogenicity of potassium bromate after subcutaneous injection to newborn mice and newborn rats. *Sci. Rep., Tohoku Univ., Ser. C.* **33,** 22-26.

Odashima, S. (1980). Cooperative programme on long-term assays for carcinogenicity in Japan. In *Molecular and Cellular Aspects of Carcinogen Screening Tests, IARC Publication No. 27* (ed. R. Montesano, H. Bartsch and L. Tomatis), pp. 315-322. Lyon: International Agency for Research on Cancer.

Ohno, Y., Onodera, H., Takamura, N., Imazawa, T., Maekawa, A. and Kurokawa, Y. (1982). Carcinogenicity testing of potassium bromate in rats (in Japanese). *Bull. Natl. Inst. Hyg. Sci.* **100,** 93-100.

Oinuma, T. (1974). 8 cases of death by intoxication of potassium bromate [in Japanese]. *Nichidaiishi* **33,** 759-766.

Onodera, H., Tanigawa, H., Matsushima, Y., Maekawa, A., Kurokawa, Y. and Hayashi, Y. (1985). Eosinophilic bodies in the proximal renal tubules of rats given potassium bromate (in Japanese). *Bull. Natl. Inst. Hyg. Sci.* **103,** 15-20.

Packer, L. and Cadenas, E. (1998). Oxidative Stress in Cancer, AIDS and Neurodegenerative Diseases. In *Oxidative Stress and Disease* (ed. L. Montagnier, R. Olivier and C. Pasquier), pp. 588. New York: Marcel Dekker, Inc.

Park, J. and Floyd, R. A. (1992). Lipid Peroxidation Products Mediate the Formation of 8-Hydroxydeoxyguanosine in DNA. *Free Rad. Biol. & Medicine* **12,** 245-250.

Park, J. and Floyd, R. A. (1994). Generation of Strand Breaks and Formation of 8-Hydroxy-2'-deoxyguanosine in DNA by a Thiol/Fe3+/O2-Catalyzed Oxidation System. *Arch. Biochem.* **312,** 285-291.

Park, J.-W. and Floyd, R. A. (1997). Glutathione/Fe3+/O2-Mediated DNA strand breaks and 8-hydroxydeoxyguanosine formation: Enhancement by copper,zinc superoxide dismutase. *Biochimica et Biophysica Acta* **1336,** 263-268.

Patnaik, P. (1992). A Comprehensive Guide to the Hazardous Properties of Chemical Substances. New York: Van Nostrand Reinhold.

Patten, E. J. and DeLong, M. J. (1999). Temporal effects of the detoxification enzyme inducer, benzyl isothiocyanate: activation of c-Jun N-terminal kinase prior to the transcription factors AP-1. *Biochem. Biophys. Res. Comm.* **257,** 149-155.

Sai, K., Takagi, A., Umemura, T., Hasegawa, R. and Kurokawa, Y. (1991). Relation of 8-Hydroxydeoxyguanosine Formation in Rat Kidney to Lipid Peroxidation, Glutathione Level and Relative Organ Weight after a Single Administration of Potassium Bromate. *Jpn. J. Cancer Res.* **82,** 165-169.

Sai, K., Umemura, T., Takagi, A., Hasegawa, R. and Kurokawa, Y. (1992). The Protective Role of Glutathione, Cysteine and Vitamin C against Oxidative DNA Damage Induced in Rat Kidney by Potassium Bromate. *Jpn. J. Cancer Res.* **83,** 45-51.

Saura, M., Zaragoza, C., Bau, C., McMillan, A. and Lowenstein, C. J. (1999). Interaction of interferon regulatory factor-1 and nuclear factor kappaB during activation of inducible nitric oxide synthase. *J. Mol. Biol.* **289,** 459-471.

Scandalios, J. G. (1997). Oxidative Stress and the Molecular Biology of Antioxidant Defenses. In *Cold Spring Harbor Monograph Series* (ed. J. G. Scandalios). Cold Spring Harbor: Cold Spring Harbor Press.

Schiaffonati, L. and Tiberio, L. (1997). Gene expression in liver after toxic injury: analysis of heat shock response and oxidative stress-inducible genes. *Liver* **17,** 183-191.

Sun, Y. and Oberley, L. W. (1996). Redox Regulation of Transcriptional Activators. *Free Radical Biology and Medicine* **21,** 335-348.

Suzuki, Y. J., Forman, H. J. and Sevanian, A. (1997). Oxidants as Stimulators of Signal Transduction. *Free Radical Biology & Medicine* **22,** 269-285.

Takamura, N., Kurokawa, Y., Matsushima, Y., Imazawa, T., Onodera, H. and Hayashi, Y. (1985). Long-term oral administration of potassium bromate in male Syrian golden hamsters. *Sci. Re. Res. Inst. Tohoku univ., Ser. C.* **32,** 43-46.

Tanaka, K., Oikawa, K., Fukuhara, C., Saito, H., Onosaka, S., Min, K. S. and Fujii, M. (1984). Metabolism of potassium bromate in rats. II. in vitro studies. *Chemosphere* **13,** 1213-1219.

Tchou, J., Kasai, H., Shibutani, S., Chung, M. H., Laval, J., Grollman, A. P. and Nishimura, S. (1991). 8-Oxoguanine (8-hydroxyguanine) DNA glycosylase and its substrate specificity. *Proc. Natl. Acad. Sci. USA* **88,** 4690-4694.

Tsuji, Y., Torti, S. V. and Torti, F. M. (1998). Ferritin heavy chain. *J. Biol. Chem.* **273,** 2984-2992.

Umemura, T., Sai, K., Takagi, A., Hasegawa, R. and Kurokawa, Y. (1993). A possible role for cell proliferation in potassium bromate (KBrO3) carcinogenesis. *J. Cancer Res. Clin. Oncol.* **119,** 463-469.

Umemura, T., Sai, K., Takagi, A., Hasegawa, R. and Kurokawa, Y. (1995). A possible role for oxidative stress in potassium bromate (KBrO3) carcinogenesis. *Carcinogenesis* **16,** 593-597.

USEPA. (1998). Draft Water Quality Criteria Methodology Revisions: Human Health; Notice. *Federal Register* **63,** 43755-43828.

von Gunten, U. and Holgne, J. (1994). Bromate Formation during Ozonation of Bromide-Containing Waters: Interaction of Ozone and Hydroxyl Radical Reactions. *Environ. Sci. Technol.* **28,** 1234-1242.

Vos, T. A. and al., e. (1999). Expression of inducible nitric oxide synthase in endotoxemic rat hepatocytes is dependent on the cellular glutathione status. *Hepatology* **29,** 421-426.

Wang, X. and Ohnishi, T. (1997). p-53-Dependent Signal Transduction Induced by Stress. *J. Radiat. Res.* **38,** 179-194.

WHO. (1964). Seventh Report on the Specifications for the Identity and Purity of Food Additives and Their Toxicological Evaluation: Emulsifiers, Stabilizers, Bleaching and Maturing Agents. *World Health Organization Technical Report* **Series 281,** 164.

Table 1. Acute- and Long-term Toxicity of $KBrO_3$

ACUTE:

Duration/Reference	Method of Admin.	Dose	Species/Sex	Target Tissue	Lesion
<12 hrs.(Matsumoto, 1973)	Accidental/intentional ingest.	0.5-70 g	humans/m+f	kidney	atrophy, necrosis, degeneration & regeneration of the proximal tubular epithelium
				ear	degeneration of cochlear sensory
				heart	not specified
				liver	not specified
48 hrs.(Kurokawa, 1985)	Intragastric (IG)	0-900 mg/kg	F344 rats/m+f		
				kidney	epithelial dilatation & desquamation of distal convoluted tubules; necrotic & degenerative changes of the proximal tubular epithelium, regenerative changes in tubular epithelium
			B6C3F1 mice/m+f	stomach	hyperemia of glandular stomach mucosa
				lung	pulmonary edema
			Syrian Golden Hamster/m+f		same as for mice

SUBACUTE:

10 wks.(Kurokawa *et al*., 1986b)	Ingest. (drinking water)	250-4000 ppm	B6C3F1 mice/m+f		no adverse effects at palatable (<2000ppm) doses
13 wks.(Onodera *et al*., 1985) (Onclera, unpub.)	Ingest. (drinking water)	150-10,000 ppm	F344 rats/m+f		>1250 ppm died w/in 7 wks.
				kidney	eosinophilic droplets in proximal tubular epithelium, tubular regeneration
					decreased weight gain

Duration/Reference	Method of Admin.	Dose	Species/Sex	Target Tissue	Lesion
4,8,12 wks.(WHO, 1964)	Ingest. (trtd. flour/trtd. flour as bread)	84% flour diet from flour trtd. w/75 ppm $KBrO_3$			
			rat		no adverse effects
			dog		no adverse effects
			monkey		no adverse effects
16 days (bread) (WHO, 1964)	Ingest. Of flour or bread				
10 wks. (flour)		bread from flour trtd. w/200 ppm $KBrO_3$			
		flour trtd. w/200 ppm $KBrO_3$			
			rat		no adverse effects
			dog		no adverse effects
6 wks. (WHO, 1964)	Ingest. of flour	flour trtd. w/70 ppm $KBrO_3$			
			dog		no adverse effects
17 mos. (WHO, 1964)	Ingest. of flour	flour trtd. w/200 ppm $KBrO_3$			
			dog		no adverse effects
multigenerational (WHO, 1964)	Ingest. of flour trtd. bread				
(3 generations)		flour trtd. w/14 or 100 ppm $KBrO_3$			
			rat/m+f		no adverse effects
multigenerational (WHO, 1964)	Ingest. of flour	flour trtd. w/15 ppm $KBrO_3$			
(8 & 5 generations)			mouse		no adverse effects
			rat		no adverse effects
104/80 wks. (Fisher *et al*., 1979)	Ingest. of bread from trtd. flour				
	diet = 79% bread		Wistar Porton rat/m+f		
				pancreas	periarteritis (males)
				adrenals	increased aging pathology (m+f)
					no accum. of $KBrO_3$ in tissues
					total tumor incidence in females> control ($p< 0.01$)

Duration/Reference	Method of Admin.	Dose	Species/Sex	Target Tissue	Lesion
			Theiler mouse/m+f		small amts. Accum. In adipose tissue No adverse effects

Long-term, (not specified) (Fisher *et al*., 1979; Ginocchio *et al*., 1979)

Ingestion of (a) flour trtd. w/50 ppm $KBrO_3$, 30 ppm ascorbic acid, 50 ppm benzoyl peroxide, or (b) flour trtd. w/50 ppm $KBrO_3$, 30 ppm ascorbic acid, 50 ppm benzoyl peroxide, 15 ppm chlorine dioxide

			rat/m+f	pancreas	periarteritis (males)
				adrenals	increased aging pathology (m+f)

CHRONIC:

110 wks. Ingest. (drinking water) 0 - 500 ppm F344 rat/m+f decreased survival time @500 ppm

(Hayashi *et al*., 1986; Kurokawa, 1985; Kurokawa *et al*., 1985; Kurokawa *et al*., 1986a; Kurokawa *et al*., 1982; Kurokawa *et al*., 1983a; Kurokawa *et al*., 1983b; Kurokawa *et al*., 1986b; Ohno *et al*., 1982; Onodera *et al*., 1985)

(reduced high dose to 400 ppm at wk 60)

	kidney (m)	renal cell tumors (RCT) (high dose: 88%) low dose: 60%, control: 6%) dysplastic foci (DF) (77%, 60%, 11%) adenocarcinoma (AC) (85%, 45%, 6%) adenoma (A) (10%, 19%, 0%) similar for (f) except DF peritoneal mesothelioma (m only) mesothelioma (M) (59%, 33%, 11%)

No peritoneal mesotheliomas in trtd. or Control female rats.

Duration/Reference	Method of Admin.	Dose	Species/Sex	Target Tissue	Lesion
104 wks. (Kurokawa *et al*., 1986a)	Ingest. (drinking water)	0-500 ppm	F344 rat/m		decreased survival time @500 ppm kidney RCT, DF, AC, A thyroid follicular adenoma (FA) follicular adenocarcinoma (FAC)
Ltd. Duration study (Kurokawa *et al*., 1987a) 13 - 104 wks.	Ingest. (drinking water) (H_2O, $KBrO_3$, $KBrO_3$ followed by H_2O only)	500 ppm	F344 rat/m	kidney thyroid	RCT, DF, AC, A FA, FAC perit. Mesothelium M Effects irreversible. Tumor Incidence High overall in discont.-trtd. groups receiving same dose as continuously-trtd.
					(high dose + short time>low dose + long time)
87 wks. (Oinuma, 1974)	Intragastric	0- 600 mg/kg	F344 rat/m	kidney	RCT (but NS: 13.6%, 0%, 0%) finding may be sig. Due to low backgrnd. incidence of RCT in F344 rat.
78 wks. + 26 wks. tap water (Kurokawa *et al*., 1986b)		500-1000 ppm	B6C3F1 mouse/f		
				lung liver lymph node	tumor incidence NS “ “
88 wks. (Oinuma, 1974)	Ingest. (drinking water)	750 ppm	B6C3F1 mouse/m	kidney	AC (NS), A (NS), DF (NS)
			BDF1 mouse/m	small intestine	adenoma ($p<0.01$)
			CDF1 mouse/m	liver	adenoma ($p<0.05$)

Duration/Reference	Method of Admin.	Dose	Species/Sex	Target Tissue	Lesion
89 wks. (Takamura *et al*., 1985)	Ingest. (drinking water)	125 - 2000 ppm	Syrian Golden Hamster/m	kidney	A (9.3%, 0%)
78/82 wks. (Matsushima *et al*., 1986)	Subcut. Inj.; single or 4/wk. Until weanling	12.5 - 200 mg/kg	ICR mouse (newborn)	Kidney	DF in trtd. & ctrls.
			F344 rat (newborn)	Kidney	few tumors (NS)

Table 2. Mutagenicity Assay Results For $KBrO_3$ and Related Compounds

Strain	Concentration	Compound	Result	Metabolic Activation?
S. typhimurium, TA100[a,f]	3 mg/plate	$KBrO_3$	weak +	+
" TA102[f]	2 to 4 mg/plate	"	+	+
" TA104[f]	"	"	+	+
" TA98[a,b,c]	"	"	-	+/-
" TA1535[a,b,c]	"	"	-	+/-
" TA1537[a,b,c]	"	"	-	+/-
" TA1538[a,b,c]	"	"	-	+/-
E. coli, WP2try-[a,b,c]	"	"	-	+/-
" WP2try-his-[a,b,c]	"	"	-	+/-
Sarcina cerevisiae[e]	ns	"	-	+/-
Bacillus subtilis, 17Arec+[a]	ns	"	-	+/-
" 45Trec+[a]	ns	"	-	+/-
S. typhimurium, TA98[f]	ns	KBr	-	+/-
" TA100[f]	ns	"	-	+/-
ns[f]	ns	$NaBrO_3$	-	+/-
ns[f]	ns	$AgBrO_3$	-	+/-

[a] (Kawachi *et al*., 1980) ns = not specified
[b] (Ishidate *et al*., 1984)
[c] (Ishidate *et al*., 1982)
[d] (Levin *et al*., 1982)
[e] Litton Bionetics, unpublished
[f] Kurokawa, et al., unpublished

Chapter 2. Origin and Distribution of Potassium Bromate-Induced Testicular and Peritoneal Mesotheliomas

Authors and Affiliations:

Lynn M. Crosby[1], Kevin T. Morgan[2], Betty Gaskill[2], D.C. Wolf[3], and A.B. DeAngelo[3]

[1]US EPA Trainee in Environmental Carcinogenesis and North Carolina State University Department of Toxicology, Research Triangle Park, North Carolina 27711

[2]GlaxoWellcome Inc., 5 Moore Drive, Research Triangle Park, NC 27709

[3]US EPA, TW Alexander Drive, Research Triangle Park, NC 27711

ABSTRACT

Tissue sections from a 2-year bioassay of male F344 rats treated with potassium bromate administered in drinking water were examined. All animals exhibiting peritoneal mesotheliomas also had mesotheliomas of the tunica vaginalis testis mesorchium, but not the reverse, and were highly correlated statistically ($r^2 = 0.98$). Mapping of the tunica vaginalis tumors at all time points and at all bromate concentrations revealed a pattern of increasing incidence of tumor formation on the mesothelium of the tunica vaginalis testis as a function of proximity to the mesorchial ligament. Thus it was concluded that the mesorchium is the major mesothelial target site for potassium bromate-mediated carcinogenesis. The frequency of occurrence of mesotheliomas by location was: tunica vaginalis testis (25%), mesosplenium (20%), mesentery (10%), mesojejunum/mesocolon (8%), bladder (6.5%), mesogastrium (13%), liver serosa (5%); and kidney, small intestine, and rectum (1% each). A complete cross-section of the rat testis was prepared and used to construct a complete map of the mesothelium. Any attempt to determine the role of local dose and tissue susceptibility for the purpose of interspecies risk extrapolation must take into account the complex anatomy and physiology of this region of the visceral and testicular suspensory apparatus. Improved histological approaches are needed for adequate assessment of this delicate suspensory system.

Glossary of Terms:

mesothelium – tissue consisting of a one cell thick layer surrounding all bodily organs and lining the inside of all bodily cavities.

suspensory apparatus/ligament – the anatomic attachment of an organ to the body cavity wall, lined on its outer surface by mesothelial cells

mesorchium – suspensory apparatus of the testis

mesosplenium – suspensory apparatus of the spleen

tunica vaginalis visceralis – (or, “mesothelial tunic”) the mesothelial covering on the outside of the rete testis, just external to the tunica albuginea

tunica vaginalis parietalis – the mesothelial covering on the inside of the scrotum

tunica albuginea – the fibrous covering of the testis, a fibrous membrane

INTRODUCTION

Potassium bromate is produced during the ozonation or chlorination of surface water, via hydroxyl radical generation (Hijnen *et al*., 1995). This chemical mechanism is of particular concern in waters with high bromine content, such as certain highly brackish aquifers. The US EPA has promulgated proposed standards for the regulation of bromate content in finished drinking waters (USEPA, 1998b). More information is needed, however, regarding the effects of potassium bromate upon human health, since mechanistic data can now be more readily incorporated into risk assessment models based upon the US EPA guidelines (USEPA, 1998a).

The historical uses and acute toxicity of potassium bromate have been well characterized (IARC, 1986; WHO, 1964). A very strong oxidizing agent, potassium bromate represents a severe hazard in both acute and chronic scenarios. Potassium bromate is a complete carcinogen. Potassium bromate reportedly produced cancerous lesions in the kidney, thyroid, and peritoneal mesothelium of the male F344 rat, the kidney of the female F344 rat, the kidney of male Syrian Golden hamsters, the kidney and small intestine of B6C3F1 male mice, and the liver of male CDF1 mice (Fisher *et al*., 1979; Ginocchio *et al*., 1979). Kurokawa (Kurokawa *et al*., 1990) and colleagues have extensively investigated the etiology and mechanism(s) of potassium bromate carcinogenesis in the rat kidney. The rat mesothelium has received little or no attention in the laboratory, however, due to the inherent difficulties of working with this delicate and anatomically complex tissue. This fact by no means diminishes the importance of this target organ toxicity; indeed, in a recent USEPA bioassay, 62.8% of animals fed drinking

water containing 0.4g/L potassium bromate ($KBrO_3$) developed peritoneal mesotheliomas (DeAngelo *et al*., 1998).

Mesothelioma occurs in species ranging from lower vertebrate to avian, marsupial, and domestic mammalian (Ilgren, 1993). Mesothelioma can be ideopathic in origin, or may be induced. Induction may occur by any one of three asbestiform and 19 other natural fibers, nine man-made mineral fibers, at least 27 separate chemicals (e.g.: acetamide N-2-Fluorenyl, dichlorobucil, ethylene oxide and synthetic estrogen), 14 metals, at least 12 polymers, and eight different viruses (Ilgren, 1993). In the rat, spontaneous mesotheliomas have been noted in Fischer F344, Sprague-Dawley, Wistar and Norvegicus strains, in both males and females. In male rats, the usual location of these neoplasms is either the tunica vaginalis testis or the peritoneum, while in females the location is typically the ovary or peritoneum. The pleura is the next most frequently cited location in both males and females; occasionally the peritoneum and pleura are both involved. Most tumors are observed in aged rats (≥ 2 years) and therefore would not appear in studies of short duration.

Historically, the frequency of spontaneous mesothelioma occurrence in rats of these species ranges from 0.2 to 5%. It has been previously reported that in spontaneously occurring mesotheliomas most tumors begin in the tunica vaginalis testis mesothelium and spread to the peritoneal mesothelium via seeding (Gould, 1977; Tanigawa *et al*., 1987). The causes of spontaneous mesothelioma have been attributed to hormonal imbalance, and it has been speculated that the mesothelium of the tunica vaginalis testis represents an especially susceptible tissue because tumors were induced there by ENU at doses not inducing tumors in any other location (Maekawa *et al*., 1984).

We were curious as to whether an anatomical pattern of distribution exists in potassium bromate-induced mesothelial tumors in the male F344 rat. Significant species/gender differences in the metabolism and consequent disposition of potassium bromate and its metabolite(s) during the development of malignant mesotheliomas would be of great interest because new information on mechanisms of carcinogenesis in the rat might be found, which might inform new mechanisms of carcinogenesis in humans. Such information may assist in formulating risk assessment guidelines for human health. The objective of this study was the more precise determination of the site of origin and incidence of these mesothelial tumors.

METHODS

Bioassay materials

Materials from a 2-year bioassay (DeAngelo *et al*., 1998) were re-examined and lesions mapped. H & E-stained, 5 μm thick sections from formalin-fixed tissues were used. Tissues from all time points (13, 26, 52, 96 and 100 wks) were examined at all potassium bromate concentrations (0, 0.02, 0.1, 0.2 and 0.4 g/L). All 'found dead' and 'moribund sacrifice' tissues available were also examined. Slides were available from at least six animals per treatment group per time point, giving a total of 352 animals examined.

Lesion Mapping

A lesion recording map was designed (Fig. 1) using two landmarks as reference points: the mesorchium of the tunica vaginalis testis and the testicular artery and adjacent vein (Fig. 2) which were generally prominent. Where these features were not distinguishable due to tissue destruction, mapping was omitted (2 cases). All cases included in this assessment displayed at least one morphologically intact testis of the pair, i.e. not missing

the mesothelial tunic. The map was divided into eight equal sectors of the roughly circular testicular cross-section. The mesorchial ligament was placed at the top of the map, at the juncture of segments one and eight. The branch of the testicular artery used as a landmark may occur either just to the left or right of the mesorchial attachment, depending upon orientation of the tissue on the slide. Using this template, tumor distribution was mapped as it appeared on the slide. The number of tumors that occurred in each octant as well as the defined stages (according to pre-established criteria, see below, and stages 1-6) was quantified. Additionally, the number and stage of mesotheliomas on the spleen and/or mesosplenium were recorded.

Statistical Tests

The probability of chance occurrence with greater frequency on the mesorchium than at other locations on the tunica vaginalis (decreasing frequency with distance) was assessed by the student's t-test. The probability of chance concomitant occurrence on both the tunica vaginalis mesorchium and the mesosplenium was tested by calculation of a correlation coefficient. The observed frequency of occurrence of tumors in the mesorchium and mesosplenium was summed and compared with the expected frequency, based on random probability.

Testicular Cross-section & Fixation

In order to observe the spatial arrangement and relationship of the mesorchium to the epididymis and testis, a six-month old male F344 rat was euthanized by CO_2 asphyxiation and the head, tail and other extremities removed. Deep incisions were made inguinally. The trimmed rat was fixed by whole-body immersion in 10% neutral buffered formalin for two months, after which it was washed in running tap water for 24 hours and the

scrotum trimmed away from the rest of the tissue. The whole scrotum was shaved and dehydrated through a graded series of alcohols to xylene as follows: 70% alcohol for seven days (two changes), 75% ethanol for two days, 85% ethanol for 24 hours (two changes), 95% ethanol for 24 hours (three changes), 100% ethanol for 24 hours (four changes), 50:50 absolute ethanol:xylene (one change, three hours), 100% xylene (18 hours, two changes). The whole scrotum was then embedded in paraffin (three changes paraplast, three hours each, at 65 ^{o}C), mounted on a steel chuck (approximately 3 cm x 1 cm), and 5 μm-thick sections were prepared from the approximate center of the block. Slides were stained with H & E using standard techniques.

RESULTS

Control Animals

A non-neoplastic tunica vaginalis testis seen in cross-section (Fig. 3) consists of a single, contiguous layer of fusiform mesothelial cells lining the outside of the tunica albuginea, a cover external to the testis. These cells have a single oval nucleus and delicate faintly eosinophilic cytoplasm.

$KbrO_3$-Treated Animals

Tumor Classification. Abnormal mesothelial growth was classified according to the following criteria (developed in-house).

1. Reactive mesothelium - (Figs. 4, 6) cells with darkly staining nuclei and an increased nuclear to cytoplasmic ratio, a rounded outline which projects outward from the serosal surface resulting in a “cobblestone” appearance.

2. Hyperplasia - increase in the thickness of the mesothelium to >1 cell.

3. Pre-neoplasia - (Fig. 5. 5a compare to Fig. 3); all characteristics of (1) and (2).

4. Early stage - solid expansion or papillary growth and all characteristics of (3).

5. Intermediate-stage mesothelioma - stromal proliferation and some obscuring of normal tissue structure or evidence of deteriorated normal structures and all characteristics of (4).

6. Late-stage mesothelioma (Fig. 7) – growth which overwhelms, obliterates, compacts and/or strangulates normal tissues; smaller, compacted tumor cells; may contain necrotic centers; and all characteristics of (5).

The incidence and stage of mesotheliomas occurring during this study are summarized in Table 1 and Figs. 8-11.

Tumor Incidence. Of 370 animals treated by oral administration of potassium bromate in this study, from 8.2% (0.02 g/L) to 62.8% (0.4 g/L) developed mesotheliomas, with a control incidence of 0% (DeAngelo *et al*., 1998). A detailed examination of the data collected at necropsy revealed that 25% of all observed mesotheliomas occurred on the tunica vaginalis testis and 20% on the mesothelium of the spleen. The remainder of the mesotheliomas occurred on the mesentery (10%), jejunum and colon (8%), pancreas (7%), urinary bladder (6.5%), stomach (6%), liver (5%); and caecum, rectum and kidney (1% each) mesothelium.

Tumor Location. Hyperplastic and pre-neoplastic lesions were first visible on the mesorchium of the tunica vaginalis testis and the mesosplenium at week 13. While from week 13 onward, hyperplastic and pre-neoplastic lesions were visible in both locations (mesorchium and mesosplenium), at week 52 frank mesotheliomas appeared on the mesorchium (at 13 weeks on the mesosplenium)(Table 1). All six stages (reactive mesothelium, hyperplasia, pre-neoplasia, early-, intermediate- and late-stage mesothelioma) were present from week 52 onward, in all potassium bromate-exposed

groups (Table 1 and Figs. 8,11). Two pre-neoplastic lesions and one mesothelioma located on the mesorchium of the tunica vaginalis testis were identified in control animals at 96 weeks. On the surface of the splenic capsule/mesosplenium of control animals, 8 cases of reactive mesothelium (week 26 onward), 8 cases of pre-neoplasm (week 13 onward), and 2 cases of frank mesothelioma (weeks 78 and 96) (Table 1) were observed. In the 'found dead' and 'moribund sacrifice' groups, 14 mesotheliomas were noted on the mesorchium and 9 on the mesosplenium for all doses of potassium bromate administered (none in control animals)(weeks of treatment duration unknown, doses noted in Table 1).

Lesion Mapping

Mapping of the mesotheliomas of the tunica vaginalis testis revealed a pattern of decreasing incidence of tumor formation as a function of distance from the mesorchial ligament: see Fig. 9, at all doses and time points (100 week time point shown), and Fig. 10 (all doses combined shown). At 100 weeks, the number of tumors in sectors 1 and 8 was significantly higher in all dose groups ($p<0.001$) than in sectors farther away from the mesorchium. The proliferative response increased with increasing dose administered. On the surface of the splenic capsule, all observed mesotheliomas were confined to or involved the mesosplenium.

Pre-neoplastic and hyperplastic lesions were seen by 13 weeks on both the mesorchium (Fig. 11 and Table 1) and mesosplenium, but not at other mesothelial locations examined. Mesorchial locations outside of the testis (i.e. within the peritoneum) were not available for examination. The correlation coefficient (r^2) for relatedness between occurrence in both the mesorchium and mesosplenium (columns 1 and 2, Table 2) was 0.98 (for all time points combined) when numbers of tumors were compared at each dose.

Furthermore, the number of animals with tumors on the tunica vaginalis testis mesorchium was 61 (all doses/times) in 352 (17.3%), and the number of animals with tumors on the mesosplenium was 48 (all doses/times) in 352 (13.6%). Thus the probability of observing tumors in both tissues by chance is 0.173 x 0.136 = 0.023, or 2.3% (8 in 352 animals). However, the actual occurrence of tumors in both sites concurrently was 28/352 or 7.9%, therefore, there is an excess risk of 5.7% or 1 in 18 over that expected given random probabilities (which are based on actual observed numbers of tumors in each tissue individually). Based on these calculations, the probability that the occurrence of tumors in these two sites is linked is very high.

Histology

Fig.12 is a photomicrograph of the H & E section (1x) of the whole rat scrotum. The testicular coverings are, starting from the outermost layer, (1) skin and tunica dartos (the tunica dartos forms the scrotal septum) (2) external spermatic fascia, (3) cremaster muscle and cremasteric fascia covering it, (4) internal spermatic fascia, and (5) tunica vaginalis parietalis. The testis (T) is surrounded by the tunica albuginea (A), a thick fibrous wall, and outside of this, by the tunica vaginalis visceralis (V). The tunica vaginalis visceralis extends from the vaginal ring at the extremitas capitata of the testis, to the extremitas caudata of the testis, where lies the epididymis caudata. The border of the testis that is attached to the scrotal wall is the epididymal border, opposite of which is the free border. The proper ligament of the testis attaches the epididymis to the testis along the epididymal border. A testicular bursa (B) occurs between the epididymis and the testis. This consists of a recess in the fold of the proper ligament. The duct of the epididymis (E) is long and coiled, and its diameter increases as it (cauda epididymis)

nears the ductus deferens, with which it is contiguous. The ductus deferens (D) is enclosed within its own mesothelial covering, the mesoductus deferens. The ductus deferens, testicular artery and vein, lymphatics and nerves run together enclosed within the spermatic cord, which passes into the abdominal cavity via the inguinal canal, through the vaginal ring. Between the tunica vaginalis parietalis and visceralis lies the cavum vaginale (C), a narrow capillary space contiguous with the peritoneal cavity at the vaginal ring. The tunica vaginalis parietalis is contiguous with the peritoneal parietal mesothelium. The visceral tunic is contiguous to the mesorchium (M), a long serosal fold suspending the testis. It contains the spermatic cord, etc. as mentioned above. The long, narrow fold of serosal tissue attaching the epididymal border of the testis to the tunica vaginalis parietalis (proper ligament of the testis) is also part of the mesorchium. From it ensues a further fold, the mesepididymis (ME), which passes laterally along the epididymis. The mesepididymis and mesorchium bound the testicular bursa, mentioned above. The mesorchium from the vaginal ring to the testicular caput is called the mesofuniculum (which would be visible upon longitudinal or extremitas capitata section of the testis only), which attaches the spermatic cord to the tunica vaginalis parietalis by means of mesothelial tissue. The ligament of the tail of the epididymis is otherwise known as the distal free end of the mesorchium. According to Fig. 12C, all structures outward starting from the mesofuniculum are typically lost at necropsy, however, in some cases, removal of the testis includes some tearing of tissue, which may mean none of the mesorchial structure remains. Only very rarely is the parietal mesothelium included in the sectioned tissue. Commonly, tunica vaginalis visceralis is disrupted, at least briefly, at one or more points surrounding the testis.

It is concluded that mesotheliomas occur first on the mesorchium or the mesosplenium, or at some point on the mesothelium lying in between these suspensory apparati (which is lost during routine necropsy procedures and therefore could not be observed in this study).

DISCUSSION

With time the potassium bromate-induced proliferative response on the mesorchium became more frequent (Fig. 11), extensive and biologically aggressive. Taken together with the increased incidence of mesotheliomas at 0-1 map units from the mesorchium vs. greater distances, we conclude that the probability of tumor origination on the tunica vaginalis mesorchium is greater than in all other sites of the tunica vaginalis examined. This pattern is consistent with tumor spreading from the mesorchium of the tunica vaginalis testis to the peritoneal mesothelium via the inguinal canal, but is also consistent with spread from the mesosplenium to the mesorchium. A distinct possibility is that the actual origin lies somewhere in between these two locations, but since tissue was not available for examination, it cannot be concluded from these data. It was observed that more tumors occurred in the mesorchium without concomitant mesosplenic occurrence at later time points, while more occurred in the mesosplenium at earlier time points and in both “found dead “and “moribund sacrifice” groups (Table I). (Other types of tumors observed in “found dead” and “moribund sacrifice” included thyroid follicular cell adenoma/carcinoma, splenic mononuclear cell leukemia, renal tubular cell adenoma.) One possible explanation for this set of circumstances is that mesosplenic malignant mesotheliomas resulted in early deaths. The incidence of tunica vaginalis mesorchial

mesotheliomas may, in fact, be higher at later time points because they were less lethal, or for other unknown reasons.

The spermatic cord (Fig. 13) runs through the abdominal ring and leads from the peritoneal cavity into the scrotal sac. The spermatic cord contains the spermatic artery, (carrying blood to the testis) (Fig. 2), testicular lymphatic drainage portals, the source of enervation to the testis, the pampiniform plexus (venous bed allowing blood drainage and facilitating cooling of the blood entering the testis), and musculature supplying the testis. The mesorchium connects the testis to the epididymis (Fig. 2) and scrotal wall, and extends laterally along the entire testis and through the inguinal canal at least to the lumbar peritoneal region. The data presented here indicate that a significant number of potassium bromate-induced tumors occur in the mesorchium (sections cut approximately midway through testes) of the treated rats. These mesotheliomas might have originated on the mesorchium at the juncture of the spermatic cord with the testis or at any distance, cranial or caudal, along the mesorchium. If in fact a “hotspot” along the mesorchium exists, it cannot be located solely from the data of the present study. The focus now points to the mesorchial ligament as the point of origin for tumor development. It remains for improvements in histological techniques to facilitate clearing up this question.

Factors which may contribute to the development of tumors in the mesothelium at the convergence of the mesorchium with the testis include; 1) blood flow, 2) direction of flow of peritoneal fluid, 3) heating and cooling processes, 4) lymphatic drainage, 5) enervation and 6) metabolic or other physiologic properties of target mesothelial cells, combined with one or more of the above.

Blood flow may be intimately involved with the process of tumor development because of the swift delivery through the spermatic cord of substances via the circulation. Kurokawa, et al. (1990) investigated the disposition of potassium bromate given intragastrically to male Wistar rats. Bromate and bromide levels in various organs were measured. After 24 hours, approximately 30% of parent compound was detected in the urine, while bromide levels were increased significantly in the plasma, red blood cells, kidney, pancreas, stomach, small intestine and urine. Bromate was absorbed and degraded within 2 to 4 hours in the stomach, small intestine, plasma and urine. No bromate was detected in the urine at doses of less than 2.5 mg/kg; however at doses of 5 mg/kg upward, the amount of bromate in the urine increased proportionally to dose. Thus it appears that potassium bromate administered orally is rapidly distributed throughout the body via the circulatory system. Some of the potassium bromate is then excreted unchanged; however, 70% remains in the body at 24 hours. The testicular artery originates from the abdominal aorta, following a tortuous path to enter the scrotal sac via the abdominal ring and branching to supply the vas deferens before entering the rete testis. The vas deferens branch follows the epididymis and both are attached to the testis by a visceral fold of the tunica vaginalis (part of the mesorchium). The spermatic, cremasteric and vas deferens arteries anastomose juxtatesticularly, maintaining close contact within the spermatic cord. This arrangement could allow for diffusion of potassium bromate out of one or more of the vessels and into the other(s), as well as into the immediately surrounding tissues (e.g. tunica vaginalis, epididymis). Unfortunately, the majority of these structures are destroyed during routine necropsy procedures, rendering meaningful observations about their role in the development of lesions

speculative at best. Not yet explored are the mesorchial reaches in the lumbar region within the peritoneal cavity, where in some species it may extend to the aorta.

The direction of the flow of peritoneal fluid may assist in the distribution of blood-borne potassium bromate quickly and directly to the testicular tunic versus other anatomic sites, but there is no detailed knowledge of the flow field. With respect to heating and cooling processes, the valved spermatic veins leave the testis dorsalis, are joined by veins from the epididymis and form the spermatic plexus (*plexus pampiniformis*). This large and convoluted mass of vessels fills most of the spermatic cord, and effectively cools arterial blood passing into the testis by means of a countercurrent mechanism. The nest of veins coalesces into first several, then two veins as it passes upward through the inguinal canal into the abdomen. The testicle is maintained at a significantly cooler temperature than the trunk, facilitating optimal spermatogenesis as well as maintaining constitutive antioxidant enzyme activity (Ahotupa and Huhtaniemi, 1992). Thus the cooling function of this plexus is essential to health, especially in the event of oxidative stress, such as that reportedly induced by potassium bromate administration (Ballmaier and Epe, 1995; Sai *et al*., 1994; Umemura *et al*., 1995). Such oxidative stress reportedly induces lipid peroxidation, 8-OH-deoxyguanosine adducts, and/or DNA glycosylase activity (the repair enzyme for 8-OH-deoxyguanosine lesions) (*vide supra*). On the other hand, cold or physical stress stimulates withdrawal of the testes into the abdomen, as a result of which the activities of antioxidant enzymes superoxide dismutase (Cu/Zn form), and catalase are greatly reduced. If the testes remained in this position over extended periods of time, especially during exposure to potassium bromate, the ensuing toxicity might be exacerbated. Experiments are underway to investigate whether Cu/Zn SOD expression is

increased 24 hours after potassium bromate exposure *in vitro*, using gene expression array technology. If true, this may be a compensatory response to oxidation or to suppressed SOD enzyme function. Thus it can be seen that the venous drainage from the testicle and physiologic processes such as withdrawal into the abdominal position may be important in the local toxicity of some circulating compounds. One may speculate, as well, that the countercurrent mechanism of cooling may assist potassium bromate deposition in the testis, perhaps by changing the solubility and therefore the partitioning of potassium bromate between the testis (*via* the tunica vaginalis) and the venous blood.

Of note, the visceral and parietal tunica vaginalis is a completely enclosed pouch in humans (Nickel *et al*., 1973), but not in other animals. In the rat, the parietal tunica vaginalis is contiguous with the parietal peritoneal mesothelium at the abdominal ring, and the visceral tunic is contiguous to the mesorchium, the length of which differs among species. Therefore, the spread of mesothelioma from the testicular tunica vaginalis mesothelium into the peritoneum (or the reverse) by "seeding" can proceed unimpeded by anatomic blockage in rats and other animals, but not in humans.

The superficial lymphatic vessels of the testes begin on the tunica vaginalis surface and merge to form larger vessels as they enter the spermatic cord while deep lymphatic vessels originate in the rete testis and epididymis, merging at the spermatic cord. Lymphatic drainage thus occurs through one of several large vessels contained within the spermatic cord and terminating in the lumbar lymph nodes. It is interesting that the hilus of the kidney and of the spleen contain the lymphatic drainage sites for those organs as well, since these three separate organs are targets for potassium-bromate associated tumor development. All specifically show a preponderance of mesothelial lesions located on the

suspensory apparati. Through lymphatic drainage ports within the suspensory ligaments, the passage of toxic products of metabolism occurring at or through them could be responsible for the nascence of lesions at these sites. This mechanism of occurrence may be independent of that which results in thyroid neoplasms.

Mesothelial cells are especially plastic and immortalize spontaneously with ease [20]. This factor has made mesothelial cells an attractive model for *in vitro* studies in the study of asbestos carcinogenicity, for which mesothelium is the target tissue (Mossman *et al*., 1994). It has been proposed that there may be a missing tumor suppressor function in these cell populations, leading to a self-perpetuating autocrine growth factor loop under certain circumstances. Additionally, mesothelial cells (at least *in vitro*) do not contain as much endogenous reduced or total glutathione reserves as do non-target cells (e.g. HepG2 (Crosby, 1998)). Since glutathione plays an important role in oxidative stress (and potassium bromate) toxicity (Sai *et al*., 1991; Sai *et al*., 1992) (notwithstanding it is as yet unclear what that role may be), this may mean that mesothelial cells are intrinsically less capable of dealing with the insult of oxidative stress from potassium bromate. Alternatively, a combination of anatomic uniqueness and mesothelial cell population sensitivity may account for the appearance of these tumors in significant numbers at this location. The carcinogen ***o***-nitrotoluene bears an interesting similarity to that of potassium bromate (Dunnick *et al*., 1994). During 13 weeks of treatment (oral), male rats developed mesotheliomas of the tunica vaginalis and mesothelial cell hyperplasia, and kidney toxicity including hyaline droplet nephropathy and increased α_{2U}-globulin concentration was observed. Furthermore, spleens of male and female rats showed increased hematopoiesis, hemosiderin deposition and/or congestion. The study of ***o***-

nitrotoluene, or that of any of the ≈100 other agents that induce mesothelioma, may provide clues as to the confluence of events precipitating the development of neoplasms at this location. The role of oxidative stress in the generation of mesotheliomas needs to be addressed through further study of one or more of these carcinogenic compounds. Studies of these lesions should be directed toward their tissue of origin, despite its complex and difficult nature. We strongly advocate the inclusion of whole tissue cross-sectioning techniques during necropsy where possible, in order to avoid the inadvertent destruction of essential information.[1]

REFERENCES

Ahotupa, M. and Huhtaniemi, I. (1992). Impaired Detoxification of Reactive Oxygen and Consequent Oxidative Stress in Experimentally Cryptorchid Rat Testis. *Biol. of Reprod.* **46,** 1114-1118.

Ballmaier, D. and Epe, B. (1995). Oxidative DNA damage induced by potassium bromate under cell-free conditions and in mammalian cells. *Carcinogenesis* **16,** 335-342.

Crosby, L. M. (1998). Unpublished Observations.

[1] This work was supported by the US Dept. of Education, Graduate Assistance in Areas of National Need Fellowship Program, North Carolina State University/US EPA Cooperative Training Grant Program CT-826512, and GlaxoWellcome, Inc. The views expressed in this manuscript do not necessarily represent official US EPA policy.

DeAngelo, A., George, M., Kilburn, S., Moore, T. and Wolf, D. (1998). Carcinogenicity of Potassium Bromate Administered in the Drinking Water to Male B6C3F1 Mice and F344/N Rats. *Toxicol. Pathol.* **26,** 724-729.

Dunnick, J., Elwell, M. and Bucher, J. (1994). Comparative Toxicities of o-, m-, and p-Nitrotoluene in 13-Week Feed Studies in F344 Rats and B6C3F1 Mice. *Fund. and Appl. Tox.* **22,** 411-421.

Fisher, N., Hutchinson, J., Hardy, J., Ginocchio, A. and Waite, V. (1979). Long-term toxicity and carcinogenicity studies of the bread improver potassium bromate. 1. Studies in rats. *Food Cosmet. Toxicol.* **17,** 33-39.

Ginocchio, A., Waite, V., Hardy, J., Fisher, N., Hutchinson, J. and Berry, R. (1979). Long-term toxicity and carcinogenicity studies of the bread improver potassium bromate. 2. Studies in mice. *Food Cosmet. Toxicol.* **17,** 41-47.

Gould, D. H. (1977). Mesotheliomas of the Tunica Vaginalis Propria and Peritoneum in Fischer Rats. *Vet. Path.* **14,** 372-379.

Hijnen, W., Voogt, R., Veenendaal, H., Jagt, H. and Kooij, D. (1995). Bromate Reduction by Denitrifying Bacteria. *Appl. & Env. Micro.* **61,** 239-244.

IARC. (1986). Some Naturally Occurring and Synthetic Food Components, Furocoumarins and Ultraviolet Radiation. *IARC Monographs on the Evaluation of the Carcinogenic Risk of Chemicals to Humans* **40,** 207-220.

Ilgren, E. G. (1993). Mesotheliomas of Animals; A Comprehensive, Tabular Compendium of the World's Literature, pp. 356. Oxford: CRC Press.

Kurokawa, Y., Maekawa, A., Takahashi, M. and Hayashi, Y. (1990). Toxicity and Carcinogenicity of Potassium Bromate - A New Renal Carcinogen. *Env. Hlth. Persp.* **87,** 309-335.

Maekawa, A., Ogiu, T., Matsuoka, C., Onodera, H., Furuta, K., Kurokawa, Y., Takahashi, M., Kokubo, T., Tanigawa, H., Hayashi, Y., Nakadate, M. and Tanimura, A. (1984). Carcinogenicity of low doses of N-ethyl-N-nitrosourea in F344 rats: A dose-response study. *GAANN* **75,** 117-125.

Mossman, B. T., Quinlan, T. and Spivack, S. (1994). Regulation of Antioxidant Enzymes in Lung after Oxidant Injury. *Env. Hlth. Persp.* **102,** 79-87.

Nickel, R., Schummer, A., Seiferle, E. and Sack, W. O. (1973). The Viscera of the Domestic Mammals, pp. 392. New York: Springer-Verlag.

Sai, K., Takagi, A., Umemura, T., Hasegawa, R. and Kurokawa, Y. (1991). Relation of 8-Hydroxydeoxyguanosine Formation in Rat Kidney to Lipid Peroxidation, Glutathione Level and Relative Organ Weight after a Single Administration of Potassium Bromate. *Jpn. J. Cancer Res.* **82,** 165-169.

Sai, K., Tyson, C. A., Thomas, D. W., Dabbs, J. E., Hasegawa, R. and Kurokawa, Y. (1994). Oxidative DNA damage induced by potassium bromate in isolated rat renal proximal tubules and renal nuclei. *Cancer Lett.* **87,** 1-7.

Sai, K., Uchiyama, S., Ohno, Y., Hasegawa, R. and Kurokawa, Y. (1992). Generation of active oxygen species in vitro by the interaction of potassium bromate with rat kidney cell. *Carcinogenesis* **13,** 333-339.

Tanigawa, H., Onodera, H. and Maekawa, A. (1987). Spontaneous Mesotheliomas in Fischer rats - A Histological and Electron Microscopic Study. *Toxicol. Pathol.* **15,** 157-163.

Umemura, T., Sai, K., Takagi, A., Hasegawa, R. and Kurokawa, Y. (1995). A possible role for oxidative stress in potassium bromate (KBrO3) carcinogenesis. *Carcinogenesis* **16,** 593-597.

USEPA. (1998a). Draft Water Quality Criteria Methodology Revisions: Human Health; Notice. *Federal Register* **63,** 43755-43828.

USEPA. (1998b). National Primary Drinking Water Regulations: Disinfectants and Disinfection Byproducts Notice of Data Availability: Proposed Rule. *Federal Register 40 CFR Parts 141-142* **63,** 15673-15692.

WHO. (1964). Seventh Report on the Specifications for the Identity and Purity of Food Additives and Their Toxicological Evaluation: Emulsifiers, Stabilizers, Bleaching and Maturing Agents. *World Health Organization Technical Report* **Series 281,** 164.

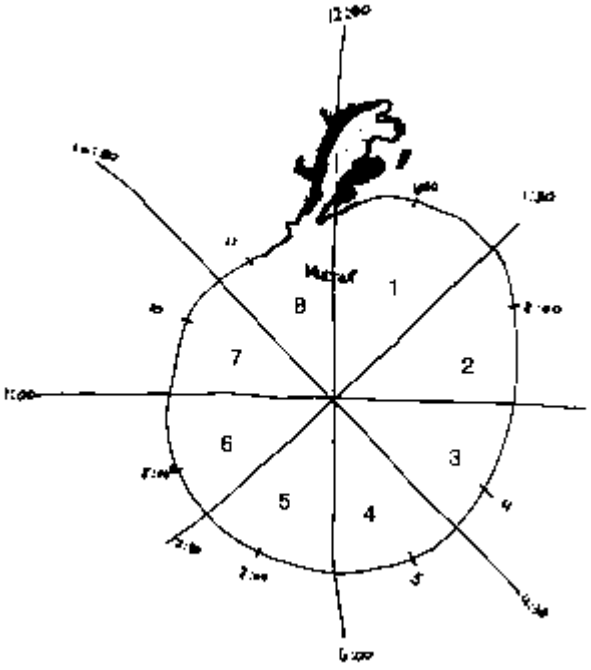

Fig. 1. Representation of the tunica vaginalis testis used to map tumors

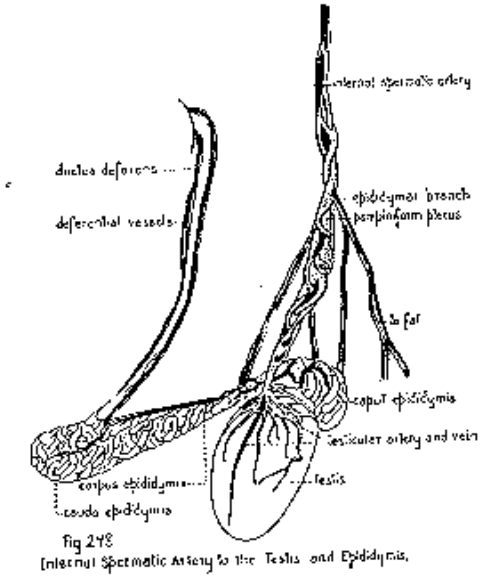

Fig. 2. Testicular Blood Supply. Adapted from “Anatomy of the Rat”, E.C. Greene. Hafner Publ., N.Y. (1963).

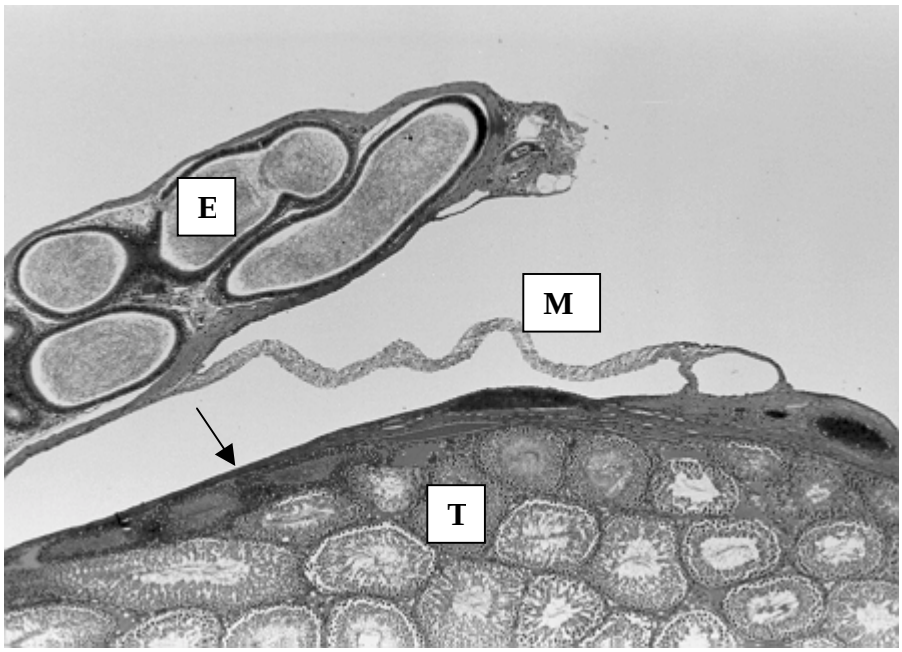

Fig.3. Healthy mesorchial ligament (M) attaching testis (T) to epididymis (E) and tunica vaginalis visceralis (arrow) (H&E, 10x)(Week 13).

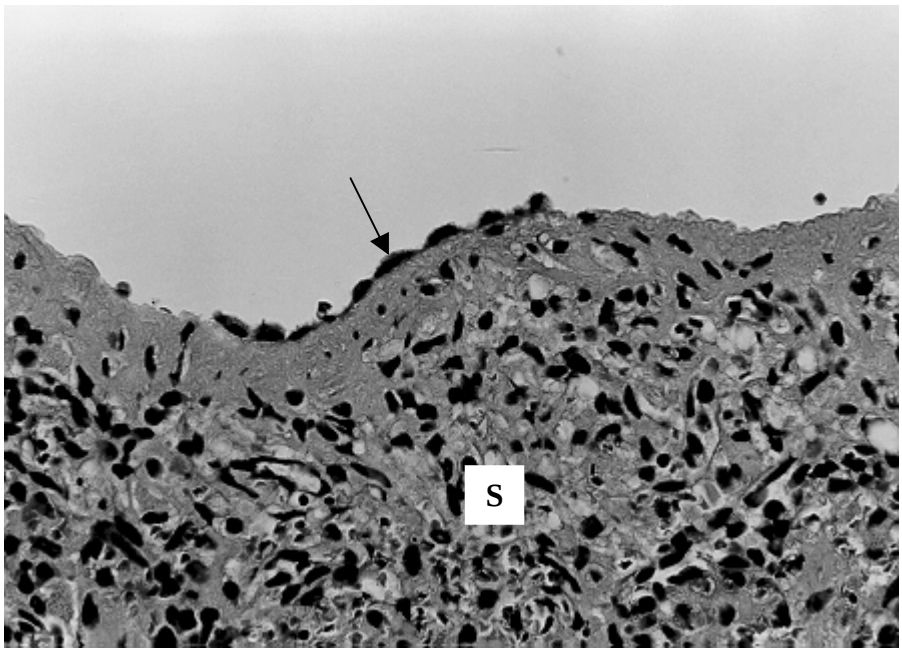

Fig. 4. Reactive mesothelial cells (arrow), part of the mesothelial covering on the spleen (S) (H&E, 200x) (Week 100).

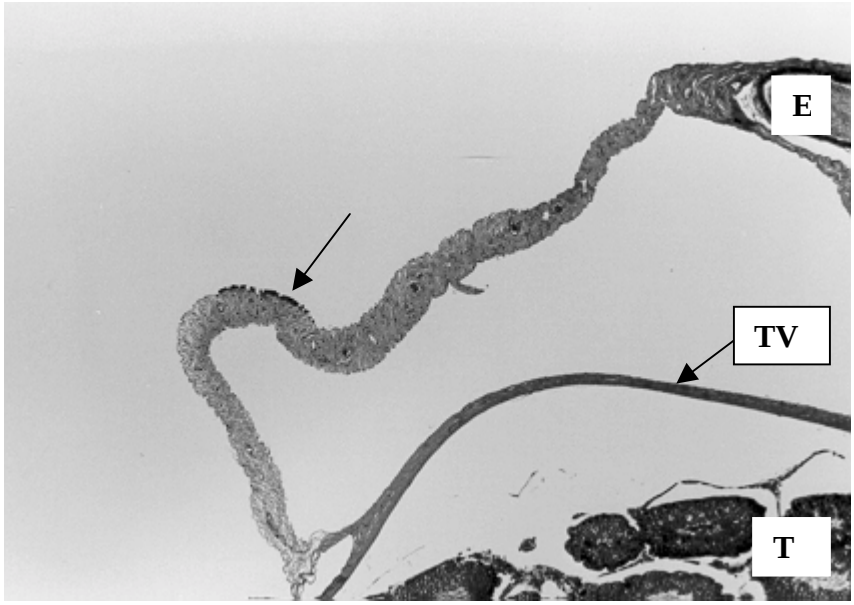

Fig. 5. Pre-neoplastic lesion (arrow) on the mesosplenium (H&E, 20x) (Week 52). Epididymis (E), Testis (T), Tunica Vaginalis (TV).

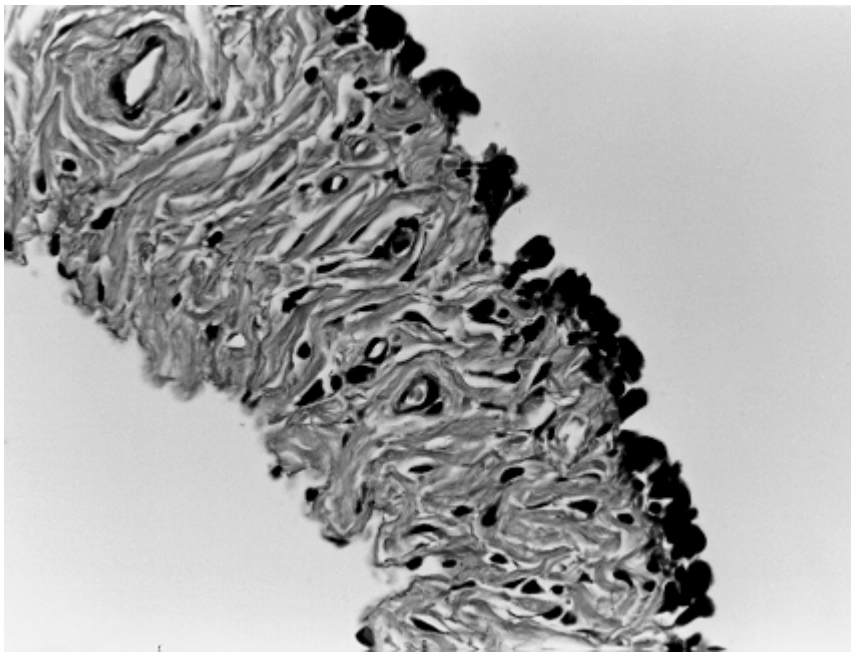

Fig. 5a. Higher magnification of Fig. 5 (400x) showing pre-neoplastic lesion.

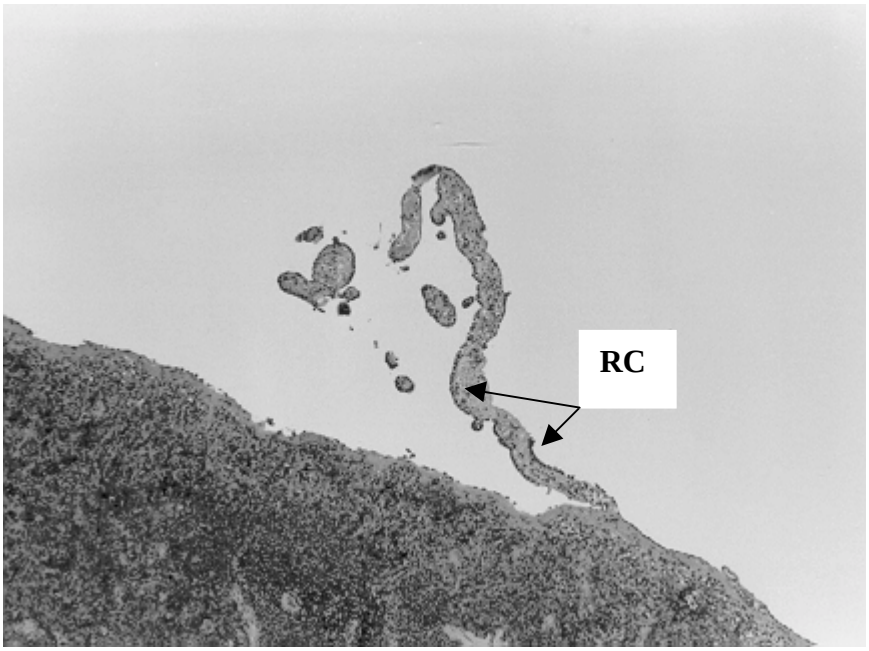

Fig. 6. Reactive mesothelial cells (RC) covering the mesosplenium (H&E, 37x) (Week 100).

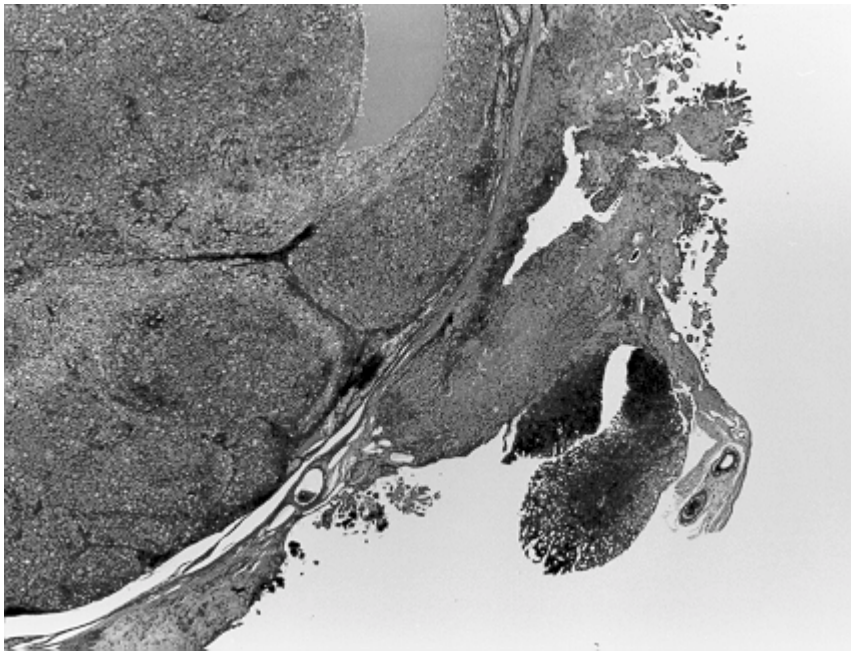

Fig. 7. Late stage malignant mesothelioma (H&E, 10x) (Week 96).

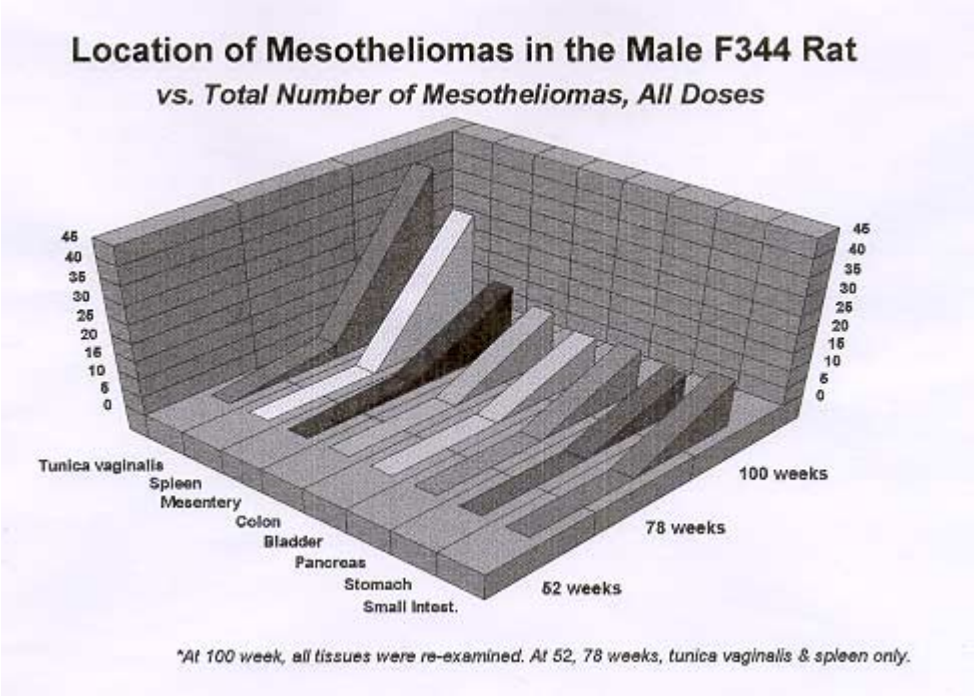

Fig. 8. Location of Mesotheliomas in the Male F344 Rat vs. Total Number of Mesotheliomas, All Doses.

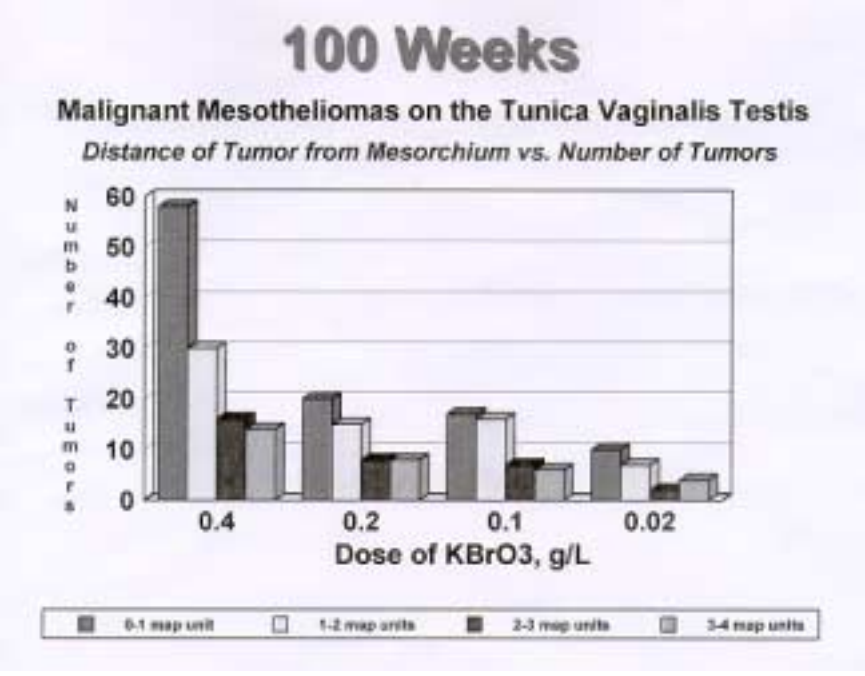

Fig. 9. Malignant Mesotheliomas on the Tunica Vaginalis Testis: Distance of Tumor from Mesorchium vs. Number of Tumors (100 weeks).

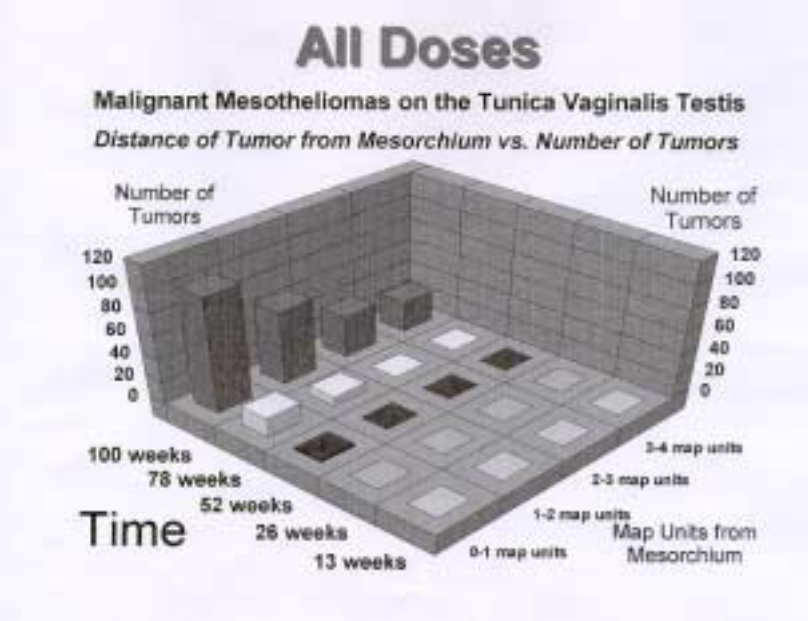

Fig. 10. Malignant Mesotheliomas on the Tunica Vaginalis Testis: Distance of Tumor from Mesorchium vs. Number of Tumors (All Doses).

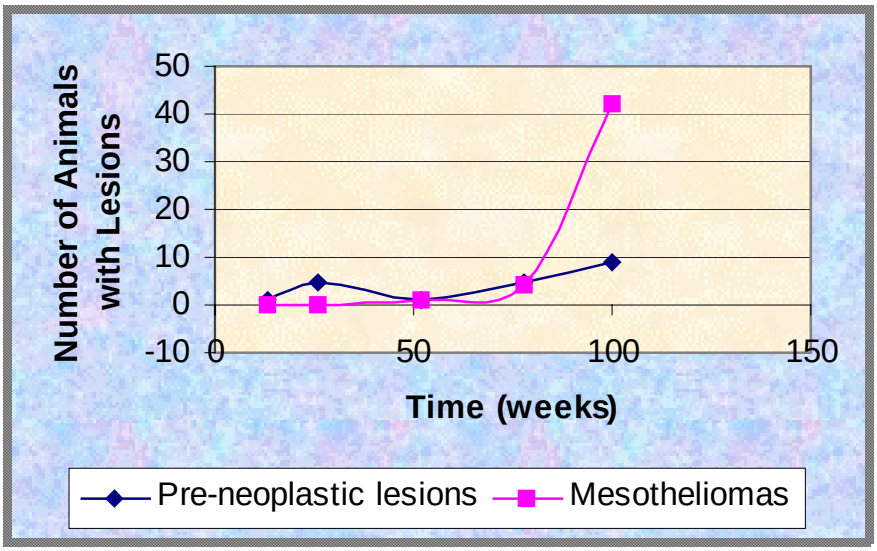

Fig. 11. Incidence of Pre-Neoplastic and Neoplastic Lesions formed on Mesorchium vs. Time.

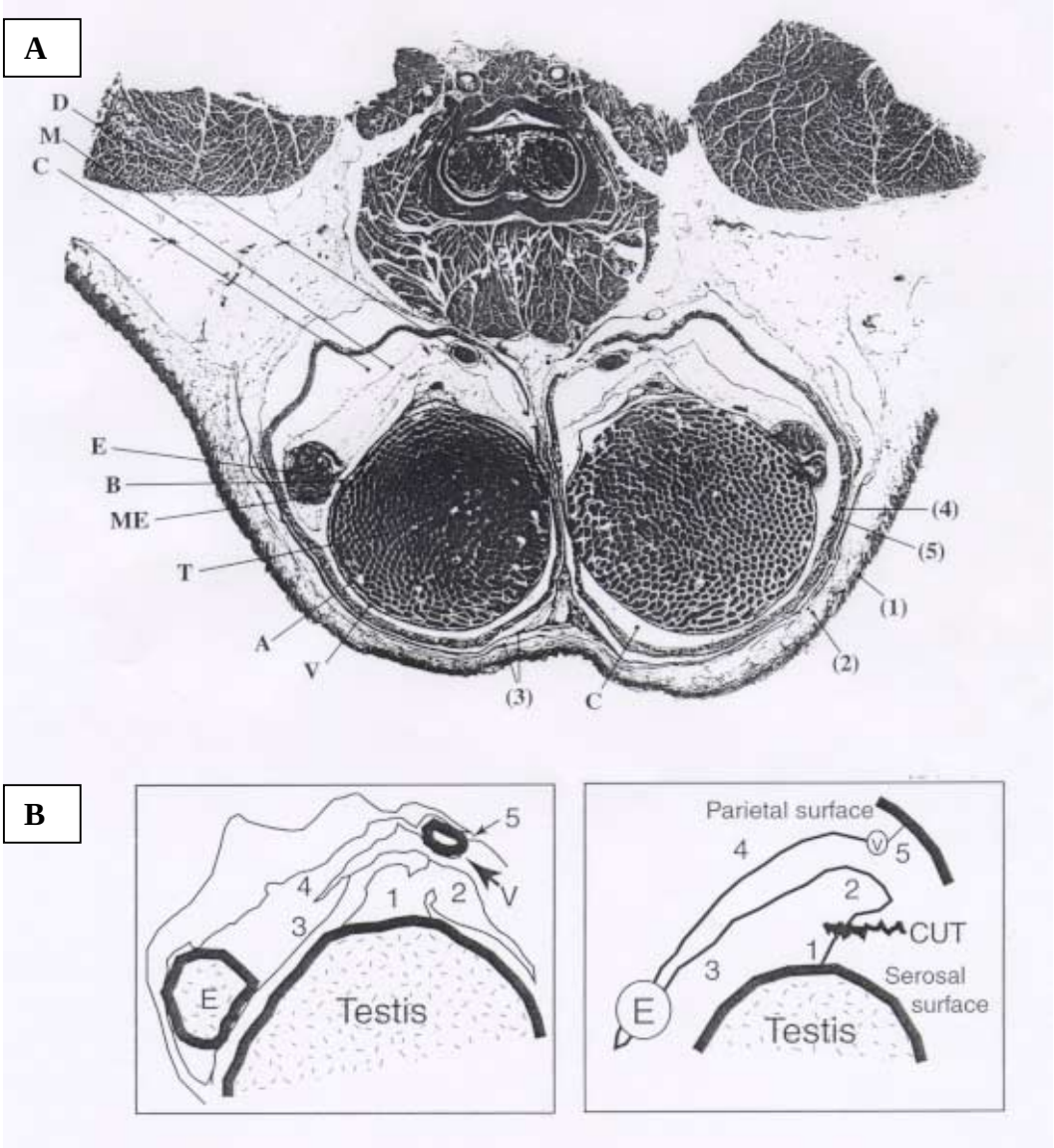

Fig. 12A. Rat scrotum cross section (H&E, 1x). (1) skin and tunica dartos, (2) external spermatic fascia, (3) cremaster muscle and cremasteric fascia, (4) internal spermatic fascia, (5) tunica vaginalis parietalis. T= testis, A= tunica albuginea, V= tunica vaginalis visceralis, B= testicular bursa, E= epididymis, D= ductus deferens, C= cavum vaginale, M = mesorchium, ME= mesepididymis.

Fig. 12B. Drawing (left) and simplified diagrammatic representation (right) of a portion of Fig. 12A showing detailed structure of the mesothelial covered suspensory apparatus of the vas deferens, epididymis and testis, including (1) the testicular attachment, (2) fat-laden medial fold, (3) ventral and (4) dorsal portions of the lateral fold, and (5) the parietal attachment to the scrotal wall. The epididymis (E) and vas deferens (V) lie within this delicate suspensory apparatus between the testicular and scrotal attachments. Much of this potential target tissue is lost from close to the testicular attachment (CUT) during routine toxicology studies.

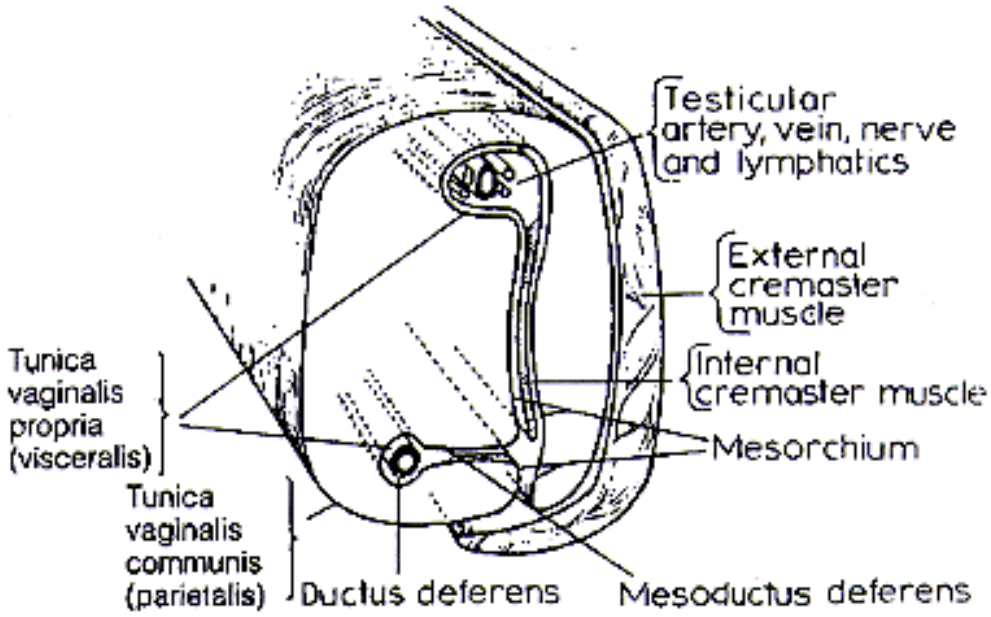

Fig. 13. Spermatic cord. Reprinted from Frandson RD, Spurgeon TL. Anatomy and physiology of farm animals. 5th Ed. Philadelphia: Lea & Febiger, 1992.

Table 1

Incidence of Pre-neoplastic & Neoplastic Lesions vs. Time

		Mesorchium						Mesosplenium					
	Exp. Conc.	***Week***											
	(g/L)	13	26	52	78	96	FD	13	26	52	78	96	FD
Reactive mesothelium							/MS						/MS
	0	0	0	0	0	0	0	0	4	0	1	3	1
	0.4	0	2	0	0	0	7	0	5	1	1	0	2
	0.2	0	1	0	2	2	3	0	5	3	3	0	2
	0.1	0	0	0	1	0	8	0	5	1	1	2	4
	0	0	1	0	0	1	0	4	6	3	1	1	0
Pre-neoplasm													
	0	0	0	0	0	2	0	1	2	0	1	4	3
	0.4	1	0	1	1	0	5	2	2	1	1	1	3
	0.2	0	0	0	1	2	0	1	1	0	1	3	1
	0.1	0	1	0	0	0	4	3	3	3	1	4	1
	0	0	0	0	0	2	2	2	2	0	1	8	1
Mesothelioma													
	0	0	0	0	0	1*	0	0	0	0	1*	1*	0
	0.4	0	0	0	4	20	8	0	0	0	3	15	3
	0.2	0	0	1	0	9	2	0	1	0	0	5	4
	0.1	0	0	0	0	5	3	1	0	1	0	6	0
	0	0	0	0	0	7	1	0	0	0	0	6	2

*Differs from previously reported [4] data.

FD/MS= found dead/moribund sacrifice

Table 2.

Number of Mesotheliomas on Mesorchium and Mesosplenium vs. Dose

Mesorchium	Mesosplenium	Dose Administered (g/L)
1	2	0
8	8	0.02
8	8	0.1
12	10	0.2
32	21	0.4

r^2= 0.98 for relatedness between columns 1 & 2.

Chapter 3. Studies of Mesothelial and HepG2 Cells Demonstrate That GSH Depletion Plays a Key Role in $KBrO_3$ Toxicity

Authors and Affiliations:

Lynn M. Crosby[1], Kevin T. Morgan[2], A.B. DeAngelo[3]

[1]US EPA Trainee in Environmental Carcinogenesis and North Carolina State University Department of Toxicology, Research Triangle Park, North Carolina 27711

[2]GlaxoWellcome Inc., 5 Moore Drive, Research Triangle Park, NC 27709

[3]US EPA, TW Alexander Drive, Research Triangle Park, NC 27711

ABSTRACT

We examined the role of GSH in $KBrO_3$–induced toxicity (protective or potentiating). Derived rat mesothelial cell lines (peritoneal, pleural) were compared to other rat and human mesothelial and hepatocellular carcinoma cell lines for species/target tissue comparison. $KBrO_3$ toxicity was quantified and the ED_{50} determined. GSH content in the cell lines was approximately 8 nmol/10^6 cells (HepG2) and from 0.4 to 2.0 nmol/10^6 in mesothelial cells. $KBrO_3$-treated (5 mM) mesothelial cells were 41% GSH depleted (15 min), 93% (4 h), 58% (12 h), 80% (24 h), 100% (48 h). Treatment with buthionine sulfoximine, $KBrO_3$, or diethylmaleate depleted GSH (visualized by the GSH-specific stain mercury orange). In untreated mesothelial cells, bright peri-spindle staining infers a protective role for GSH during replication. Cells were treated with buthionine sulfoximine, diethylmaleate and $KBrO_3$ to determine whether pre-treatment with N-acetylcysteine or glutathione-o-ethyl ester could protect, and whether combinations of the former three chemicals would shift the $KBrO_3$ toxicity curve. Glutathione-o-ethyl ester protected all mesothelial cell lines, N-acetylcysteine protected 1 of 2, but neither protected HepG2. GSH depletors plus $KBrO_3$ exacerbated toxicity. Br^- ion selective electrode studies were performed characterizing the reaction between GSH and $KBrO_3$ in H_2O, cell culture media, sonicated cells or cellular supernatant. A two-step reaction was observed in an aqueous medium (pH 2.7, 37 °C), while at buffered pH, a one-step reaction occurred, implying the two-step reaction is not extracellular and not necessarily enzymatic. GSH protects mesothelial cells *in vitro*, target tissue susceptibility playing a major role in $KBrO_3$-mediated toxicity.

INTRODUCTION

Glutathione (GSH, L-γ-glutamyl-L-cysteinylglycine) has been studied extensively for over one hundred years, and yet new information can be found regarding this ubiquitous tripeptide in the literature on an almost daily basis. For extensive reviews on the subject, the reader is referred to the excellent work of Mary E. Anderson and Alton Meister (Anderson, 1998)' (Meister and Anderson, 1983) and others referenced therein. In addition, several enlightening texts exist (Arias and Jakoby, 1976; Flohe *et al*., 1973; Sies and Ketterer, 1988; Taniguchi *et al*., 1989). It is usually possible to discover, by perusal of the literature, further data concerning the function and importance of glutathione. Therefore, scanning of both "classic" references and new ones is encouraged, for the edification of the interested scientist.

GSH has been implicated in protein and DNA synthesis, amino acid transport, enzyme activity, intermediary metabolism and protection of cells (Anderson, 1998; Arias and Jakoby, 1976). To the toxicologist, GSH is best known as the prime mover in the formation of mercapturic acids using the enzymes glutathione S-transferase, γ-glutamyl transpeptidase, dipeptidase, and N-acetyl transferase, accomplishing the detoxication of a wide range of xenobiotics (as well as, occasionally, activation of same) (Meister and Anderson, 1983). To those studying the phenomenon of oxidative stress in the eukaryotic cell, GSH is known for its general properties as an antioxidant (Gutteridge and Halliwell, 1994). GSH plays the role of reducing agent in the presence of free radicals, lipid/organic peroxides and other reactive oxygen species, in close alliance with its associated peroxidase and reductase, and other major electron-carriers such as α-tocopherol, citrate and urate (Gutteridge and Halliwell, 1994). According to H.F. Gilbert, GSH is "the intracellular thiol/disulfide redox buffer of highest concentration" (Taniguchi *et al*., 1989). Not to be ignored are the important functions of amino acid biosynthesis

and degradation, DNA synthesis, γ-glutamyl amino acid transport, and co-factor role for other enzymes (glyoxalase, DDT dehydrochlorinase,etc.) (Meister and Anderson, 1983).

$KBrO_3$ is a byproduct of drinking water disinfection and is formed in greater amounts where water is brackish and/or contains higher amounts of bromine (von Gunten and Holgne, 1994). Either chlorination or ozonation will form bromate compounds, but ozonation has been found to cause increased formation over other methods of disinfection. $KBrO_3$ has other uses, both in food and non-food items (IARC, 1986). As a food additive, however, it is not viewed as a danger to consumers since in baking all bromate is converted to bromide, which has been demonstrated to be non-toxic (Gould, 1977; WHO, 1993).

The major focus of public concern with regard to this chemical is its potential carcinogenicity in humans via chronic ingestion of drinking water. Therefore, for obvious reasons, animal models have been utilized to study this possibility (DeAngelo *et al*., 1998; Hiasa *et al*., 1991; Kurokawa *et al*., 1983a; Kurokawa *et al*., 1990; Kurokawa *et al*., 1986b; Lee *et al*., 1996; McLaren *et al*., 1994; Sai *et al*., 1992a).

The estimated excess lifetime cancer risk for $KBrO_3$ in humans is 1 in 10^{-5} for a dose of three μg/L based upon a linearized multistage model which assumes a drinking water consumption of two L/day (70 kg adult) (WHO, 1993). Bromide (Br^-) concentrations in untreated drinking waters range from micrograms to several milligrams per liter. It is presently held that waters with levels of bromide >200 μg/L (>1.2 μM) require treatment to reduce bromate (BrO_3^-) levels in finished drinking waters (von Gunten and Holgne, 1992) . A regulatory guideline of 25 μg/L has been recommended by the World Health Organization (WHO) (WHO, 1993), based upon technically feasible removal and detection. However, it is not

clear whether the risk to humans is equivalent to that which has been predicted by the use of animal models.

$KBrO_3$ is known to act as a direct carcinogen in the male F344 rat, causing tumor formation in the kidney (renal cell), thyroid (follicular cell), and tunica vaginalis testis (mesothelial cell) (DeAngelo *et al*., 1998; Kurokawa *et al*., 1990). From the latter site, the neoplasm spreads to the peritoneal mesothelium via "seeding"(Gould, 1977).

Curiously, mesotheliomas in female rats have not been observed (Hayashi *et al*., 1986; Kurokawa, 1985; Kurokawa *et al*., 1985; Kurokawa *et al*., 1986a; Kurokawa *et al*., 1982; Kurokawa *et al*., 1983a; Kurokawa *et al*., 1990; Kurokawa *et al*., 1983b; Kurokawa *et al*., 1986b; Ohno *et al*., 1982; Onodera *et al*., 1985), nor is there evidence that mice or other species are susceptible. Thus, further studies paying close attention to the possible mechanism(s) of toxicity in the rat versus human are warranted. Collection of cross-species data is of heightened importance since the USEPA has recently encouraged the use of mechanistic data in risk assessments for human health (USEPA, 1998). Plainly, determination of the mechanism(s) of action of $KBrO_3$ would allow the formulation of realistic water treatment regulatory requirements, with increased confidence of adequate human health protection.

$KBrO_3$ is a known oxidizing agent. Since it has been shown that the biological reducing capacity of tissues is diminished during exposure to oxidative stress (Kohen *et al*., 1992), one possible mechanism leading to toxicity may be the depletion of cellular reserves of reduced GSH, a major source of reducing power within the cell. GSH has previously been demonstrated to be an important factor in $KBrO_3$ toxicity in the rat kidney (Kurokawa *et al*., 1990; Sai *et al*., 1991; Sai *et al*., 1992b). Reports have identified the role of GSH in the induction of DNA damage as one of activation *in vitro* or under cell free conditions (Ballmaier and Epe, 1995) and

protection *in vivo* (Sai *et al*., 1991; Sai *et al*., 1992b). This issue was considered to deserve further examination. Additionally, limited data exist as to the effects of GSH upon mesothelial cells and concerning the amount of endogenous GSH found in mesothelial cells either *in vitro* or *in vivo* (Breborowicz, 1996; Breborowicz *et al*., 1996; Kinnula *et al*., 1998; Ogretman *et al*., 1998). Therefore, we have studied the effects of *in vitro* $KBrO_3$ administration in association with GSH augmentation (as GSH-o-ethyl ester or its precursor, N-acetyl cysteine, NAC) or depletion via diethylmaleate (DEM) or buthionine sulfoximine (BSO).

Kurokawa (Kurokawa *et al*., 1990) measured the stoichiometric degradation of BrO_3^- to Br^- for a range of GSH concentrations however experimental conditions such as buffering solution, temperature, and time were not given. This reaction was "cell free". We determined whether the same reaction could be observed in the presence of intact or sonicated cells, and whether the kinetics of said reaction might be the same/similar or entirely different from the kinetics of the "cell free" chemical reaction. Kurokawa also measured $KBrO_3$ in rat tissue homogenates and found that after three min, substantial degradation occurred in liver, kidney, spleen, stomach, small intestine, red blood cells, and gastric juice (*vide supra*). We wished to determine the kinetics of these reactions in mesothelial cells, and to better characterize the reaction(s) between $KBrO_3$ and GSH.

MATERIALS AND METHODS

Derivation & Characterization of Cell Lines. The following cell lines were used:

Cell Line	Tissue of Origin	Source
NRM-LC	rat pleural mesothelial	derived in-house
Fred-Pe	rat peritoneal mesothelial	" "
Hep-G2	human hepatocellular carcinoma	ATCC, Rockville, MD
MeT-5A	human pleural mesothelioma	" "
NRM-2	rat pleural mesothelial	P. Ferriola, CIIT, RTP, NC
II-14	rat peritoneal mesothelioma	" "

Cell lines derived in-house were collected from three month-old male F344 rats asphyxiated with carbon dioxide (CO_2) gas and exsanguinated. A small incision was made in the peritoneal wall and approximately ten mL of a solution of Type IV collagenase (10 ug/mL) was injected. After 30 min incubation on a warming pad kept at 37 °C, the solution was withdrawn and placed in a sterile petri dish containing DMEM/Ham's F12 + 10% FCS + HITS. (HITS = 0.1 μg/mL hydrocortisone, 1.0 μg/mL insulin, 2.5 μg/mL transferrin and 2.5 ng/mL selenium). Five mL of penicillin/streptomycin were added per liter media, and the cells were incubated under standard cell culture conditions (5-7% CO_2, 37 °C). Cells were passaged after growth breakthrough occurred, as evidenced by burgeoning colony formation without contact inhibition, phase-contrast microscope luminosity of cell borders indicating lack of desmosome formation and disappearance of cells displaying differentiated characteristics of mesothelial cells. Differentiated mesothelial cells are comparatively large, polyhedral to round with fine lines visible in the cytoplasm (possible cytoskeletal fibers), a prominent nucleus with several darkly staining nucleoli, ruffled cell margins, and sometimes needle-like projections reaching to other cells. They are largely contact inhibited.

Characterization of cells as mesothelial *per se* was accomplished by standard peroxidase anti-peroxidase immunohistochemical staining using primary antibodies to pan-cytokeratin and vimentin, and secondary biotinylated anti-mouse IgG, followed by horseradish peroxidase and streptavidin, and detection using the ABC Kit (Vector Labs). Cells staining positively for both pan-cytokeratin and vimentin are considered to be mesothelial in origin (Mossman, 1998). MeT-5A cells were used as positive control cells, and negative control slides were prepared by substituting antibody diluent (PBS containing 0.1% Brij™) without primary antibody, in the primary antibody incubation step.

All mesothelial-type cell lines were grown in DMEM/F12 + 10% FCS + HITS (*vide supra*), while the HepG2 cell line was grown in DMEM + 10% FCS, under standard cell culture conditions, without antibiotics after the first passage.

$KBrO_3$ Exposure Concentration-Response Time Course.

To establish the range of toxicity of $KBrO_3$ in the cell lines of interest, the following experiment was performed. Six freshly (≤ one week) subcultured cell types (HepG2, MeT-5A, NRM-2, NRM-LC, Fred-Pe and II-14) were plated in a 96-well format at a density of 20,000 cells per well (2×10^5 cells/mL, 100 μL/well) and grown overnight. Cells were then treated with $KBrO_3$ (0, 0.05, 0.1, 0.25, 0.5, 1, 2, 3, 4, 5, 7.5 and 10 mM) for 0, 4, 8, 12, 24 and 48 h. Cell viability was assayed by the MTS assay (Promega CellTiter 96 Aqueous One Solution™), which measures the reductive capacity of the cells, largely as a function of cellular NADPH/NADH content (Ferrari *et al*., 1990; Gergel *et al*., 1995; Hussain *et al*., 1993; Jiao *et al*., 1992; Jost *et al*., 1992; Marshall *et al*., 1995; Shi *et al*., 1993; van de Loosdrecht *et al*., 1991; Wong and Goeddel, 1994). Twenty μL of MTS reagent were added to each well of a 96-well plate, and the plate was incubated for 1 h at 37 °C and the spectrophotometric absorbance read at 490 nm. Results were graphed as percent reducing capacity vs. exposure concentration for 4, 8, 12 and 24 h. Results presented are representative of at least two experiments.

The MTS assay was compared to cell counts and morphology, and LDH (lactate dehydrogenase) release in HepG2 cells after treatment with $KBrO_3$, in order to assess the utility of the MTS assay as an endpoint of cellular viability for $KBrO_3$ (Marshall *et al*., 1995).

Determination of Endogenous Glutathione Levels.

In order to investigate the interaction between GSH and $KBrO_3$, it was necessary to establish the baseline amount of GSH found in the cell types under study. The amounts of total

and oxidized GSH in HepG2, MeT-5A, II-14, NRM-LC, Fred-Pe and NRM-2 cell lines was determined using the Cayman Chemical Co. Glutathione Assay Kit™ (a spectrophotometric method employing Ellman's Reagent). Reduced GSH was determined by difference between total GSH and oxidized GSH measurements. Cell pellets of from 1 x 10^6 to 1 x 10^8 cells were trypsinized using 0.25% Trypsin-EDTA. Cell pellets were collected in sterile PBS (pH 7.4) centrifuged at 175 g for three min at 4 °C and the trypsin-containing PBS was removed by aspiration. Thereafter, cells were kept on ice. After resuspension in 10 mL of fresh PBS, representative samples were counted. Samples were then re-centrifuged and the total volume of each sample reduced to 0.5-1.0 mL. Metaphosphoric acid (MPA, 10% aq. w/v) was added (1:1 v/v) and samples were sonicated for 30 s (0.5 s pulses) using a Virsonic™ cell sonicator (setting three), then frozen at ⁻80 °C until assayed. After thawing, cell lysates were centrifuged at 16,000 g for five min at room temperature and the supernatant removed for assay. Cell supernatants were then assayed according to the manufacturer's protocol in a 96-well plate format, and absorbance was read at 405 nm. For range-finding, four dilutions were performed for each cell type, in duplicate, with a total of 16 measurements per cell type. Later experiments were performed with 3x or 4x dilutions of cellular lysates, (for HepG2: 10x, 100x, and 500x). Duplicate standard curves were run for each plate assayed. The amount of GSH determined was normalized as nmol/10^6 cells.

Glutathione Determination in $KBrO_3$-Treated Cells.

To determine the effects of $KBrO_3$ on the GSH content of mesothelial cells, NRM-2 cells were treated with 0 or 5 mM $KBrO_3$ for 5, 10, 15, 30 min, two, three, four, five, six, eight, 12, 18, 24, or 48 h and the amount of GSH present assayed by the Cayman Scientific Inc. Glutathione Assay Kit™. Briefly, T225 flasks were seeded with 5.45 x 10^5 cells/flask, grown to

confluence (36 h), treated with $KBrO_3$ and harvested after the above-specified times by trypsinization (0.25% trypsin, five min). The determination of GSH was carried out as above.

GSH AUGMENTATION

GSH Protection Assay.

To determine whether GSH could protect cells from $KBrO_3$-induced toxicity, cell populations were pre-treated with GSHoET and then exposed to $KBrO_3$ and the resulting toxicity quantitated. Recently subcultured cells were plated at 2 x 10^5 cells/mL and grown overnight before treatment. The following represents the treatment regimen:

HepG2		0-100 mM		Remove	⇒	0/5 mM $KBrO_3$,6 h	
Fred-Pe	⇒	GSHoET	⇒	GSHoET			⇒ MTS Assay
NRM-LC		(30 min)		(aspirate)	⇒	0/7.5 mM $KBrO_3$, 24 h	
Met-5A							

Cell lines were assayed in a 96-well plate format using the above-mentioned assay for cellular reducing capacity.

In order to confirm the effectiveness of the reducing capacity assay for $KBrO_3$ –mediated toxicity, the protective effects of GSHoET pre-treatment were also measured by quantitation of live cells/mm^2. Cells were grown in chamber wells (Nalge-Nunc™ four-well chamber well slides, 1 mL media/well). In this assay, cells were pre-treated for 30 min with 0, 10 or 20 mM GSHoET, followed by 0 or 5 mM $KBrO_3$ exposure for 24 h, and afterwards fixed in 100% ice-cold ethanol and stained routinely with H&E.

NAC Protection Assay.

HepG2, II-14, and NRM-2 cells were plated on chamber wells and grown overnight before treatment. Cells were treated for 30 min with 0, 0.03, 0.3, or 3 N NAC, (a GSH precursor) in serum free medium (SFM). Since one molecule of $KBrO_3$ will oxidize six molecules of NAC, the exposure concentration was calculated as normality (all other

experimental exposure concentrations were calculated as molar equivalents, but the strength difference was taken into account when setting same). Cells were then rinsed with PBS and then treated with 0, 0.03, 0.3 or 3 N $KBrO_3$ in SFM for 15 min and allowed to recover for 24 or 36 h. Cells on slides were then fixed in absolute ethanol at ¯20 °C for 24 h, stained (H&E) by standard histologic methods, and counted (duplicate experiments) under 20x magnification using a light microscope.

GSH DEPLETION

GSH Localization by Mercury Orange Staining.

$KBrO_3$, DEM-Treated Cells. An experiment was performed to compare and contrast the effects of treatment with $KBrO_3$, DEM, or both on cellular morphology and the localization of GSH. The method of Keller(Keller *et al*., 1990) was used; it is essentially specific for GSH staining with mercury orange (HgO) incubation times < five min. Fred-Pe/NRM-2 cells were grown overnight in chamber wells (seeded at $2x10^5$ cells/mL) and treated with 3.0 (Fred-Pe) or 2.5 (NRM-2) mM $KBrO_3$, 1 mM DEM or both simultaneously, for 24 h. Media was removed and slides were then immersed in 50 μM HgO in 9:1 acetone:water for 30 s, rinsed in 9:1 acetone:water, air-dried and cover slipped. Fluorescence microscopy was used to visualize the staining, with excitation wavelengths of 450-490 nm and emission wavelengths >515 nm. Images were captured in Adobe Photoshop™. Results presented are from duplicate experiments.

BSO Depletion of GSH. To visualize the diminution of GSH with increasing [BSO], an experiment was performed using concentrations of 0 - 10.0 mM BSO for 24 or 48 h to treat NRM-2 cells grown in chamber wells. Cells were plated at a density of 2×10^5 cells/mL and grown overnight before treatment. At the end of 24 or 48 h, cells were immediately stained with HgO as above and cover-slipped. Fluorescence images were captured as above.

EXACERBATION OF $KBrO_3$ TOXICITY BY GSH DEPLETORS

Treatment of Cells with DEM, BSO or DEM+BSO. Duplicate experiments were performed in order to determine whether addition of BSO, DEM or both along with $KBrO_3$ to cells would increase/decrease the toxic effects on cellular reducing capacity, as follows:

NRM-2 cells	2.5 mM $KBrO_3$ 250 μM DEM 10 mM BSO 2.5 mM $KBrO_3$ + 10 mM BSO 2.5 mM $KBrO_3$ + 250 μM DEM 2.5 mM $KBrO_3$ + 10 mM BSO + 250 μM DEM 250 μM DEM + 10 mM BSO No Treatment (change to fresh media)	⇒	24/48 h	⇒ Remove (aspirate), MTS Assay

The experiment addressed the question of whether, under conditions of GSH depletion, $KBrO_3$-mediated toxicity would increase or decrease. If toxicity were to increase under dual/triple treatments, it would imply that the presence of GSH was protective.

MEASUREMENT OF THE REACTION BETWEEN $KBrO_3$ AND GSH

Characterization of Chemical Reaction of $KBrO_3$ & GSH.

A reaction was carried out by adding 0.05 M GSH to 0.05 M $KBrO_3$ in ultrapure water or in cell culture media (both HepG2 and MeT-5A media were tested). Readings were taken on the pre-calibrated (using 0.1 to 1000 ppm NaBr) ion-selective electrode (ISE) from 10 s to 70 min at room temperature and 37 °C. Reactions measured in media were carried out in a cell culture incubator without stirring, at 37 °C in an atmosphere of 5% CO_2.

Characterization of the Reaction of 50 μM $KBrO_3$ & Cellular GSH in the Presence of Cellular Lysates of Intact Cells.

HepG2 and MeT-5A cells (two T225 flasks per cell type) were grown until confluent and one flask was trypsinized. The second flask was not trypsinized; Br^- formation was measured in

the supernatant of intact cells (see (b) below). Cells from the trypsinized flask were collected in sterile PBS, pH 7.4 and pelleted by centrifugation at 175 g for 5 min in a Dupont/Sorvall GLC2B centrifuge. Trypsin-containing supernatant was removed by aspiration and replaced with fresh PBS. A drop-size aliquot was counted and the remaining pellet was centrifuged again (as above), then resuspended in 1 mL of sterile PBS, pH 7.4. Each pellet was sonicated for 30 s using a Virsonic cell sonicator (0.5-s pulses at setting three) while kept on ice.

a) The sonicated pellet was added to 50 mL of the appropriate cell culture media, and treated as follows:

1. 50 μM $KBrO_3$ in 50 mL of appropriate media + 1 mL VWR Ionic Strength Adjuster (ISA) was equilibrated in the incubator.
2. The previously calibrated (using 0.1 to 1000 ppm NaBr) bromide ISE and pH probe (using pH buffers 4.0 and 7.0) and temperature probe ('ATC probe') were placed into the $KBrO_3$ solution (to obtain background Br^-) and allowed to equilibrate in the incubator (5% CO_2 and 37 °C).
3. The initial concentration of bromide, temperature and pH were measured after the $KBrO_3$ was equilibrated.
4. Reaction timing was not initiated until the ATC probe reading was at least 36.2 °C. The cell sonicate was added at once and timing of the reaction was begun.
5. The ISE reading was taken at 10 s, 30 s, one min, and at one-min intervals thereafter up to 30 min, and then at 35, 40, 45, 50, 60, 70 min, (or until seven consecutive readings were essentially identical).

b) The second T225 flask of cells was treated as follows:

1. The flask was equilibrated in the incubator and 1 mL of ISA added, and the three probes were placed into the flask inside the incubator.
2. The temperature, pH and Br^- content were allowed to reach equilibrium and measured. Reaction timing was not begun until temperature was at least 36.2 °C.
3. A solution of 50 μM $KBrO_3$ in 40 mL media with 2% ISA (v/v) was equilibrated at the same time in the incubator (for a total reaction volume of 102 mL).
4. The $KBrO_3$ solution was added and reaction timing begun. Measurements were taken as in a) (duplicate experiments).

Statistical methods.

For the comparison between cell lines to determine whether HepG2 cells contain a significantly different amount of GSH than mesothelial cell lines, an F-test of the ratio of σ^2 from means of the two sample populations and σ^2 from individuals in the entire population was performed (Steel and Torrie, 1980), where the square root of F has Student's *t* distribution. The standard deviation appropriate to a difference between two random means from a normal population was calculated. For all other statistical comparisons, a two-tailed Student's *t* Test was performed (Steel and Torrie, 1980). Results at significance levels lower than 95% ($p < 0.05$) were not reported.

RESULTS

Characterization of Cell Lines

Both the NRM-LC (rat pleural) and Fred-Pe (rat peritoneal) cell lines proved to be of mesothelial cell lineage as evidenced by morphological characteristics and positive

immunostaining for both vimentin and pan-cytokeratin (data not shown). The NRM-2 cell line stained positively for vimentin and pan-cytokeratin, as has previously been shown (Crosby *et al*., 1997) and was used as a positive control for staining of Fred-Pe and NRM-LC mesothelial cell lines developed in-house. II-14, MeT-5A and HepG2 cell lines were previously authenticated cell lines obtained from outside sources.

$KBrO_3$ Dose-Response Time Course

Toxic responses to treatment were indicated by diminution of reducing capacity in the MTS assay, compared to untreated time-matched controls, and/or cellular degeneration and loss by light microscopy. In MeT-5A cells at four h, from 2.5 to 10 mM $KBrO_3$ produced gradually increasing levels of toxicity (data not shown). For all six cell lines tested, the threshold of severest toxicity was approximately five mM by 24 h, while in control wells reductive capacity increased (as expected, due to cellular proliferation) over time. In the two rat peritoneal mesothelial cell lines, (II-14 and Fred-Pe), (Fig. 1) percent toxicity (as decreased cellular reducing capacity) was similar. At 7.5 and 10 mM, $KBrO_3$ gave evidence of toxicity at four h; by 24 h the limit of severe toxicity was lowered to five mM. NRM-2 and NRM-LC (data not shown) differed somewhat, with NRM-LC exhibiting the first signs of severe toxicity at four h (10 mM) and NRM-2 at 12 h (10 mM). NRM-2 cells showed a transient increase in reducing power at the 2.5 mM treatment level at 12 h, which may represent a compensatory effect for GSH depletion. NRM-2 cells were less susceptible to $KBrO_3$ toxicity than NRM-LC. HepG2 cells differed from mesothelial cell lines, exhibiting higher initial reducing capacity than all cell lines except II-14 and more resistance to KBrO3 toxicity than II-14 at 5 mM (12 and 24 h) and than II-14 and Fred-Pe at 5, 7.5 and 10 mM (12 h). Significance testing revealed that HepG2 cells differed from II-14

and Fred-Pe at exposure concentrations of 5 mM or greater for all non-zero exposure periods ($p<0.05$ except HepG2 vs. Fred-Pe at 5 mM, 12 h, where $p<0.062$).

Comparison of MTS, cell counts, cell morphology and LDH release revealed the following:

1. Cell counts: MTS results and cell counts compared over a period of five days in control and one to three N $KBrO_3$-treated HepG2 cells did not differ significantly within the first 24 h after treatment, but diverged rapidly thereafter (data not shown). Correlation coefficients calculated between the results of the two methods varied from 0.68 to 0.99 (average 0.85) for eight determinations, when all five days data were taken into account.
2. LDH release: LDH release from HepG2 cells treated with 2.5 mM $KBrO_3$ for three, six, nine or 12 h was not significantly different from controls (data not shown). At 24 h, release was significantly higher, or about twice that of controls.
3. Morphology: HepG2 cells treated with 2.5 mM $KBrO_3$ for 24 h displayed the following characteristics (0 = no effect, 10 = severe effect);

loss of	- normally large cytoplasmic vacuoles	10
	- mitotic figures	10
	- cell-cell contact	4
retraction of cellular processes/cytoplasmic shrinkage		2
decrease in cell number (sample count)		2
increased nuclear/cytoplasmic ratio		2

Determination of Endogenous GSH Levels

The amount of GSH in cell lines (nmol/10^6 cells) is shown in Table 1. The total amount of GSH in HepG2 cells is four to 20 times higher than that of the mesothelial cell lines tested (confirmed by HPLC, data not shown). HepG2 cells contain the most, and II-14 the least GSH. Statistical comparisons between the [GSH] of individual mesothelial cell lines and HepG2 cells revealed significant differences ($p<0.0001$ or lower).

Determination of GSH Levels in $KBrO_3$-Treated Cells

NRM-2 cells treated with five mM $KBrO_3$ for up to 48 h were 41% depleted of GSH after 15 min ($p < 0.01$) (Fig. 2, Table 2). The concentration of GSH continued to drop until four h, when it was 93% depleted. Beginning at five h, a steady increase in GSH occurred, up to 12 h (58% depleted). At 18 h, GSH began to drop off again, and at 48 h GSH was not detected. At all time points after 5 min, differences between treated and control samples were highly significant ($p < 0.001$).

GSH AUGMENTATION

Glutathione Protection Assay

Using the MTS reducing capacity assay, 30 min pre-treatment with GSHoET was protective at 24 h to all mesothelial cell types (Table 3), but to HepG2 only slightly. Stimulatory effects upon the cellular reducing capacity were observed in cells treated with GSHoET alone for 30 min in every cell type tested; these effects could be observed either at six or 24 h, depending on experimental conditions. Protective effects were observed in NRM-LC, II-14 and NRM-2 at 24 h with little or no accompanying stimulatory effect in time-matched controls treated with GSHoET alone. For the II-14 cell line, the protective effect declined between six and 24 h. In Fred-Pe cells, the protective effect observed after six h of treatment was not apparent at 24 h. In the case of HepG2 cells, a stimulatory surge in reducing power occurred at six h, and disappeared by 24 h.

Using the number of live cells remaining on chamber well slides as an indication of GSHoET pre-treatment protection, NRM-LC cells showed a clear protective effect, Fred-Pe cells and MeT-5A showed a significant, but less marked effect, and HepG2 cells displayed no

protective effect, when these cell types were given 10 or 20 mM GSHoET 30 minutes prior to 5 mM $KBrO_3$ exposure for 24 h (Fig. 3).

From these results, a sensitivity advantage is inferred from the use of the reducing capacity assay over the live cell counting method.

NAC Protection Assay

In HepG2 cells (Table 4), NAC pre-treatment for 30 min followed by 24 h recovery afforded slight protection from $KBrO_3$-induced toxicity at a concentration of three normal (0.5 M), as measured by cells remaining attached per field. In NRM-2 cells, no protective effect was observed at these time/exposure concentrations. For II-14 cells a marked protective effect was observed at 0.3 and three normal; no cells remained on the slide at three N $KBrO_3$ without NAC pre-treatment. These results agree with those observed when GSHoET was added as a pre-treatment, noted above.

GSH DEPLETION

GSH Localization by HgO Staining

Untreated cells. HgO staining for identification of GSH in tissues (Keller *et al*., 1990) revealed a characteristic pattern of GSH localization in untreated Fred-Pe cells (Fig. 4) in the cytoplasm and especially in a crescent-shaped region adjacent to the nucleus, possibly the golgi apparatus. Less GSH staining appears in the nucleus than the cytoplasm. Extremely strong GSH staining surrounding the aggregated chromosomes was apparent in cells undergoing mitosis (Fig. 4).

$KBrO_3$, BSO, DEM-Treated Cells. In Fred-Pe cells treated with 3mM KBrO3 for 24 h (data not shown), the nucleus appeared to have a greater GSH concentration, but the whole cell stains strongly. Cells appeared shrunken and drawn away from one another and cellular processes also stained positively for GSH. Compared to control, NRM-2 cells treated with $KBrO_3$ show partial

depletion of GSH (Fig. 5A & B). BSO-treated NRM-2 cells (Fig. 5C) were not as severely depleted as those treated with $KBrO_3$. In DEM-treated cells (Fig. 5D), GSH depletion is evident, as well as large vacuoles of unknown composition. In cells treated with both DEM and $KBrO_3$, (data not shown) all cells were apparently dead and stained only faintly, being mostly shrunken.

$KBrO_3$ Toxicity Curve Shift Experiment

Treatment of Cells with DEM, BSO or DEM+BSO. Exposure of cells to $KBrO_3$, DEM and BSO produced significant toxicity at 24 h in MeT-5A, HepG2, and NRM-2 cells (Table 5.) In combination, DEM and $KBrO_3$ or BSO and $KBrO_3$ produced more severe toxicity than either substance alone. The toxicity of $KBrO_3$ was exacerbated under conditions in which GSH was depleted or partially depleted in these cell types.

MEASUREMENT OF THE REACTION BETWEEN $KBRO_3$ AND GSH

Characterization of Chemical Reaction of $KBrO_3$ & GSH

During the reaction in water (Fig. 6A and B), a large drop in pH occurred (from 6.5 to 2.7) upon the addition of 0.05 M GSH to the 0.05 M $KBrO_3$-containing beaker, and thereafter remained relatively constant. Br^- was 23-40 ppm in the $KBrO_3$-containing beaker before the start of the reaction. Immediately upon mixing, the evolution of Br^- commenced (Fig. 6A-D). Under the conditions studied, where the reaction was carried out at room temperature (Fig. 6B) (but temperature was not controlled), 600 ppm Br^- was evolved within 17 min. Heat was also produced; from an initial condition of 23 °C, temperature rose to 27.5 °C over the 70-min period of monitoring (using manual mixing). Br^- production reached a peak at 17 min, and declined thereafter until 25 min, when it again began to climb. Br^- concentration rose to 1050 ppm by 70 min (Fig.6B). Step One of the reaction that was carried out at 37 °C (Fig. 6A) was more rapid, evolving the first Br^- peak by three min post-mixing. Approximately 1500 ppm Br^- was

generated during Step One. During Step Two of the reaction, approximately 1700 ppm Br^- was generated, with a peak at 30, and another peak by 70 min. The shape of the reaction curve was the same at both temperatures, and the reaction obeyed Arrhenius temperature dependency (Gillespie *et al*., 1986). The first minimum of [Br^-] occurred at 3 min at 37 °C (Fig. 6A) and 25 min at room temperature (Fig. 6B).

Characterization of the Reaction of 50 μM $KBrO_3$ & Cellular GSH in the Presence of Cell Lysates or Intact Cells

In mesothelial or HepG2 cell culture media (Fig.6C), the reaction pH was buffered around 7.4, and therefore the pH change was small, or from 8.0 to 7.6 upon the mixing of reagents. Temperature and CO_2 concentration were also held constant in the incubator where the reaction was carried out. *In situ* heat production could not be measured accurately under these conditions. The background level of Br^- in cell culture media or in the supernatant of cells in flasks was 23-60 ppm prior to the start of the reaction. The production of Br^- occurred in every reaction carried out, in cell culture media (Fig. 6C), in cellular sonicates (data not shown, but similar to Fig. 6D), and in the supernatant in contact with intact, live cells (Fig. 6D). The maximum [Br^-] concentration was reached in ten s [Br^-] then declined gradually over 70 min. The second maximum of [Br^-] production was not observed. In all buffered reactions, the shape of the reaction curve was an initial sharp peak of Br^- production followed by a slow decline. The reaction of $KBrO_3$ with intact HepG2 cells produced 25-30 ppm Br^- while that with MeT-5A produced 14-17 ppm. The sonicated cell reactions produced only 2 to 5 ppm in the two cell types assayed.

DISCUSSION

In previous work (Crosby *et al*., 2000) the location of mesotheliomas in the male F344 rat was studied at selected times during a two-year cancer bioassay. The results of that study led to the conclusion that the lesions probably originated between the testicular mesorchium and the splenic mesosplenium, in a mesothelial milieu. Yet, it was not known whether the cells where these lesions developed were especially predisposed to become mesotheliomas, or might be optimally located to receive the highest local dose of $KBrO_3$. The development of immortalized rat peritoneal (Fred-Pe) and pleural mesothelial (NRM-LC) cell lines enabled comparison between target and non-target mesothelial regions in the F344 male rat, and between rat and human pleural mesothelial cells.

The toxicity threshold of $KBrO_3$ for all cell lines was comparable at 24 h, (about 5 mM). For all sources and sites, GSH content of mesothelial lines more closely resembled one another than the GSH content of HepG2 cells. For rat peritoneal vs. pleural mesothelial cells, pre-treatment of cells with NAC was protective only for peritoneal mesothelial cells. Protection of mesothelial cells by GSHoET varied by cell type and time of treatment, but all five mesothelial cell lines displayed significant protection from toxicity at one or more times/exposure concentrations, the reducing capacity assay being the more sensitive of the two assays employed. In the toxicity curve shift experiment, human and rat mesothelial cells responded similarly to one another.

Notably, important differences have been uncovered between the behavior and interaction of the non-target HepG2 cell line and the five target mesothelial cell lines studied with respect to GSH. The threshold of toxicity for HepG2 cells was higher than that for any of the five mesothelial cell lines tested. The mesothelial cell lines were a tumor cell line, an SV40-

transformed cell line, and three spontaneously immortalized cell lines, thus the presence or absence of tumorigenicity or method of immortalization does not appear to be important to the threshold of $KBrO_3$ toxicity these cell populations. Although differences between the mesothelial cell lines were apparent, all behaved similarly with respect to $KBrO_3$ toxicity.

Importantly, the GSH content in untreated mesothelial cell lines is significantly lower than that of HepG2 cells in culture. HepG2 cells were found to contain 8.3 ± 1.3 nmol/10^6 cells, comparing reasonably well with the experience of others (Griffin, 1998) of 40 to 60 nmol/mg (4 to 6 nmol/10^6 cells). Primary hepatocytes have been shown to contain 23 nmol/10^6 cells (Palmeira *et al*., 1994), and as much as 60 nmol/10^6 cells in replete cells (Lu, 1999). The amount of GSH may vary considerably, as GSH turnover in normal hepatocytes is 12 nmol/10^6 cells/hr (Lu, 1999). MeT-5A cells have been shown to contain 23.5 nmol/mg (Kinnula *et al*., 1998), which would be equivalent to 2.35 nmol/10^6 cells if it is assumed that 1 g contains approximately 10^8 cells, as is true for hepatocytes. Our value of 1.03 nmol/10^6 cells compares well in consideration of probable high GSH turnover rates and the unavailability of fresh GSH sources in cells in culture between feedings. The next highest GSH-containing cell line (Fred-Pe) has approximately 24% of the content of HepG2 populations. The II-14 cell line, with 0.4 nmol/1x10^6 cells, contains the least, or about 1/20^{th} that of HepG2. This difference may represent an artifact of cell culture, i.e. not be observed *in vivo* because of intra-organ transport of GSH and uptake by cells that contain γ-glutamyl transpeptidase on the external membrane surface (Taniguchi *et al*., 1989).

The differences in GSH content of HepG2 and mesothelial cells may help explain the divergent responses of the two cell types to $KBrO_3$ toxicity. The addition of GSH in a cell that normally contains high concentrations of GSH will result in harmful reductive stress (Sies and

Ketterer, 1988). Kinnula (Kinnula *et al*., 1998) and Breborowicz (Breborowicz, 1996) have demonstrated increased resistance in cells containing higher amounts of GSH to free radical injury and epirubicin toxicity. The effects of GSH depletion are increased radiosensitivity, thermosensitivity, oxidative stress sensitivity and sensitivity to the effects of certain drugs, decreased synthesis of leukotrienes, certain prostaglandins, decreased lymphocyte response to mitogens and increased response to teratogens (Taniguchi *et al*., 1989).

All five mesothelial cell lines pre-treated with GSHoET for 30 min and then $KBrO_3$ for six or 24 h exhibited increased reducing capacity compared to HepG2 cells treated in the same manner, at one or both time points in the reducing capacity assay. In the "live cell count" assay, three mesothelial cell lines tested all displayed significant differences between GSHoET-pretreated, and non-pretreated wells exposed to $KBrO_3$, indicative of protection, while no differences were apparent for HepG2. One (II-14) of 2 mesothelial cell lines pre-treated with NAC for 15 min, and then allowed to recover for 36 h, was protected compared to HepG2 cells, similarly treated. Thus, cells containing less GSH experience a lower threshold of $KBrO_3$ toxicity and can be partially protected from this toxicity by augmentation of intracellular stores of GSH. In the $KBrO_3$ toxicity curve shift experiment, both mesothelial and HepG2 cells experienced an exacerbation of the toxic effect when given DEM or BSO in addition to $KBrO_3$. Since DEM depletes GSH in a GST-catalyzed reaction, and BSO prevents the synthesis of GSH by inhibiting generation of the γ-glutamylcysteine intermediate by γ-glutamyl cysteine synthetase (GCS), it is expected another GSH depletor will potentiate the effects of BSO or DEM. In this experiment $KBrO_3$ toxicity was substantially increased in the presence of DEM or BSO. Of note, for HepG2 cells effects were less severe in the dual treatment samples than in the mesothelial cells, with respect to controls. This may be due to the higher basal level of GSH found in HepG2

cells. It was previously posited that $KBrO_3$ treatment of cells results in the evolution of reactive species (Ballmaier and Epe, 1995). We have here demonstrated that the reaction of GSH with $KBrO_3$ results in cellular protection rather than increased toxicity. Therefore, reactive species, if formed upon $KBrO_3$ treatment, most likely proceed from a state of GSH depletion.

$KBrO_3$ behaved as an efficient and complete depletor of reduced GSH. By 15 min exposure time, NRM-2 cells experienced 41% depletion in GSH versus controls, and at four h, a minimum was reached. Thereafter, the amount of GSH began to climb until 12 h. An effort to regain control over GSH homeostasis may have been mounted. The level of GSH did not return to the level of control, recovering only to the 58% depletion level, and at 48 h levels were undetectably low. Throughout the course of the exposure, GSSG remains essentially unchanged, however, extracellular GSH was not measured. It must be noted that GSSG levels have traditionally been difficult to quantitate due to technical considerations, and possibly to rapid export into the extracellular media. Others (Kurokawa *et al*., 1987; Tanaka *et al*., 1984) have reported that $KBrO_3$ oxidizes GSH to GSSG *in vitro* and *in vivo* in the rat.

These interactions between GSH and $KBrO_3$ led to curiosity regarding the true nature of the reaction between these two molecules. Is this a purely chemical reaction, or are enzymes involved? What are the kinetics of this reaction over time? Kurokawa, et al. (Kurokawa *et al*., 1990) demonstrated that when varying amounts of GSH were reacted with $KBrO_3$, Br^- was evolved in stoichiometric amounts. Our results indicate that the reaction between these moieties is at least two-step in nature. In a water-based reaction with uncontrolled pH at room temperature or 37 °C, step one of the reaction evolved substantial Br^- within 17 or three min (respectively), fell thereafter, (minimum at 25 or five min) then climbed again. At the end of monitoring (60 min), [Br^-] had climbed higher than its step one maximum and was still rising slowly. We

interpret this sequence of events to represent a two-step or two-stage reaction, the first step of which evolved Br^- (Fig. 7, step 4 and dashed box), the second of which both consumed and produced Br^- (not depicted in Fig. 7). In buffered (pH 7.4) media, cellular sonicates, or in the supernatant of intact, live cells (as measured at 5% CO_2, 37 °C), the second stage of the reaction was not observed (Fig. 6A and B). Instead, after the initial evolution of Br^- resulting from the combination of GSH and $KBrO_3$ (as represented by Fig. 7 step 4 and dashed box) the [Br^-] began dropping and reached a steady state concentration by approximately 20 min. If the start of reaction two is hypothesized to begin with the consumption of Br^- (Fig. 7, step 5), then it is possible that in buffered media, Br^- instead reacts with another molecule ('X') and is unavailable to participate in reaction two. Br^- would then not be present as such, and would not be measurable by this method. After the model of P. Vani (Vani *et al.*, 1995), where cysteine was reacted with $KBrO_3$ in acidic medium, the reaction might be as follows:

$$H_2Br_2O_3 + 4Br^- + 4H^+ \xrightarrow[\text{several fast steps}]{} 3Br_2 + 3H_2O \qquad (1)$$

$$3\{\ R\text{-}S\text{-}H + Br_2 + H_2O \xrightarrow{\text{fast}} R\text{-}S(=O)_2 + 2Br^- + 2H^+\ \} \qquad (2)$$

where R = $-CH_2-CH(NH-CO-CH_2-CH_2-CH(NH_3^+)-COO^-)-CO-NH-CH_2-COO^-$

(The rest of the GSH molecule).

The final product of equation (2) (see above) is a sulfone or a sulfoxide. Br^- would be released concomitantly. The reader is referred to Wefers and Sies (Wefers and Sies, 1983; Wefers and Sies, 1986a; Wefers and Sies, 1986b) for a discussion of possible mechanisms to account for the production of GSO_2/GSO_3^- and singlet molecular oxygen in the oxidation of GSH by superoxide generating enzyme systems (e.g., peroxysulphenyl radicals) with GSH. It is assumed that this

reaction could occur in an aqueous milieu of suitably low pH, because in our (aqueous milieu) experiment, pH was monitored and found to drop to 2.7 after the addition of GSH. In the presence of lactoperoxidase/myeloperoxidase, a further reaction could occur, producing HBrO, such as occurs in polymorphonuclear leukocytes (PMN's) during the "oxidative burst". Mesothelial cells are phagocytic *in vitro* (Boorman *et al*., 1990) and may share these properties with PMN's.

A simple disproportionation of $KBrO_3$ does not occur in water: the molecule is stable for at least one year as iodometrically titrable $KBrO_3$ (Crosby, 1998; Kurokawa *et al*., 1990). Therefore, the appearance of Br^- in this experiment represents a reaction between two molecules. The cellular concentration of GSH was seen to be depleted by approximately one-half between ten and 15 min after exposure to $KBrO_3$ *in vitro*, and this fits well with the reaction kinetics showing that the reaction producing, and then consuming [Br^-] has reached steady-state in 20 min or less. Since we were able to protect cells from $KBrO_3$-mediated toxicity by 30 min pre-treatment with the membrane-permeable molecule GSHoET, and to deplete total endogenous GSH after $KBrO_3$ treatment, we conclude that GSH and $KBrO_3$ present inside the cell react together under the conditions described in these experiments.

Regarding the enzymatic or chemical nature of this reaction, it is of note that the same reactions that take place between GSH and xenobiotics chemically can occur through the catalysis of GST's (Sies and Ketterer, 1988) with rates increased by10^4 to10^6-fold. The results presented here provide a crude estimate of reaction kinetics, and are not suitable for a thorough analysis, but indicate that in media where GST's may be present, reaction time to first maximum is lowered (from one to three min to five to ten s), or between six- and 18-fold (Fig. 6A vs. C).

The localization of GSH in a juxtanuclear region which may be the golgi apparatus or the endoplasmic reticulum, and the markedly increased GSH content in cells undergoing mitosis are consistent with the observations of others (Li and Oberley, 1998). A protective role for GSH can be inferred from the HgO staining results, where it appears to aggregate around the nuclear material during mitosis, when the chromosomes are most vulnerable to oxidative damage. Similarly, GSH in the golgi may function to protect nascent lipids or proteins against oxidation.

In summary, it is demonstrated here that GSH plays an important, and cell type specific protective role against $KBrO_3$-mediated toxicity *in vitro*, and the toxic effects of this chemical upon the cell occur in association with GSH depletion.

ACKNOWLEDGMENTS

Support for this work was provided by a US EPA/North Carolina State University Co-operative Agreement Traineeship and by GlaxoWellcome, Inc. The authors wish to thank Roger Brown, Bill Benson, Gary Hatch, Nik Liv and Tracy Brainerd for their assistance. The views expressed herein do not represent US EPA policy.

REFERENCES

Anderson, M. E. (1998). Glutathione: an overview of biosynthesis and modulation. *Chemico-Biological Interactions* **111-112,** 1-14.

Arias, I. M. and Jakoby, W. B. (1976). Glutathione: Metabolism and Function. In *Kroc Foundation Series*, vol. 6. New York: Raven Press.

Ballmaier, D. and Epe, B. (1995). Oxidative DNA damage induced by potassium bromate under cell-free conditions and in mammalian cells. *Carcinogenesis* **16,** 335-342.

Boorman, G. A., Eustis, S. L., Elwell, M. R. and Montgomery, C. A. (1990). Pathology of the Fischer Rat; Reference and Atlas. New York: Academic Press, Inc.

Breborowicz, A. (1996). L-2-Oxothiazolidine-4-carboxylate and N-acetylcysteine as precursors of intracellular glutathione in human peritoneal mesothelial cells. *Blood Purification* **14,** 1-7.

Breborowicz, A., Rodela, H., Martis, L. and Oreopoulos, D. G. (1996). Intracellular glutathione in human peritoneal mesothelial cells exposed in vitro to dialysis fluid. *International Journal of Artificial Organs* **19,** 268-75.

Crosby, L. M. (1998). Unpublished Observations.

Crosby, L. M., Everit, J. I. and Mangum, J. (1997). Transforming growth factor alpha expression in mineral fiber-induced malignant mesothelioma. *Proc. Amer. Assoc. Canc. Res.* **38**.

Crosby, L. M., Morgan, K. T., Gaskill, B., Wolf, D. C. and DeAngelo, A. B. (2000). Origin and Distribution of Potassium Bromate-Induced Testicular and Peritoneal Mesotheliomas. *Toxicol. Pathol.* **28**.

DeAngelo, A., George, M., Kilburn, S., Moore, T. and Wolf, D. (1998). Carcinogenicity of Potassium Bromate Administered in the Drinking Water to Male B6C3F1 Mice and F344/N Rats. *Toxicol. Pathol.* **26,** 724-729.

Ferrari, M., Fornasiero, M. C. and Isetta, A. M. (1990). MTT colorimetric assay for testing macrophage cytotoxic activity in vitro. *J. Immunol. Methods* **131,** 165-172.

Flohe, H., Benohr, H. C., Sies, H., Waller, H. D. and Wendel, A. (1973). Glutathione. In *Proceedings of the 16th Conference of the German Society of Biological Chemistry, Tubingen, March 1973*, pp. 302. Tubingen, Germany: Academic Press, Inc., New York, Georg Thieme Publishers Stuttgart.

Gergel, D., Misik, V., Ondrias, K. and Cederbaum, A. I. (1995). Increased Cytotoxicity of 3-Morpholinosydnonimine to HepG2 Cells in the Presence of Superoxide Dismutase. *J. Biol. Chem.* **270,** 20922-20929.

Gillespie, R. J., Humphreys, D. A., Baird, N. C. and Robinson, E. A. (1986). Chemistry. Boston: Allyn & Bacon, Inc.

Gould, D. H. (1977). Mesotheliomas of the Tunica Vaginalis Propria and Peritoneum in Fischer Rats. *Vet. Path.* **14,** 372-379.

Griffin, M. (1998). The Characterisation of the HepG2 Cell Line in different Culture Media. London: The School of Pharmacy, University of London.

Gutteridge, J. M. C. and Halliwell, B. (1994). Antioxidants in Nutrition, Health and Disease, pp. 143. Oxford: Oxford University Press.

Hayashi, Y., Kurokawa, Y., Maekawa, A. and Takahashi, M. (1986). Strategy of long-term animal testing for quantitative evaluation of chemical carcinogenicity. In *New Concepts*

and developments in Toxicology (ed. P. L. Chambers, Gehring, P. and Sakai, F.), pp. 383-391. New York: Elsevier Science Publishers.

Hiasa, Y., Konishi, N., Nakaoka, S., Nakamura, M., Nishii, S., Kitahori, Y. and Ohshima, M. (1991). Possible Application to Medium-term Organ Bioassays for Renal Carcinogenesis Modifiers in Rats Treated with N-Ethyl-N-hydroxyethylnitrosamine and Unilateral Nephrectomy. *Jpn. J. Cancer Res.* **82,** 1385-1390.

Hussain, R. F., Nouri, A. M. E. and Oliver, R. T. D. (1993). A new approach for measurement of cytotoxicity using colorimetric assay. *J. Immunol. Meth.* **160,** 89-96.

IARC. (1986). Some Naturally Occurring and Synthetic Food Components, Furocoumarins and Ultraviolet Radiation. *IARC Monographs on the Evaluation of the Carcinogenic Risk of Chemicals to Humans* **40,** 207-220.

Jiao, H., Y. Soejima, Ohe, Y. and Saijo, N. (1992). A new MTT assay for examining the cytotoxicity of activated macrophages towards the non-adherent P388 leukaemia cell line. *J. Immunol. Meth.* **153,** 265-266.

Jost, L. M., Kirkwood, J. M. and Whiteside, T. L. (1992). Improved short- and long-term XTT-based colorimetric cellular cytotoxicity assay for melanoma and other tumor cells. *J. Immunol. Meth.* **147,** 153-165.

Keller, D. A., D'A Heck, H., Randall, H. W. and Morgan, K. T. (1990). Histochemical Localization of Formaldehyde Dehydrogenase in the Rat. *Tox. & Appl. Pharm.* **106,** 311-326.

Kinnula, K., Linnainmaa, K., Raivio, K. O. and Kinnula, V. L. (1998). Endogenous antioxidant enzymes and glutathione S-transferase in protection of mesothelioma cells against hydrogen peroxide and epirubicin toxicity. *Br. J. Cancer* **77,** 1097-1102.

Kohen, R., Tirosh, O. and Gorodetsky, R. (1992). The Biological Reductive Capacity of Tissues is Decreased Following Exposure to Oxidative Stress: A Cyclic Voltammetry Study of Irradiated Rats. *Free Rad. Res. Comms.* **17,** 239-248.

Kurokawa, Y. (1985). Overview on the toxicity and carcinogenicity of potassium bromate (in Japanese). *Kosankinbyo Kenkyuzasshi* **37,** 139-149.

Kurokawa, Y., Aoki, K., Imazawa, T., Hayashi, Y., Matsushima, Y. and Takamura, N. (1985). Dose-related enhancing effect of potassium bromate on renal tumorigenesis in rats initiated with N-ethyl-N-hydroxyethylnitrosamine. *Jpn. J. cancer Res. (Gann)* **76,** 583-589.

Kurokawa, Y., Aoki, S., Matsushima, Y., Takamura, N., Imazawa, T. and Hayashi, Y. (1986a). Dose-response studies on the carcinogenicity of potassium bromate in F344 rats after long-term oral administration. *J. Natl. Cancer Inst.* **77,** 977-982.

Kurokawa, Y., Hayashi, Y., Maekawa, A., Takahashi, M. and Kokubo, T. (1982). Induction of renal cell tumors in F344 rats by oral administration of potassium bromate, a food additive. *Gann* **73,** 335-338.

Kurokawa, Y., Hayashi, Y., Maekawa, A., Takahashi, M., Kokubo, T. and Odashima, S. (1983a). Carcinogenicity of Potassium Bromate Administered Orally to F344 Rats. *J. Nat'l. Cancer Inst.* **71,** 965-971.

Kurokawa, Y., Maekawa, A., Takahashi, M. and Hayashi, Y. (1990). Toxicity and Carcinogenicity of Potassium Bromate - A New Renal Carcinogen. *Env. Hlth. Persp.* **87,** 309-335.

Kurokawa, Y., Takahashi, M., Kokubo, T., Ohno, Y. and Hayashi, Y. (1983b). Enhancement by potassium bromate of renal tumorigenesis initiated by n-ethyl-N-hydroxyethylnitrosamine in F-344 rats. *Gann* **74,** 607-610.

Kurokawa, Y., Takamura, N., Matsuoka, C., Imazawa, T., Matsushima, Y., Onodera, H. and Hayashi, Y. (1987). Comparative studies on lipid peroxidation in the kidney of rats, mice and hamsters and on the effect of cysteine, glutathione and diethyl maleate treatment on mortality and nephrotoxicity after administration of potassium bromate. *J. Am. Coll. Toxicol.* **6,** 489-501.

Kurokawa, Y., Takayama, S., Konishi, Y., Hiasa, Y., Asahina, S., Takahashi, M., Maekawa, A. and Hayashi, Y. (1986b). Long-term in vivo carcinogenicity test of potassium bromate, sodium hypochlorite and sodium chlorite conducted in Japan. *Environmental Health Perspect.* **69,** 221-235.

Lee, Y., Choi, J., Park, M., Choi, E., Kasai, H. and Chung, M. (1996). Induction of oh-8 Gua glycosylase in rat kidneys by potassium bromate (KBrO3), a renal oxidative carcinogen. *Mutation Research* **364,** 227-233.

Li, N. and Oberley, T. D. (1998). Modulation of antioxidant enzymes, reactive oxygen species, and glutathione levels in manganese superoxide dismutase-overexpressing NIH/3T3 fibroblasts during the cell cycle. *J. Cell Physiol.* **177,** 148-60.

Lu, S. c. (1999). Regulation of hepatic glutathione synthesis: current concepts and controversies. *FASEB J.* **13,** 1169-1183.

Marshall, N. J., Goodwin, C. J. and Holt, S. J. (1995). A Critical Assessment of the Use of Microculture Tetrazolium Assays to Measure Cell Growth and Function. *Growth Regulation* **5,** 69-84.

McLaren, J., Boulikas, T. and Vamvakas, S. (1994). Induction of poly(ADP-ribosyl)ation in the kidney after in vivo application of renal carcinogens. *Toxicology* **88,** 101-112.

Meister, A. and Anderson, M. E. (1983). Glutathione. *Ann. Rev. Biochem.* **52,** 711-60.

Mossman, B. T. (1998). Personal Communication.

Ogretman, B., Bahadori, H., McCauley, M., Boylan, A., M., G. and A.R., S. (1998). Lack of correlation of MRP and gamma-glutamylcysteine synthetase overexpression with doxorubicin resistance due to increased apoptosis in SV40 large T-antigen-transformed human mesothelial cells. *Cancer Chemotherapy & Pharmacology* **42,** 441-6.

Ohno, Y., Onodera, H., Takamura, N., Imazawa, T., Maekawa, A. and Kurokawa, Y. (1982). Carcinogenicity testing of potassium bromate in rats (in Japanese). *Bull. Natl. Inst. Hyg. Sci.* **100,** 93-100.

Onodera, H., Tanigawa, H., Matsushima, Y., Maekawa, A., Kurokawa, Y. and Hayashi, Y. (1985). Eosinophilic bodies in the proximal renal tubules of rats given potassium bromate (in Japanese). *Bull. Natl. Inst. Hyg. Sci.* **103,** 15-20.

Palmeira, C. M., Moreno, A. J. and Madeira, V. M. C. (1994). Metabolic alterations in hepatocytes promoted by the herbicides paraquat, dinoseb and 2,4-D. *Archives of Toxicology* **68,** 24-31.

Sai, K., Takagi, A., Umemura, T., Hasegawa, R. and Kurokawa, Y. (1991). Relation of 8-Hydroxydeoxyguanosine Formation in Rat Kidney to Lipid Peroxidation, Glutathione

Level and Relative Organ Weight after a Single Administration of Potassium Bromate. *Jpn. J. Cancer Res.* **82,** 165-169.

Sai, K., Uchiyama, S., Ohno, Y., Hasegawa, R. and Kurokawa, Y. (1992a). Generation of active oxygen species in vitro by the interaction of potassium bromate with rat kidney cell. *Carcinogenesis* **13,** 333-339.

Sai, K., Umemura, T., Takagi, A., Hasegawa, R. and Kurokawa, Y. (1992b). The Protective Role of Glutathione, Cysteine and Vitamin C against Oxidative DNA Damage Induced in Rat Kidney by Potassium Bromate. *Jpn. J. Cancer Res.* **83,** 45-51.

Shi, Y., Kornovski, B., Savani, R. and Turley, E. A. (1993). A rapid, multiwell colorimetric assay for chemotaxis. *J. Immunol. Meth.* **164,** 149-154.

Sies, H. and Ketterer, B. (1988). Glutathione Conjugation: Mechanisms and Biological Significance, pp. 480. London: Academic Press Limited.

Steel, R. G. D. and Torrie, J. H. (1980). Principles and Procedures of Statistics: A Biometrical Approach, pp. 95-97. New York: McGraw-Hill Inc.

Tanaka, K., Oikawa, K., Fukuhara, C., Saito, H., Onosaka, S., Min, K. S. and Fujii, M. (1984). Metabolism of potassium bromate in rats. II. in vitro studies. *Chemosphere* **13,** 1213-1219.

Taniguchi, N., Higashi, T., Sakamoto, Y. and Meister, A. (1989). Glutathione Centennial: Molecular Perspectives and Clinical Implications, pp. 441. New York: Academic Press, Inc.

USEPA. (1998). Draft Water Quality Criteria Methodology Revisions: Human Health; Notice. *Federal Register* **63,** 43755-43828.

van de Loosdrecht, A. A., Nennie, E., Ossenkoppele, G. J., Beelen, R. H. J. and Langenhuijsen, M. M. A. C. (1991). Cell mediated cytotoxicity against U 937 cells by human monocytes and macrophages in a modified colorimetric MTT assay; a methodological study. *J. Immunol. Meth.* **141,** 15-22.

Vani, P., Rajeswari, T. R. and Dikshitulu, L. S. A. (1995). Kinetics and Mechanism of Oxidation of DL-Methionine by Potassium Bromate in Sulphuric Acid Medium. *J. Indian Chem. Soc.* **72,** 867-871.

von Gunten, U. and Holgne, J. (1992). *Aqua* **41,** 299-304.

von Gunten, U. and Holgne, J. (1994). Bromate Formation during Ozonation of Bromide-Containing Waters: Interaction of Ozone and Hydroxyl Radical Reactions. *Environ. Sci. Technol.* **28,** 1234-1242.

Wefers, H. and Sies, H. (1983). *Eur. J. Biochem.* **137,** 29-36.

Wefers, H. and Sies, H. (1986a). . In *Superoxide and Superoxide Dismutase in Chemistry* (ed. G. Rotilio), pp. 103-107. Amsterdam: Elsevier.

Wefers, H. and Sies, H. (1986b). *Adv. Exp. Med. Biol.* **197,** 505-512.

WHO. (1993). Guidelines for Drinking Water Quality. In *WHO Technical Reports*. Geneva: World Health Organization.

Wong, G. H. W. and Goeddel, D. V. (1994). Fas Antigen and p55 TNF Receptor Signal Apoptosis Through Distinct Pathways. *J. Immunol.* **152,** 1751-1755.

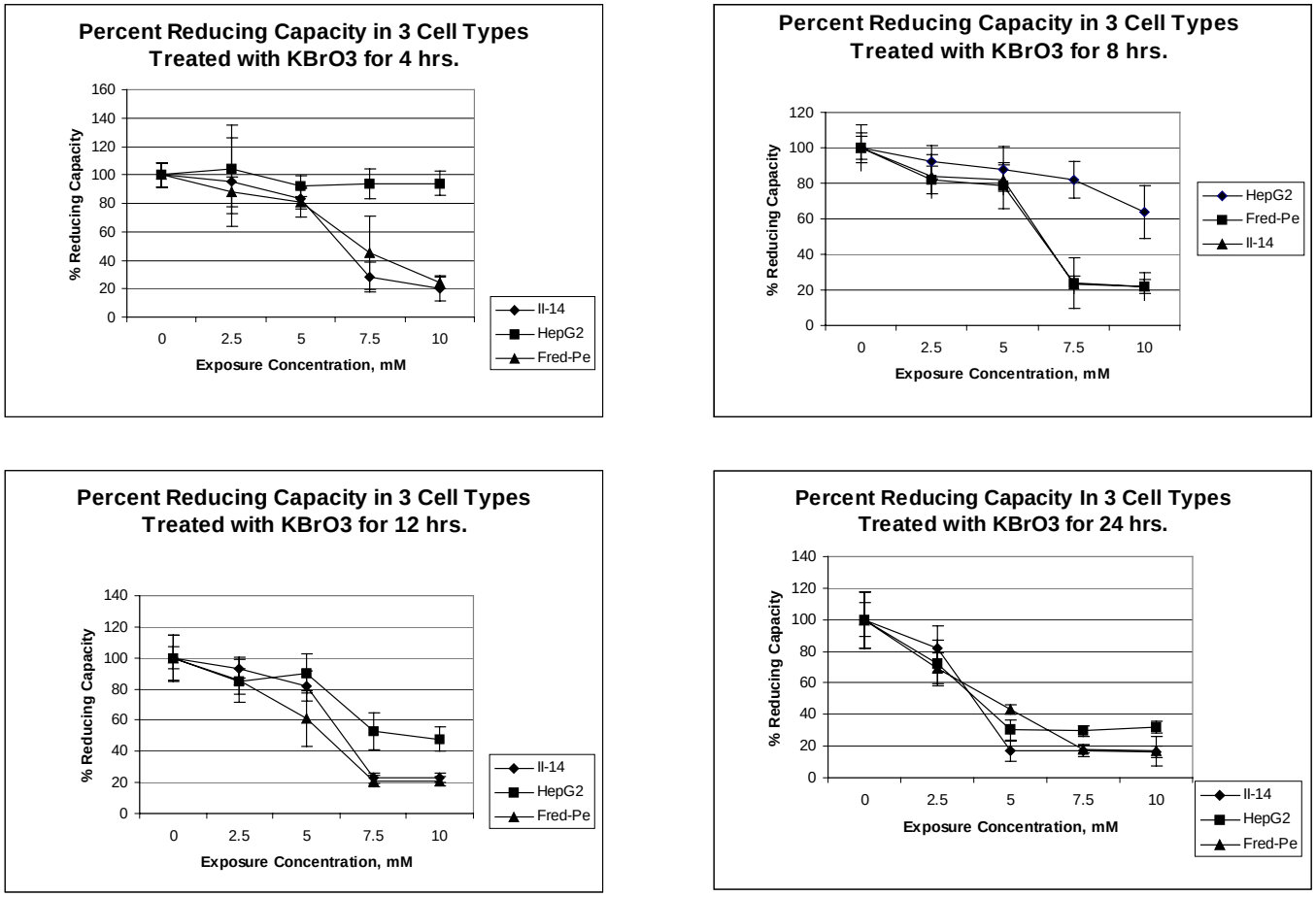

Fig. 1. Dose-response curves at; (top left) 4, (top right) 8, (lower left) 12 and (lower right) 24 h for three cell lines (HepG2, II-14 and Fred-Pe). Error bars represent ± 1 standard deviation. HepG2 differed significantly ($p<0.05$) from II-14 and Fred-Pe at ≥ 5 mM for 4, 12 or 24 h exposures (except HepG2 v. Fred-Pe at 5 mM, 12 h where $p<0.062$).

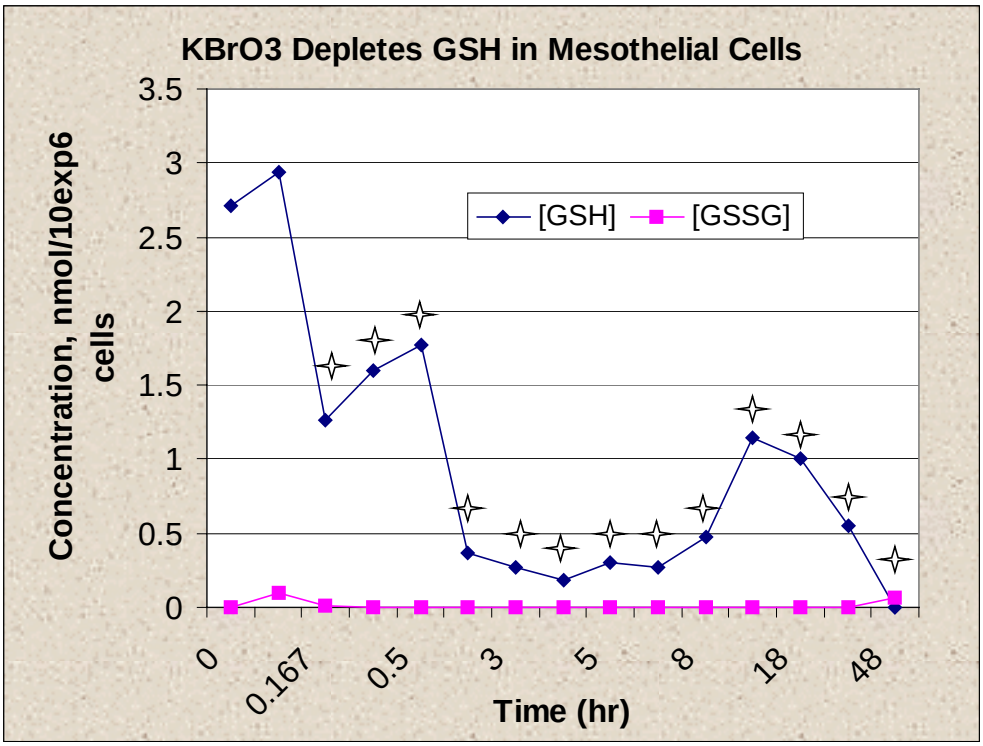

Fig. 2. Depletion of GSH (nmol/10^6 cells) vs. time (five min to 48 h) after $KBrO_3$ treatment in NRM-2 cells. All values at or later than 10 min treatment are significant at $p < 0.01$ (starred values).

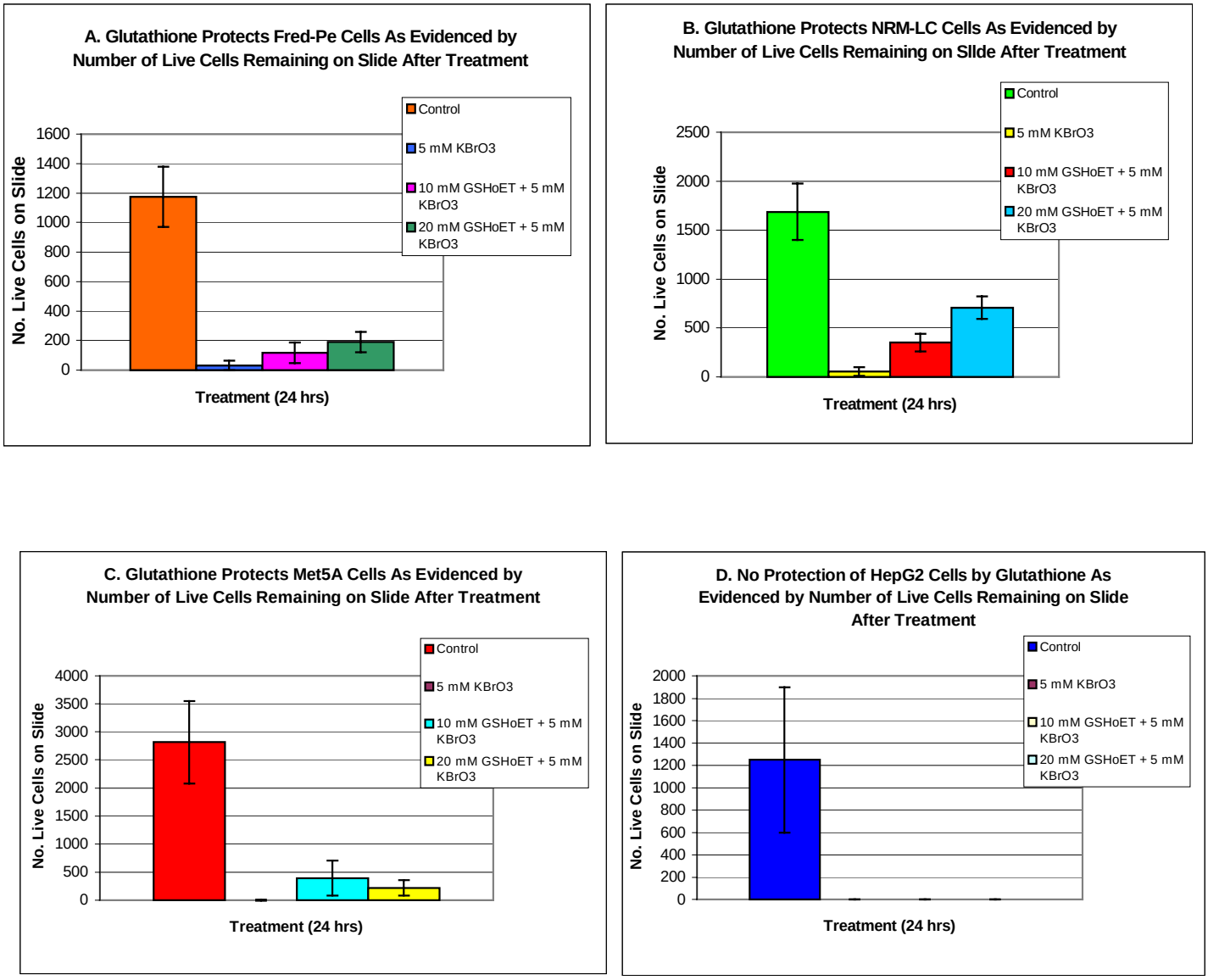

Fig. 3. GSH pre-treatment protects mesothelial, but not HepG2 cells from $KBrO_3$-induced cytotoxicity, as evidenced by number of live cells remaining on slide at 24 h. All GSHoET-treated wells were significantly different than those treated with KBrO3 alone ($p<0.005$) in the 3 mesothelial cell types (A-C). In HepG2 cells (D), wells treated with GSHoET at 10 or 20 mM were not significantly different than those treated with $KBrO_3$ alone.

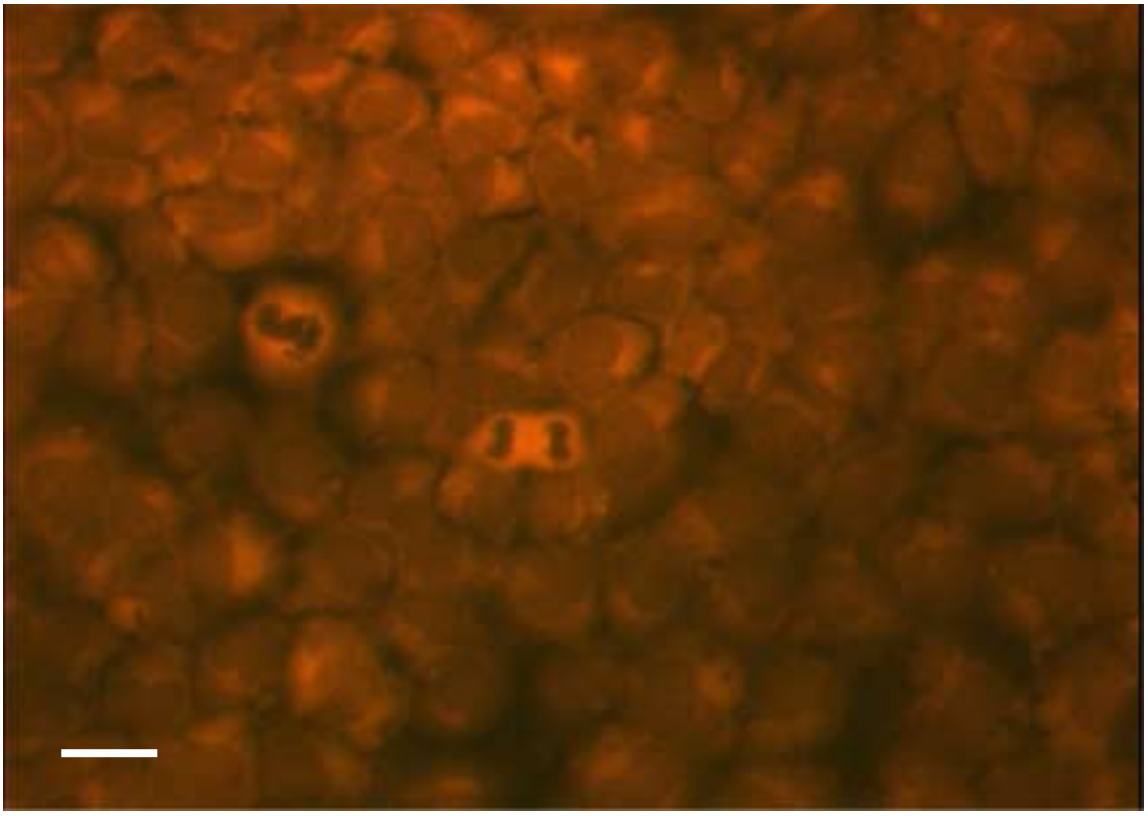

Fig. 4. Fluorescent mercury orange stain specific for GSH in untreated Fred-Pe cells: mitotic cells stain brightly (20x), while non-dividing cells display a bright crescent of staining surrounding the nucleus, possibly representing localization to the golgi apparatus. Bar = 20 μm.

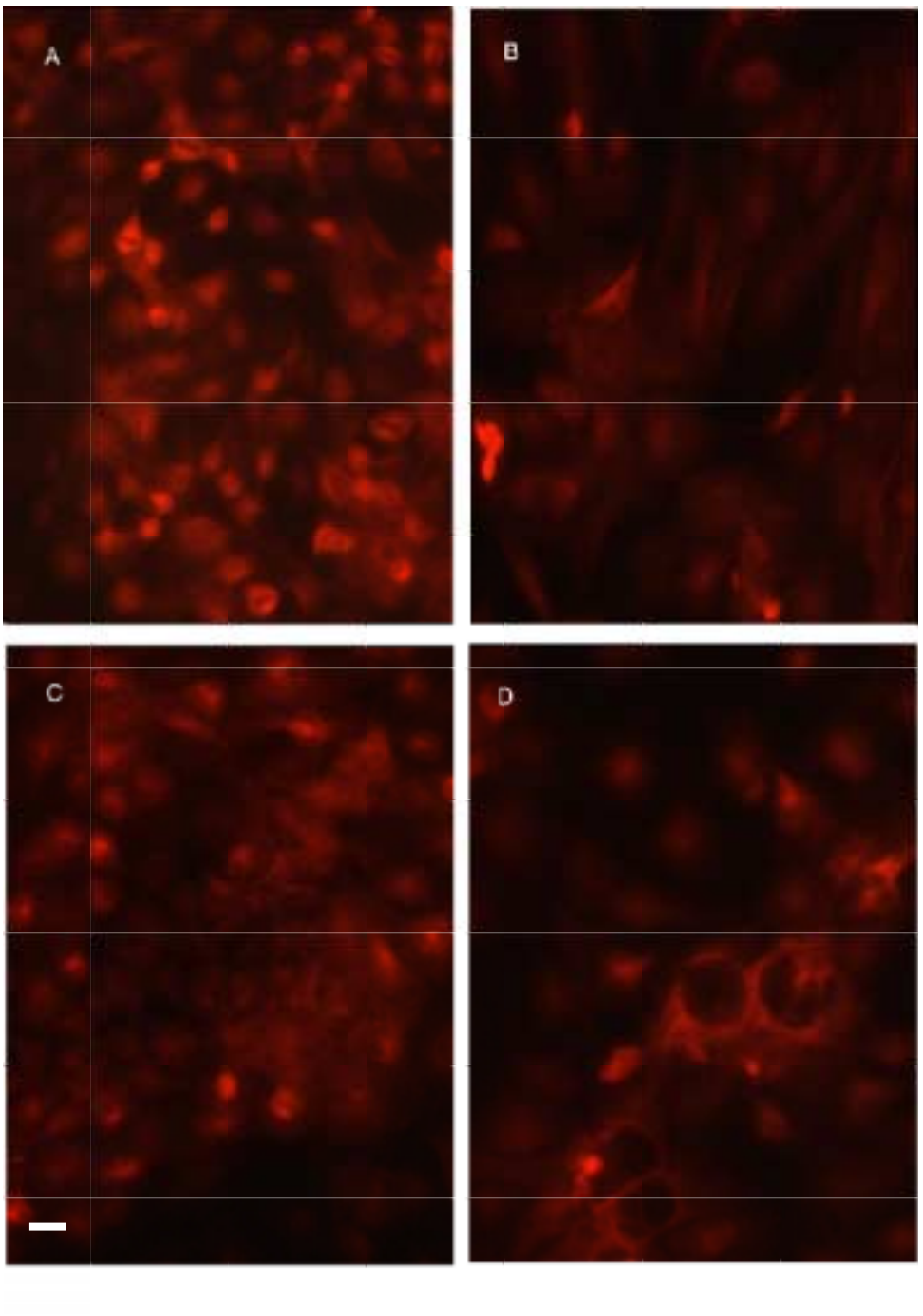

Fig. 5. NRM-2 cells stained with fluorescent mercury orange stain specific for GSH treated for 24 h as follows: A) control, B) 2.5 mM $KBrO_3$, C) 10 mM BSO, D) 1 mM DEM.10x. Bar = 30 μm.

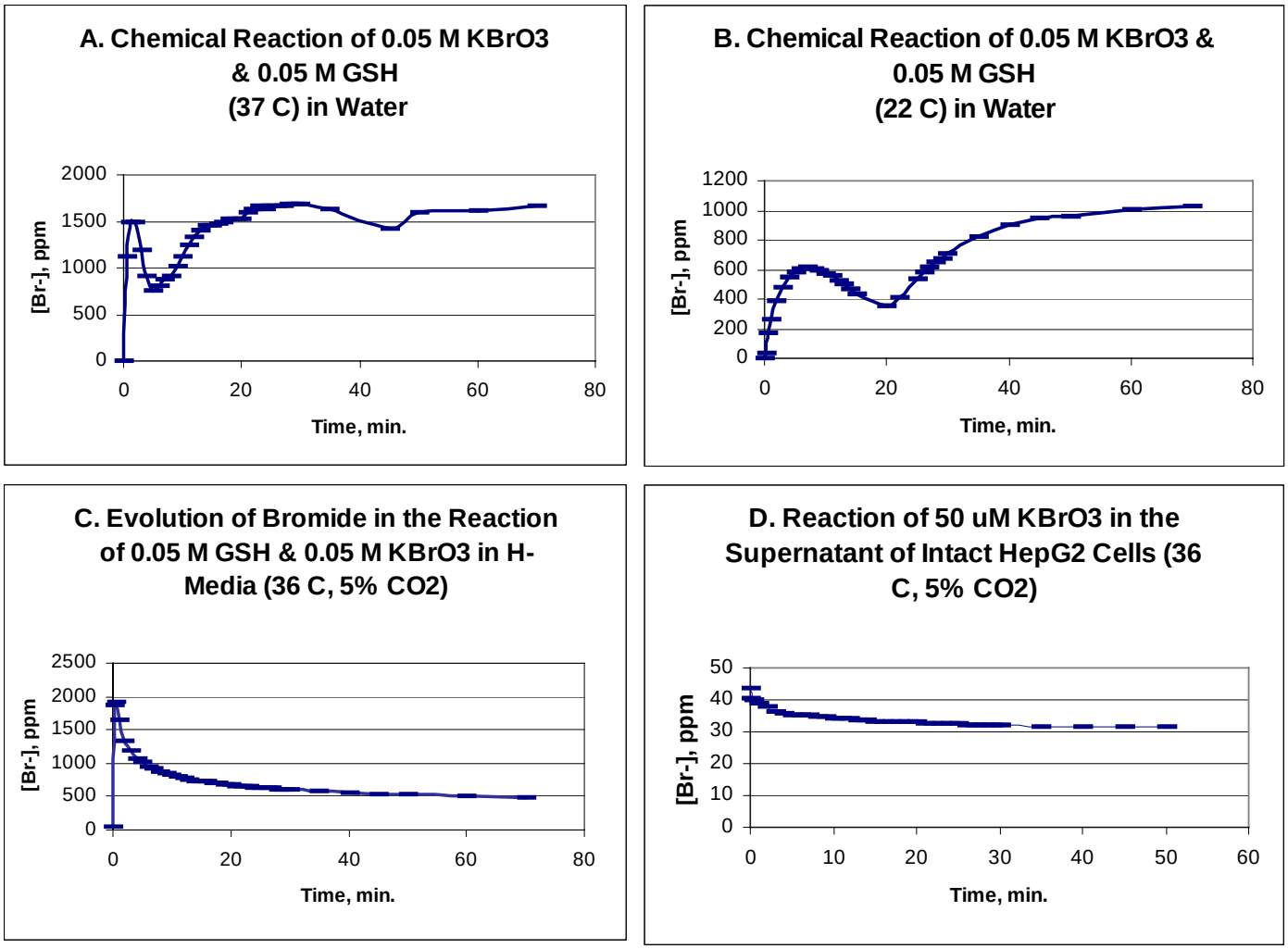

Fig. 6. Reactions of reduced GSH and $KBrO_3$ generating Br^- (ppm) vs. time in A) 37°C, (aq); B) room temperature, (aq); C) HepG2 cell culture media; D) cellular supernatant of HepG2 cells.

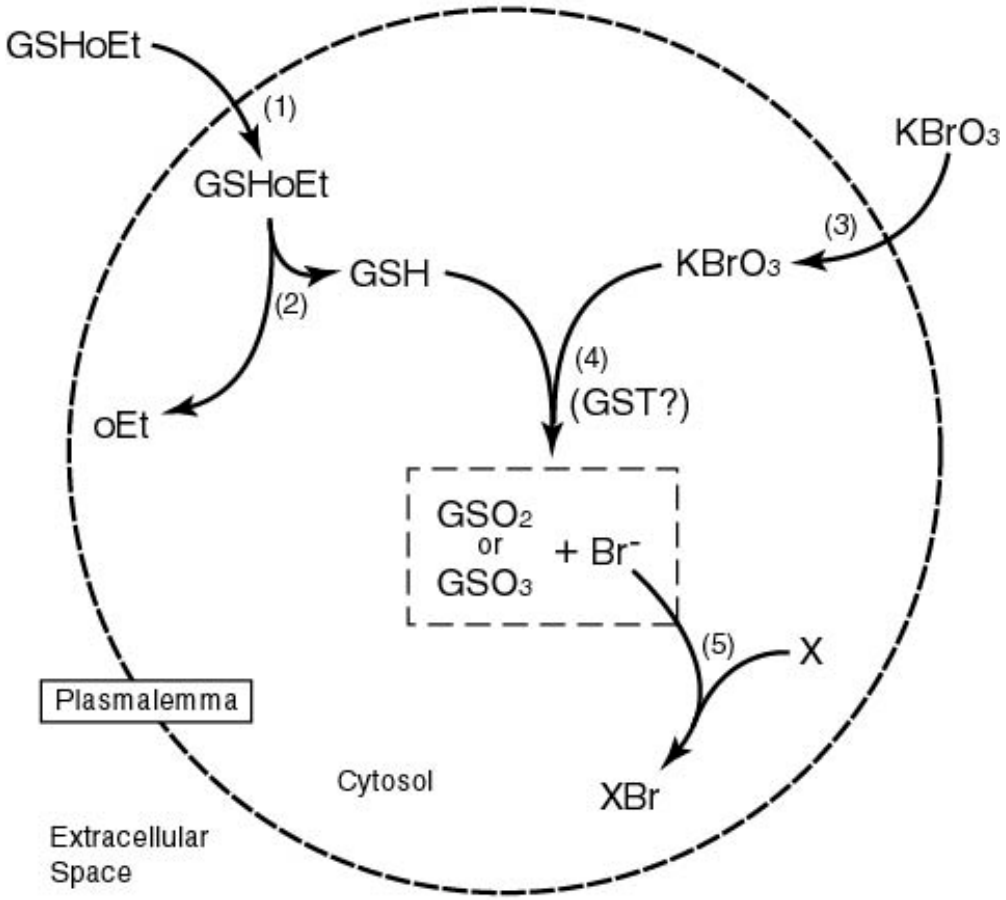

Fig. 7. Possible pathway of GSHoET within the cell, and proposed reaction with $KBrO_3$. (1) GSHoET diffuses across the cell membrane (as indicated by protection assay). (2) Cleavage of the ethyl ester portion of GSHoET results in free GSH within the cell (Anderson, 1998). (3) Free GSH reacts together with $KBrO_3$ (as indicated by Br^- selective electrode experiments) inside the cell. (4) GST(s) may catalyze in the reaction of $KBrO_3$ and GSH, producing a GSH-sulfone or -sulfoxide product + Br^- (dashed box). (5) An unknown molecule (X) is proposed to combine with Br^-, forming the product XBr.

Table 1. Total Glutathione Content in Untreated Cell Lines (nmol/1 x 10^6 cells)

All cell lines differ from HepG2 in [GSH] significantly ($p<0.0001$).

Cell Line	GSH Avg.	Std. Dev.	GSSG Avg.	Std. Dev.	Ratio of GSH:GSSG	n
HepG2	8.27	±1.34	0.22	±0.02	38	7
MeT-5A	1.03	±0.04	0.14	±0.02	7	4
Fred-Pe	1.40	±0.04	0.04	±0.05	35	4
II-14	0.43	±0.02	<0.02	±0.01	22	4
NRM-2	1.18	±0.03	<0.02	±0.01	59	4
NRM-LC	2.00	±0.05	0.38	±0.03	5	4

Table 2. Depletion of GSH vs. Time in NRM-2 Cells

Time (h)	[GSH]± s*, nmol/10^6 cells	[GSSG]± s*, nmol/10^6 cells
0	2.71 ± 0.10	0.10 ± 0.03
0.08	2.94 ± 0.09	0 ± 0.03
0.17	1.26 ± 0.06	0.06 ± 0.02
0.25	1.60 ± 0.09	0.01 ± 0.04
0.5	1.77 ± 0.08	0 ± 0.01
2	0.37 ± 0.09	0 ± 0.02
3	0.27 ± 0.38	0 ± 0.11
4	0.18 ± 0.09	0 ± 0.02
5	0.30 ± 0.06	0 ± 0.02
6	0.27 ± 0.07	0 ± 0.01
8	0.47 ± 0.12	0 ± 0.02
12	1.14 ± 0.32	0 ± 0.10
18	1.00 ± 0.46	0 ± 0.11
24	0.55 ± 1.06	0.07 ± 0.07
48	0 ± 0.17	0 ± 0.09

*s = standard deviation.

Table 3. Glutathione Protection Assay

					Cellular Reducing Capacity as % Control Using MTS** Assay (n=6)						
						6 h (5 mM $KBrO_3$)					
			$KBrO_3$ + GSHoET						GSHoET only		
	$KBrO_3$ only	$KBrO_3$ + 5 mM GSHoET	$KBrO_3$+10 mM GSHoET	$KBrO_3$+20 mM GSHoET	$KBrO_3$+50 mM GSHoET	$KBrO_3$+100 mM GSHoET	5 mM GSHoET	10 mM GSHoET	20 mM GSHoET	50 mM GSHoET	100 mM GSHoET
HepG2	94	86	70#	69#	70#	85	107	126*	132	405*	369*
MeT-5A	80	77	74	73	89	107	104	118	128*	209*	172*
NRM-2	94	96	92	109	98	111	116	113	136	210*	211*
NRM-LC	78	104#	103#	109#	129#	139#	132*	130	148*	220	222*
II-14	24	57#	58#	67#	66#	99	101	120	140*	211*	162
Fred-Pe	83	84	95#	84	80	117	103	102	155	217*	369*
						24 h (7.5 mM $KBrO_3$)					
HepG2	33	34	34	35	37#	39#	82*	76*	84*	103	84*
MeT-5A	42	44	38	44	47	57#	94	76	58*	52*	28*
NRM-2	27	22#	32	44#	47#	68#	72*	83*	83*	94	90*
NRM-LC	37	56#	46	52#	58#	67#	81	91	92	93	91
II-14	15	15	15	15	19	29	85*	89	90*	95	95
Fred-Pe	39	35	30#	31#	33	40	60*	50*	60*	76*	62*

Significance: (significantly different than control) *p<0.05

(significantly different than $KBrO_3$ only) #p<0.05

**Promega Celltiter 96 Aqueous One Solution cellular reducing capacity assay™.

Table 4. N-Acetylcysteine (NAC) Protection Assay

Cell Type	No. of Attached Cells/high power field (as % Control) [#]					
	0.03 N $KBrO_3$	0.03 N NAC + 0.03 N $KBrO_3$	0.3 N $KBrO_3$	0.3 N NAC + 0.3 N $KBrO_3$	3 N $KBrO_3$	3 N NAC + 3 N $KBrO_3$
NRM-2	82	62	82	48*	87	81
II-14	116	82	0	79*	0	69*
HepG2	159	84*	100	84	26	47*

*Significant difference between (NAC + $KBrO_3$) and ($KBrO_3$): $p<0.05$

The number of cells present per hpf (high power field, 50 x 50 micrometers) ranged from:

0 to > 50 (HepG2) 0 to 10 (NRM-2)

0 to 20 (II-14)

[#] Cells were pre-treated for 30 min with NAC, exposed for 15 min to $KBrO_3$ and allowed to recover for 36 h. Units are normality (N).

Table 5. $KBrO_3$ Toxicity Curve Shift

Cellular Reducing Capacity as % Control (+/- SD), Using MTS Assay

Cell Type	2.5 mM $KBrO_3$	2.5 mM $KBrO_3$+ 10 mM BSO	2.5 mM $KBrO_3$+ 250 µM DEM	250 µM DEM	10 mM BSO	250 µM DEM+ 10 mM BSO	2.5 mM $KBrO_3$+ 250 µM DEM + 10 mM BSO
HepG2	58 ± 3	39 ± 1	45 ± 2	81 ± 10	81 ± 8	56 ± 7♦	40 ± 1♦
NRM-2	45 ± 5	19 ± 0.6	19 ± 1	23 ± 3	65 ± 14	20 ± 0.5♦	19 ± 0.7♦
MeT-5A	58 ± 7	15 ± 0.6	15 ± 0.4	78 ± 6	73 ± 6	15 ± 1♦	14 ± 0.4♦

Significance: n = 16

All values $p < 0.01$

♦ = significance not determined

Significance for the column labelled 'BSO' is calculated as BSO vs. Control.

" " DEM' " as DEM vs. Control.

" " $KBrO_3$' " as $KBrO_3$ vs. Control

" " $KBrO_3$/BSO' " as $KBrO_3$/BSO vs. $KBrO_3$ alone.

" " DEM/$KBrO_3$' " as DEM/$KBrO_3$ vs. $KBrO_3$ alone.

(results are representative of duplicate experiments)

Chapter 4. Morphologic Analysis Correlates with Gene Expression Changes in Cultured F344 Rat Mesothelial Cells

Authors and Affiliations:

Crosby L.M.[1], Hyder K.S.[2], DeAngelo A.B.[3], Kepler T.B.[4], Gaskill B.[5], Benavides G.R.[5], Yoon L.[5] and Morgan K.T.[5]

[1]Dept. of Toxicology, North Carolina State University, Raleigh, NC and USEPA Trainee in Environmental Carcinogenesis

[2] Clontech Laboratories, Palo Alto, CA

[3] USEPA, NHEERL, RTP, NC

[4] Biomathematics Graduate Program, Dept. of Statistics, North Carolina State University, Raleigh, NC

[5] GlaxoWellcome, Inc., RTP, NC

ABSTRACT

The gene expression pattern of mesothelial cells *in vitro* was determined after 4 or 12 h exposure to the rat mesothelial, kidney and thyroid carcinogen, and oxidative stressor potassium bromate ($KBrO_3$). Gene expression changes observed using cDNA arrays indicated oxidative stress, mitotic arrest and apoptosis in treated immortalized rat peritoneal mesothelial cells. Increases occurred in oxidative stress responsive genes HO-1[1], QR[2], HSP70[3], GADD45[4], GADD153[5], p21[WAF1/CIP1 6], GST's[7], GAPDH[8], TPX[9] and GPX-1[10]; transcriptional regulators c-jun, c-fos, jun D, jun B, c-myc and IκB[11]; protein repair components Rδ, RC10-II, C3, RC-7, HR6B ubiquitin-conjugating enzyme and ubiquitin; DNA repair components PCNA[12], msh2[13] and O-6 methylguanine DNA methyltransferase; lipid peroxide excision enzyme PLA2[14] and apoptogenic components TNFα[15], iNOS1[16] and FasL[17]. Decreases occurred in bcl-2[18] (anti-apoptotic), bax α[19], bad[20] and bok[21] (pro-apoptotic) and cell cycle control elements (cyclins). Cyclin G,

[1] heme oxygenase-1
[2] quinone reductase, NMOR, DT diaphorase
[3] heat shock protein 70
[4] growth arrest and DNA damage protein 45
[5] growth arrest and DNA damage protein 153
[6] 21 kD protein/waf1/cip1 - inhibitor of cyclin kinases
[7] glutathione S-transferases
[8] glyceraldehyde phosphate dehydrogenase
[9] thioredoxin peroxidase
[10] glutathione peroxidase
[11] inhibitory κB subunit
[12] proliferating cell nuclear antigen
[13] mismatch repair protein 2 homologue
[14] phospholipase A2
[15] tumor necrosis factor α
[16] inducible nitric oxide synthase
[17] fas-ligand
[18] b-cell lymphoma 2
[19] bcl-2-associated X protein α
[20] bcl-XL/bcl-2 associated death promoter homologue
[21] bcl-2 related ovarian killer protein

p14ink4b[22] (which inhibit entry into cell cycle) were increased. Numerous signal transduction, cell membrane transport, membrane-associated receptor and fatty acid biosynthesis and repair components were altered. Morphologic endpoints examined were; mitotic index, apoptotic index, and antibody-specific localization of HO-1. PCR analysis confirmed HO-1, $p21^{waf1/cip1}$, HSP70, GPX1, GADD45, QR, mdr1[23], PGHS[24] and cyclin D1 changes. A model for $KBrO_3$-induced carcinogenicity in the F344 rat mesothelium is proposed, whereby $KBrO_3$ generates a redox signal that activates p53 and results in transcriptional activation of oxidative stress and repair genes, dysregulation of growth control, and imperfect DNA repair leading to carcinogenesis.

[22] p14/cyclin-dependent kinase inhibitor 4b
[23] multidrug resistance protein 1
[24] prostaglandin G/H synthase 1 precursor

INTRODUCTION

Radical damage to cellular constituents causes oxidative stress. This concept was proposed in 1956 in conjunction with radiation-induced cellular damage and its possible parallels with the aging process (Harman, 1956), and has been verified many times since (Bensasson *et al*., 1993). The generation of radical species *in situ* was demonstrated in water (1948) (Stein and Weiss, 1948) and in biological materials (1954) (Commoner *et al*., 1954; Gerschman *et al*., 1954). The source of reactive oxygen species (ROS) can be 1) mitochondrial oxidative phosphorylation via cytochrome oxidase, referred to as "leakage" (Fridovich, 1978), 2) the respiratory burst of phagocytic cells, neutrophils, monocytes, macrophages and eosinophils (Tauber and Babior, 1978), or 3) xenobiotic insult. Xenobiotics may increase the rate of oxidative phosphorylation (thus, "leakage") or directly react with cellular constituents to produce ROS (H_2O_2, $O_2^{-\cdot}$, $OH^{\cdot}$, $^1O_2$, $HO_2^{\cdot}$), or reactive nitrogen species. ROS may instigate a chain reaction, amplifying until an encounter with a second radical/ radical scavenger occurs.

ROS cause varying degrees of damage to nearby lipids, proteins, carbohydrates and nucleic acids, according to their relative reactivity and half-lives; for details see review by Beckman (1997). Direct evidence of ROS participation in tissue damage is obtained via electron spin resonance and spin trapping, while indirect evidence is three-fold. Lipid peroxidation is observed in the form of protein/DNA oxidation, and metal catalysis/xenobiotic metabolism exacerbates, while metal chelators/sequestering agents/antioxidants protect against, peroxidative damage. In mammalian cells, the superoxide radical ($O_2^{-\cdot}$) has a high potential for wreaking cellular damage. Since it is generated from $O_2^{-\cdot}$ during enzymatic dismutation and from $H_2O_2/O_2^{-\cdot}$ during the iron-catalyzed Haber-Weiss reaction, the highly reactive hydroxyl radical ($OH^{\cdot}$) is

commonly formed as well (Bensasson *et al*., 1993). Healthy mammalian cells contain several important radical scavengers (e.g., bilirubin, GSH[25], urate and α-tocopherol). (Beckman and Ames, 1997). Additionally, several enzymes (catalase, Cu/Zn SOD[26], Mn SOD[27], GPX) catalyze the removal of ROS, utilizing reducing species (GSH, NAD(P)H[28]…) as co-factors. The normal (unstressed) redox equilibrium within the cell decrees that, in general, a reducing environment prevails. Thus, under physiologic conditions, the ratio of reduced to oxidized GSH (GSH:GSSG) is typically 100: to 200:1 (Taniguchi, 1989). However, under tissue culture conditions, the ratio of GSH to GSSG in HepG2 (human hepatocellular carcinoma) cells is only about 4:1 (Palmeira *et al*., 1994). Reduced to oxidized ratios of NADP(H), G6PD(H)[29], GAPD(H), etc. may be expected to be heavily weighted in favor of the reduced state. NAD(H)[30] is an exception; most of this pool exists in the oxidized form (Taniguchi, 1989). A highly reducing environment is required surrounding the DNA double helix, in order for transcription factor binding to occur (Sun and Oberley, 1996). Further evidence for the importance of a highly reducing milieu is the observation of extremely bright staining for GSH about the mitotic apparatus during mitosis (Crosby *et al*., in Press), and a marked increase in GSH content during mitosis reported by Li and Oberley (Li and Oberley, 1998).

Oxidative stress results when the quantitative imbalance between pro- and anti-oxidant entities/activities within the cell is tipped in favor of pro-oxidant species (ROS) in aerobic organisms. A number of disease states are associated with oxidative stress including Parkinson's Disease, Alzheimer's Disease, inflammation, aging, cancer and ischemia-reperfusion injury.

---

[25] glutathione
[26] copper/zinc-containing superoxide dismutase
[27] manganese-containing superoxide dismutase
[28] nicotinamide adenine dinucleotide phosphate
[29] glucose-6 phosphate dehydrogenase
[30] nicotinamide adenine dinucleotide (reduced)

Therefore, an understanding of the origins, mechanisms and outcome of oxidative stress will assist in formulating effective treatments for these diseases.

The drinking-water disinfection by-product $KBrO_3$ is an acute oto- and nephro-toxicant in numerous species studied (Kurokawa, 1985; Matsumoto, 1973) and a carcinogen in the F344 rat (male and female) (DeAngelo *et al*., 1998; Hayashi *et al*., 1986; Kurokawa, 1985; Kurokawa *et al*., 1985; Kurokawa *et al*., 1986a; Kurokawa *et al*., 1982; Kurokawa *et al*., 1983a; Kurokawa *et al*., 1987; Kurokawa *et al*., 1983b; Kurokawa *et al*., 1986b; Ohno *et al*., 1982; Onodera *et al*., 1985), mouse (male) (Oinuma, 1974) and hamster (male) (Takamura *et al*., 1985). In the male F344 rat, carcinogenicity is specific to the kidney, peritoneal mesothelium and thymus. Recently, the mechanism of acute toxicity *in vitro* was demonstrated to involve depletion of GSH followed by oxidant damage (Crosby *et al*., in Press). To understand the molecular mechanism(s) of $KBrO_3$ toxicity and carcinogenicity, we investigated gene expression patterns after $KBrO_3$ exposure *in vitro*.

Gene expression array technology has matured, in the past few years, from an exciting and promising new method into one now in common use (an Internet search yielded close to 600 hits). The information obtained can speed up the discovery process many fold over more conventional techniques such as Northern- and Western-blotting. This technology promises to assist in the elucidation of cellular signalling networks, which previously had to be painstakingly worked out one element at a time.

Amundson, et al. (1999) have undertaken the investigation of genotoxic stress responses to ionizing radiation in human myeloid cells. They noted the induction of $p21^{CIP1/WAF1}$, mdm2 and bax, and p53-associated induction of FRA-1[31] and ATF-3[32]. Wang, et al. have studied the

[31] fos-related antigen 1
[32] ATF/CREB- cyclic AMP response element binding protein

transcriptional response of human cells to etoposide, an antitumor agent which induces apoptosis via p53 activation and topoisomerase II inhibition (Wang *et al*., 1999). The latter authors found $p21^{WAF1/CIP1}$ and PCNA (two known p53 regulated genes), GPX and S100A2 calcium-binding protein (two novel p53 target genes) and eight non-p53 associated genes to be induced by this treatment. These results implicate p53 activation-associated mRNAs in a generalized stress response program within the cell.

In these experiments, we were interested in the comparison of $KBrO_3$-induced oxidative stress with the work of others studying stress response-activated alteration of mRNA transcription levels. We observed mRNA changes in rat peritoneal mesothelial cells *in vitro* after a four or 12 h exposure to $KBrO_3$ by means of radioactively-labelled cDNA hybridization to a commercially available expression array and verified selected results by Taqman™ quantitative PCR, and examined morphology using light microscopy. The statistical program NLR (Normalization and Linear Regression) (Kepler *et al*., Submitted for Publication) was used for normalization and to perform statistical analysis.

MATERIALS AND METHODS

Cell culture. Fred-Pe immortalized rat peritoneal mesothelial cells developed in-house were grown in mesothelial cell culture media as previously described (Crosby *et al*., in Press). To prevent artifacts caused by recent thawing and acclimatization to culture conditions, cells were maintained in continuous culture for several months prior to the experiment. Also, to ensure that tested populations would be in the log phase of growth, stocks were sub-cultured weekly.

Selection of exposure concentration. Previously, the ED_{50} for cytotoxicity (MTS assay for cellular reducing capacity) in Fred-Pe cells exposed to $KBrO_3$ was determined to be 6 mM at 4 –

12 h (Crosby *et al*., in Press), and GSH depletion was found to be 93% at four h and 53% at 12 h post-treatment. Therefore, for the present study, cells were exposed to six mM $KBrO_3$ for four or 12 h.

$KBrO_3$ treatment of cells and RNA collection. Sub-cultured Fred-Pe (rat peritoneal mesothelial cell line) cells were plated at 1 x 10^7 cells/150 mm dish in 30 ml of HITS-containing media (Crosby *et al*., in Press) and grown for 24 h. Cells were then exposed to 6 mM $KBrO_3$ for four or 12 h and cells were removed from the dishes using a cell-lifter. Cells were centrifuged at 175 g for three min and the $KBrO_3$-containing media removed by aspiration, and cells were then re-suspended in 1 ml of sterile PBS and frozen at $^-$80C until RNA extraction (TRIZOL method, Gibco BRL) was performed. Poly A^+ RNA was quantitated by spectrophotometric absorption at 260 and 280 nm, and the quality judged by the 260/280 ratio and the appearance of the ethidium bromide-stained nucleic acid smear as run on a 1% native agarose gel.

Mitotic/apoptotic indices. Fred-Pe cells grown on four well Nalge Nunc™ chamber well slides were treated with 0, 5, 10 or 100 mM $KBrO_3$ for 30 min or 4 h, ethanol fixed and H&E stained. The number of mitotic figures and apoptotic cells, and the total number of cells per high power field (hpf, 40X) was counted in ten fields/slide for each time point and the average and standard deviation were reported.

Clontech 588-cDNA Atlas array and ~230-cDNA Stress array (rat). Poly A^+ mRNA was isolated from 5-50 μg total RNA from $KBrO_3$-treated Fred-Pe cells using the Atlas Pure Total RNA™ Labeling Protocol (revision 3.1). For Stress Arrays, pooled total RNA's from each time point were analyzed. First-strand cDNA was labelled according to the manufacturer's instructions. Membranes were mounted on Whatman paper, wrapped in plastic wrap and exposed to a phosphorimager screen for four days. Raw intensities were collected using a phosphorimager

system and AtlasImage™ software (Clontech Laboratories) was used to analyze the array data, followed by NLR analysis.

Taq Man ™Quantitative PCR analysis. Fred-Pe total RNA prepared above was DNase treated (Ambion DNase I) according to the manufacturer's protocol. RNA was quantified using the Molecular Probes Ribogreen™ assay and a Cytofluor 2350 fluorometer. Samples were diluted to 10 ng/μL prior to Taqman™ analysis (Perkin Elmer ABI Prism 7700 Sequence Detection system).

Primers were designed with the use of Perkin Elmer Primer Express™ software. A 96-well assay designed to detect mRNA expression of ten rat genes (cyclin D1, GADD45, GPX, HO-1, HSP70, mdr-1, QR, PGHS, $p21^{WAF1/CIP1}$, PLA2) was constructed using probes and primers from Keystone Biosource. Two control and two treated samples from the four h time point, and two control and one treated from the 12 h time point were analyzed. Each plate was divided into four segments consisting of four rows of six wells each, with each gene represented in duplicate wells. Four wells per quadrant were aliquotted without template (no template control or NTC wells). Forward and reverse primers were diluted to nine μM and probe to 2 μM and 20 μL of each was aliquotted to make the probe/primer master mix. This amount is sufficient for at least three reactions of 15 μL each (one reaction per run). The master mix for the remaining components was prepared according to the manufacturer's protocol (without probes and primers) and 35 μL was aliquotted per well into the ten-gene plate. Fifteen μL of probe/primer mix was then added using a multichannel pipette, the plate was sealed with optical grade caps, and the reaction carried out as follows:

48°C for 30 min (reverse transcriptase or RT step)

95°C for 10 min (Amplitaq activation and RT denaturation)

40 cycles of 94°C for 15 sec

60°C for 1 min

After the reaction was complete, the above software was used to create a graph of fluorescent intensity vs. cycle number. For each gene, a cycle threshold (CT) line is set such that it intersects with the line over the linear portion of the curve, which represents exponential amplification. Samples that do not reach the threshold line are not above background level (i.e., CT number is the same as the maximum number of cycles, 40). NCT wells positive for amplification are used to discount data from the corresponding quadrant. The average CT value for each gene is calculated, and the CT value of treated sample RNA subtracted from that of control RNA for the same time point. This difference (ΔCT) represents the relative expression of the treated sample with respect to control and becomes the exponent in the formula for amplification: $2^{|\Delta CT|}$, equivalent to fold change in expression level. When ΔCT is negative, the final product is assigned a negative value, reflecting down-regulation of the gene in question. Values of fold change in expression are then graphed for comparison purposes.

Immunohistochemistry. Fred Pe cells were plated at 2 x 10^5 cells/ml on 4-well glass chamber well slides (Nalge Nunc™), in a volume of 1 ml per chamber. Cells were grown for 24 h and treated with three mM $KBrO_3$ for 24 h. Slides were placed in ice cold 100% ethanol and stored at -20C until stained. A standard peroxidase-anti-peroxidase immunologic staining procedure was performed to visualize heme oxygenase 1 (HO-1) protein abundance and distribution, in treated and control cells. Rabbit anti-HO-1 antibody (StressGen Biotechnologies Corp. OSA #100) was diluted 1000:1 in PBS-Tween 20 (PBST). Quenching of endogenous peroxidases by incubation with hydrogen peroxide (3%) was followed by PBST rinse and incubation with the DAKO-

supplied protein blocking agent, a further PBST rinse and incubation with the primary antibody/negative control sera for 30 min After PBST rinsing, slides were incubated with DAKO Envision^{+} link (30 min, room temp.). Three 5-min PBST rinses followed by incubation with DAB (DAKO #K4011) (chromagen) for eight min (room temp.) were carried out. Slides were dehydrated through a graded series of alcohols to xylene and cover-slipped with permanent mounting media.

Statistical analysis. The NLR program (Kepler *et al*., Submitted for Publication) was developed to analyze large-scale gene expression array data. NLR assumes that for the majority of genes, expression levels are fairly constant between treatments, and departures from a linear response (expression level vs. signal intensity) are small but significant. A normally distributed population is also assumed. Local regression smoothing estimates both normalized expression levels and expression-level dependent error. (For a full explanation of the working equations behind this software, please see the noted reference.)

Cell cycle arrest and re-emergence from arrest. To determine whether the observed cell cycle arrest was reversible, an immortalized rat pleural mesothelial cell line (NRM-2), passage 37, was plated at 5.45 x 10^4 cells/T225 flask and treated with 5 mM $KBrO_3$, (a dose previously observed to result in cell cycle arrest) for five days. $KBrO_3$-containing media was then removed by aspiration and replaced with fresh HITS-containing medium. Cells were then continually re-fed every 48 h.

RESULTS

$KBrO_3$ treatment of cells. Control cultures exhibited characteristic morphology and patterns of gene expression. Exposure to six mM $KBrO_3$ induced a marked inhibition of cell replication in addition to degenerative cellular changes that were severe at 24 h. The marked cellular

degeneration at 24 h was associated with RNA degradation, and thus molecular biology studies were confined to the two earlier time-points. Morphologic changes are described below, prior to observations on gene expression in the respective cultures.

Mitotic/apoptotic indices. The mitotic index decreased significantly ($p < 0.05$) at 30 min and four h (Fig. 1A-B, Fig. 3,4). No dividing cells could be discerned in any of the treated fields examined at 12 h (data not shown). The treatment-associated disappearance of mitotic figures indicates that $KBrO_3$ induced essentially complete cell cycle arrest in treated cells.

The apoptotic index was significantly elevated at 30 min and at four h ($p < 0.05$) (Fig. 1A-B, Fig. 3). A dose-response effect of increasing apoptotic cells/hpf with increasing dose of $KBrO_3$ was observed.

Clontech Rat 588-cDNA Atlas, and 209-cDNA Stress arrays; comparison of treated v. control. See Table 1 (List of Selected mRNA's Significantly Up-regulated ($p < 0.05$) in Treated Fred-Pe vs. Ctrl.) and 2 (List of mRNA's Significantly Down-regulated ($p < 0.05$) in Treated Fred-Pe vs. Ctrl.). The gene changes noted in the tables represent all genes that changed significantly at 4 and 12 h, listed as a ratio of normalized treated/control values for increases, and control/treated for decreases. Actual spot intensities are available on CD-ROM by request from the author. Fig. 5 shows a typical stress array result, highlighting four genes (HSP70, $p21^{WAF1/CIP1}$, HO-1 and GADD153) that were significantly and reproducibly altered. Table 3 gives the results of the gene expression array and quantitative PCR experiments for the nine genes analyzed as raw intensities (array) and CT numbers (PCR); this information is presented graphically in Fig. 6. Shown in Fig. 7 is a portion of an Atlas array including the cDNA spots for mdr1 and HSP70. Clearly, adjacent HSP70 signal was also present in the mdr1 areas, obscuring the mdr1 signal itself. Taqman™ quantitative PCR helped to clarify the true signal strength and corroborated the mdr1 change.

A marked difference in gene expression can be misleading. As shown in Fig. 8A, the signal strength of HO-1 changes from an initial intensity (control) of 29 units to 2280 units at 12 h, a 78.7-fold change. HSP70 signal strength changes from an initial value of 298 units to 14,700 units, but the fold change is 49.2, less than that of HO-1 even though the absolute change in HSP70 signal strength was greater.

Comparison of Stress, Atlas array and Taqman data. Table 4 lists gene expression changes present on both the Rat Stress and Atlas arrays for $KBrO_3$ treated Fred-Pe cells. Check marks placed beneath 4 and 12 h signify that the listed array showed the change at the indicated time. Genes not included on the array are marked "NA". Stress and Atlas arrays results are in good agreement. The magnitude of changes varied considerably (compare Table 1 and 2 results for genes in Table 4), as might be expected for different hybridization events and their corresponding normalization. Asterisks denote Taqman-confirmed genes.

Analysis of the Platform: Ability of Data to Inform.

Noise (Background) and normalization. AtlasImage™ software allows for three kinds of background correction. The type used in this experiment was default external, which uses the median intensity of the blank area between the different panels of the array.

Bleed. Bleed can significantly confound interpretation of expression levels. For example, mdr-1 expression is increased by 66.6-fold at 12 h on the rat Atlas array (Table 1, Fig. 7), but is next to HSP70, which is expressed at 75 times the level of control, thus it was necessary to visually determine if bleed occurred. Stress array and Taqman data were also used in an attempt to determine how much of the apparent expression was real (Table 3). Taqman confirmed an

increase of six-fold for mdr-1. Therefore, array results must be interpreted with caution and results independently confirmed for a representative subset of genes.

Statistical Significance. There is no provision for determining statistical significance in the Atlas Vision 1.0™ software, necessitating the development of a suitable program (NLR) for use with gene expression arrays.

User-Friendliness. Gene expression array technology requires familiarity with basic molecular biology laboratory procedures. A skilled operator can align an array quickly in approximately 30 min, with fine tuning required. The generation of reports is straightforward, and hyperlinks provided on the template allow the user to link to key information quickly, without having to interrupt the flow of analysis.

Taqman™ analysis. Both at four and 12 h, nine gene changes were confirmed (Fig. 6 and Table 3). One gene failed to amplify in either treated or control samples, possibly due to a defect in the primer design or construction. The CT number of the failed sequence was 40, indicating that after all 40 cycles were complete, fluorescence intensity did not reach above that of background. Interestingly, the array results consistently underestimated the degree of change compared to Taqman results for up-regulated genes and overestimated the change for down-regulated genes, suggesting propagation of a determinate error (Day and Underwood, 1986). A method-based error is implied.

Immunohistochemistry. Control cells showed little or no HO-1-specific staining (Fig. 1C). Weak background staining appeared in negative control slides not treated with primary antibody. Immunostaining of $KBrO_3$-treated Fred-Pe cells revealed a distinctive pattern of specific staining (Fig. 1D). Vacuolation, or foaminess of cells was apparent starting at 4 h, and became marked at

12 h (Fig. 2). Dark staining surrounded and highlighted these “frothy” areas in the cells. Swelling of an unidentified sub-cellular compartment may account for this pattern.

Statistical analysis. Tables 1 and 2 list $p < 0.05$ values associated with fold-changes in gene expression.

Cell cycle arrest and re-emergence from arrest. After five days of exposure to 5 mM $KBrO_3$, approximately 95% of all mesothelial cells were dead and floating in the media. After replacement of the media, the remaining cells were seen to be severely damaged. Although the cells remained attached, only the nuclei had an intact periphery (putative phospholipid membrane). Cells remained phase-contrast bright at the edges, where edges could be distinguished. By light microscopic inspection, most intracellular structures appeared abolished or severely disturbed, with no-, or few/no- cell to cell contacts. Cells continued in this state for approximately four weeks, with fresh media replacement every 48 h. Attachment and phase-contrast brightness indicated cells were viable. After four weeks, slight evidence of cell repair was observed (intact plasmalemma and intracellular architecture were again visible); some cells acquired a terminally-differentiated appearance. (No cell division was visualized anywhere in the flask at this time.) Terminally-differentiated mesothelial cells are enlarged, with ruffled and irregular edges and thin, needle-like projections. Nuclei are small and usually contain several dark nucleoli. After approximately five weeks, a small nidus of 12 cells appeared. This focus grew exponentially, absorbing damaged cells nearby as it enlarged. Other foci then appeared in the flask, whether through migration or other cell divisions is not known. Cells exhibited an altered morphology from the parent (pre-exposure) line, being tiny, dark and stellate, but became indistinguishable from parent upon successive passaging. Cells of this lineage preferred to pile rather than spread horizontally, although ample living area was available (again, this tendency

decreased on further passaging). This cell population re-emerged from complete cell cycle arrest after five weeks, despite prolonged and severe toxic insult.

DISCUSSION

Gene expression array technology generates a large amount of data requiring careful interpretation. Many levels of control, in the form of both positive and negative feedback, are built into cellular physiology, ranging through chemical signals, allosteric regulation of enzymatically controlled metabolism, regulation of protein and mRNA transcript half lives, transcript copy number and speed of protein translation from such transcripts. The estimates of transcript levels revealed by expression arrays thus provide only a glimpse of the information flow circuitry of the cell. To interpret these data, gene products of interest must be divided into those that are transcriptionally regulated in response to stress, viz: γGCS (Rahman *et al*., 1996), HO-1 (Hartsfield *et al*., 1998) and a number of GSTs (Daniel, 1993), and those that are largely post-transcriptionally regulated, including p53 (Wang and Ohnishi, 1997) and ferritin (Goldenberg, 1997). For gene-related functions that are non-transcriptionally regulated, array data can provide indirect evidence of activation. For instance, up-regulation of mdm-2 and $p21^{WAF\text{-}1/CIP\text{-}1}$ (Wang and Ohnishi, 1997) or iNOS (Vos *et al*., 1999) indicate the possible activation of p53 or NF-κB, respectively. Such interpretations must also be cautiously undertaken, as alternative regulatory pathways exist (e.g., non-p53 mediated up-regulation of the influential cyclin dependent kinase inhibitor, $p21^{WAF\text{-}1/CIP\text{-}1}$)(Shao *et al*., 1995). Improved understanding of the regulatory networks underlying these events (Somogyi and Sniegoski, 1996) will lead to effective interpretation and application of data derived from gene expression platforms. The present data, however, show clear indications of oxidative stress and associated

cellular responses, including cell cycle arrest and possibly apoptosis, which have relevance to $KBrO_3$ toxicity and carcinogenicity.

How could growth arrest and apoptosis bring about cancer? Mitosis and apoptosis appear to be rather closely linked, e.g. the over-expression of c-myc in the presence of IL-2 induces proliferation but in its absence is associated with increased apoptosis (Bowen *et al.*, 1998). There seems to be a common factor of growth dysregulation to the initiation of apoptosis and mitogenesis in tumor promotion. In $KBrO_3$–induced toxicity, a few apoptosis-resistant cells, probably carrying a p53 or other mutation, may survive to become a promotable population. Gene expression array technology will allow the testing of this hypothesis using the cells propagated after re-emergence from complete cell cycle arrest in comparison with untreated populations. The investigation of how apoptosis participates in $KBrO_3$-induced toxicity may ultimately lead to an understanding of how cancer originates.

Gene expression analysis using cDNA arrays necessitates confirmation using other techniques. Taqman™ quantitative PCR compares favorably with traditional Northern analysis since it is reliable, uses less RNA and can analyze groups of ten or more genes at a time, depending on plate design. For those genes that appear to exhibit altered expression levels, how much of a fold change is statistically significant? In the method of choice, be it fluorescent or radioactive, glass slide or membrane, how much of a fold change is real, and how much is noise? How should background be calculated, signal strength normalized? The self-consistency and local regression technique used here (Kepler *et al.*, Submitted for Publication) represents an advance in these areas because it applies a rigorous statistical treatment of errors to the analytical process rather than an arbitrary cutoff based on empirical observations.

Morphologic evidence of apoptosis was seen in Fred-Pe cells by 30 min post-treatment and increased with exposure concentration and time. Array data revealed an increase in FasL, TNFα and iNOS1 at 12 h, all of which are implicated in the induction of apoptosis (Bowen *et al*., 1998). These data indicate that apoptosis and cell cycle arrest occur by four h, and are marked at 12 h. Expression of the apoptosis promoters bcl-X, bad, bax alpha and bok was decreased at 12 h and that of the anti-apoptotic gene bcl-2 increased. Thus two pathways appear to control the overall level of apoptosis. Furthermore, the activation of viral or cellular oncogenes, with concomitant growth signalling, results in apoptosis in cells expressing wild type, but not mutated p53 (Symonds *et al*., 1994). The present data show increased expression of APC[33], ODC[34] and telomerase protein component 1 at 12 h. This study also found decreased topoisomerase II transcript levels at 12 h after treatment, as well as changes in $p21^{WAF\text{-}1/CIP\text{-}1}$ and PCNA, as observed by Wang, et al. (1999) during the induction of apoptosis by etoposide. GPX1 was down-regulated after exposure of cells, in agreement with Amundson, et al. (Amundson *et al*., 1999) (who exposed human myeloid cells to ionizing radiation) for $p21^{WAF\text{-}1/CIP\text{-}1}$ and mdm2 but not for FRA-1 or ATF-3. Thus, many variations on the oxidative stress theme are possible.

As shown by others, evidence presented here implicates activation of p53 nuclear oncoprotein in cell cycle arrest and apoptosis. The regulation and function of the p53 tumor suppressor genes $p21^{WAF\text{-}1/CIP\text{-}1}$, GADD45, PCNA, cyclin G, bax, mdm-2 and IGF-BP3 as the transcriptional targets of p53 (affected during this study) is addressed in a recent review (Mansur, 1998). TNFα has also been reported to be a 'p53 inducible gene', or PIG (PIG7) (Polyak *et al*., 1997) as has a quinone oxidoreductase homologue and a microsomal GST homologue. A simplified model explaining the role of p53 in growth arrest and apoptosis (Fig. 9)

[33] adenomatous polyposis coli

suggests a change in cellular redox state stimulates activation of p53 and increases in p53 protein accumulation (possibly through an increase in $t^{1/2}$). Activated p53 then initiates transcription of its target genes, $p21^{WAF\text{-}1/CIP\text{-}1}$ protein levels increase, and CDK inactivation ensues. The present study indicates GADD45, PCNA and cyclin G were up-regulated at 12 h and mdm-2 at four and 12 h. Up-regulation of $p21^{WAF\text{-}1/CIP\text{-}1}$ (the universal CDK inhibitor) at four and 12 h and the cdk4 & cdk 6 inhibitor p14ink4b; p15ink4b occurred. Genes such as $p21^{WAF1/CIP1}$ are also up-regulated via non-p53-dependent pathways indicating a need for further investigation of these phenomena.

Several factors probably operate simultaneously to inhibit CDK's. $p21^{WAF\text{-}1/CIP\text{-}1}$ preferentially inhibits G_1 phase CDK's. Our data demonstrate a shutdown of cyclin expression. According to Fig. 9, an accumulation of hypophosphorylated activated Rb[35] protein occurs. Our results show a decrease in Rb2/p130 (retinoblastoma gene product-related protein) mRNA transcripts present in the cell at 12 h, which suggests that hypophosphorylated Rb may accumulate and inhibit complexation with the transcription factor E2F. The binding of E2F with Rb would then block the transcription of proteins needed for progression through the S phase of the cell cycle.

We observed down-regulation of cdc25B, cyclin B1, and cdk1 at 12 h, by which time no mitotic figures were present. p53 also plays a role in G_2 arrest as a mitotic checkpoint regulator (Cross, et al., 1995). p53 is largely post-translationally regulated, so its mRNA expression is not expected to change significantly during activation. However, since the level of wild type p53 protein observed in the cell does not always correlate to the level of p53 activation, protein assays for p53 might be misleading. A more accurate indicator of p53 activation is mdm2 expression. p53 activates mdm2 transcription and is itself down-regulated in a feedback loop

[34] ornithine decarboxylase
[35] retinoblastoma/p130

with mdm2. Here, the observed increase in mdm2, together with a small decrease in p53 nuclear oncoprotein mRNA transcript level, is consistent with this loop.

A dramatic and long-lasting increase in heme oxygenase 1 (HO-1) transcription occurred, together with a battery of heat shock factors and QR, and these responses were confirmed by Taqman™ analysis (HO-1, HSP70, QR). HO-1 specific immuno-staining also demonstrated increased protein levels. Since HO-1 is the rate-limiting enzyme in the catalysis of oxidized hemoglobin, producing bilirubin (an antioxidant/radical scavenger), carbon monoxide (an activator of guanylyl cyclase) and Fe^{3+}, its presence indicates oxidation of heme proteins, and represents an adaptive response to oxidative stress. HO-1 induction occurs following exposure to heavy metals, endotoxin, heat shock, inflammatory cytokines and hormones, and prostaglandins (Choi and Alam, 1996). Thus, induction of HO-1 and associated genes is a potential biomarker for oxidative stress in the male F344 rat.

$KBrO_3$ acts as a GSH depleting agent, reducing the cellular level of GSH by 41% in rat pleural mesothelial cells after 15 min and by close to 100% after four h (Crosby *et al*., in Press). $KBrO_3$ induces lipid peroxidation *in vivo* (Sai *et al*., 1992; Umemura *et al*., 1995), 8-OH deoxyguanosine adducts (Kasai *et al*., 1987; Lee *et al*., 1996; Umemura *et al*., 1998), poly-(ADP-ribosyl)ation (McLaren *et al*., 1994) and cell proliferation (Umemura *et al*., 1993) in the F344 rat kidney and micronucleated reticulocytes in CD-1 male mice (Awogi *et al*., 1992). We observed that GADD45 and GADD153, msh2 DNA mismatch repair protein, O-6 methylguanine DNA methyltransferase and PCNA, were induced by 12 h, indicating DNA repair activity. Proteasome components and ubiquitin transcription increased, indicating probable protein damage to the cell by four hours. PLA2, which cleaves lipid hydroperoxides from membranes so

that they may be metabolized to less harmful products, also increased 10-fold by 12 h, along with numerous fatty acid synthesis and metabolism components. Induction of these components is evidence of oxidative damage to DNA/RNA, proteins and lipids.

Re-emergence of rat pleural mesothelial cells from prolonged growth arrest induced by $KBrO_3$ was observed, suggesting that $KBrO_3$-induced growth arrest in cells that do not undergo the associated mitotic catastrophe, apoptosis, or necrosis seen in the majority of cells, is a reversible phenomenon. Together with gene expression array data demonstrating increased DNA repair activity within treated mesothelial cells *in vitro* (and lipid peroxidation and adduct formation *in vivo*) this finding suggests that imperfect DNA repair could result in the fixation of mutations in the genome. We have here shown that exposure of rat mesothelial cells to six mM $KBrO_3$ induces DNA, protein and lipid peroxidation, apoptosis and reversible mitotic arrest. It is suggested that $KBrO_3$-damaged cells may survive and become transformed.

In summary, we propose the following scheme, depicted in Fig. 10: $KBrO_3$ depletes GSH (A), promoting lipid peroxidation (B) and direct oxidation of key cysteine residues in cellular receptors (such as growth factor receptors), activating signal transduction (C) and generating a redox signal (D). Redox imbalance thus increases membrane lipid peroxidation, receptor and kinase cascade activation (E) (via stimulation of tyr, ser/thre phosphorylation reactions and suppression of phosphatase activity). IκB phosphorylation and ubiquitination allows dissociation from, and activation of, NFκB (F). The MAPK cascade activates transcription of early response genes c-jun and c-fos (G), followed by activation of AP-1 (H) and NFκB (F). The latter bind to promoter regions of key genes (GPX, QR, GST, HO-1) involved in the antioxidant response (I) and up-regulate their transcription (J). At the plasma membrane, PLA2 excises phospholipid hydroperoxides from the membrane (K) and GST's catalyze their reduction to the corresponding

alcohols, further depleting GSH (L). Increased transcription of proteasome components (Rδ, RC10-II, C3, RC-7), HR6B ubiquitin-conjugating enzyme, and ubiquitin in order to rid the cell of non-functional oxidized proteins may occur (M). Hallmark oxidative stress displays increased expression of heat shock proteins (chaperonins) which participate in the generation of a redox signal (D) and protein turnover (N). Oxidation of key p53 cysteine residues may lead to increased transcription of $p21^{WAF\text{-}1/CIP\text{-}1}$, GADD45, and GADD153, accompanied by increased cyclin G and decreased cyclins B, C, D1, D2, D3 and E expression (O), resulting in G_1 cell cycle arrest (P). In this scenario, the cell is stimulated by autocrine growth factor loops and autophosphorylation proceeding from the stimulation of signal transduction pathways, culminating in loss of growth control. The eventual re-emergence of the cell from G_1 into S phase coupled with severe DNA damage/incomplete repair may result in mutational fixation in the genome. Inappropriate urokinase receptor up-regulation may stimulate extracellular matrix invasive properties of cells. Data presented is consistent with this sequence of events based on gene expression patterns observed *in vitro*.

ACKNOWLEDGEMENTS

This work was supported by a GAANN Fellowship (US Dept. of Education), US EPA-North Carolina State University Co-Operative Training Grant Fellowship, and GlaxoWellcome Inc. The opinions contained herein do not represent US EPA policy.

REFERENCES

Amundson, S. A., Bittner, M., Chen, Y., Trent, J., Meltzer, P. and A.J. Fornace, J. (1999). Fluorescent cDNA microarray hybridization reveals complexity and heterogeneity of cellular genotoxic stress responses. *Oncogene* **18,** 3666-72.

Awogi, T., Murata, K., Uejima, M., Kuwahara, T., Asanami, S., Shimono, K. and Morita, T. (1992). Induction of micronucleated reticulocytes by potassium bromate and potassium chromate in CD-1 male mice. *Mutation Research* **278,** 181-185.

Beckman, K. B. and Ames, B. N. (1997). Oxidants, Antioxidants and Aging. In *Oxidative Stress and the Molecular Biology of Antioxidant Defenses* (ed. J. G. Scandalios), pp. 889. Cold Spring Harbor: Cold Spring Harbor Laboratory Press.

Bensasson, R. V., Land, E. J. and Truscott, T. G. (1993). Excited States and Free Radicals in Biology and Medicine: Contributions from Flash Photolysis and Pulse Radiolysis, pp. 431. Oxford: Oxford University Press.

Bowen, I. D., Bowen, S. M. and Jones, A. H. (1998). Mitosis and Apoptosis: Matters of Life and Death, pp. 180. New York, NY: Chapman & Hall.

Choi, A. M. K. and Alam, J. (1996). Heme Oxygenase-1: Function, Regulation, and Implication of a Novel Stress-inducible Protein in Oxidant-induced Lung Injury. *Am. J. Respir. Cell Mol. Biol.* **15,** 9-19.

Commoner, B., Townsend, J. and Pake, G. E. (1954). Free radicals in biological materials. *Nature* **174,** 689-691.

Crosby, L. M., Morgan, K. T. and DeAngelo, A. B. (in Press). Studies of Mesothelial and HepG2 Cells Demonstrate That GSH Depletion Plays a Key Role in KBrO3 Toxicity. .

Daniel, V. (1993). Glutathione S-transferases: gene structure and regulation of expression. *Critical Reviews in Biochemistry and Molecular Biology* **28,** 173-207.

Day, R. A. and Underwood, A. L. (1986). Quantitative Analysis, 5th Edn. Englewood Cliffs, NJ: Prentice-Hall.

DeAngelo, A. B., George, M. H., Kilburn, S. R., Moore, T. M. and Wolf, D. C. (1998). Carcinogenicity of Potassium Bromate Administered in the Drinking Water to Male B6C3F1 Mice and F344/N Rats. *Tox. Path.* **26,** 587-594.

Fridovich, I. (1978). Superoxide radicals, superoxide dismutases and the aerobic lifestyle. *Photochem. Photobiol.* **28,** 733-41.

Gerschman, R., Gilbert, D. L., Nye, S. W., Dwyer, P. and Fenn, W. O. (1954). Oxygen poisoning and X-irradiation: A mechanism in common. *Science* **119,** 623-6.

Goldenberg, H. A. (1997). Regulation of mammalian iron metabolism: current state and need for further knowledge. *Critical Reviews in Clinical Laboratory Sciences* **34,** 529-572.

Harman, D. (1956). Aging: A theory based on free radical and radiation chemistry. *J. Gerontol.* **2,** 298-300.

Hartsfield, C. L., Alam, J. and Choi, A. M. (1998). Transcriptional regulation of the heme oxygenase-1 gene by pyrrolidine dithiocarbamate. *FASEB J.* **12,** 1675-1682.

Hayashi, Y., Kurokawa, Y., Maekawa, A. and Takahashi, M. (1986). Strategy of long-term animal testing for quantitative evaluation of chemical carcinogenicity. In *New Concepts and Developments in Toxicology* (ed. P. L. Chambers, P. Gehring and F. Sakai), pp. 383-391. New York: Elsevier Science Publishers.

Kasai, H., Nishimura, S., Kurokawa, Y. and Hayashi, Y. (1987). Oral administration of the renal carcinogen, potassium bromate, specifically produces 8-hydroxydeoxyguanosine in rat target organ DNA. *Carcinogenesis* **12,** 1959-1961.

Kepler, T. B., Crosby, L. M. and Morgan, K. T. (In Press). Normalization and analysis of DNA hybridization microarrays by self-consistency and local regression. .

Kurokawa, Y. (1985). Overview on the toxicity and carcinogenicity of potassium bromate (in Japanese). *Kosankinbyo Kenkyuzasshi* **37,** 139-149.

Kurokawa, Y., Aoki, K., Imazawa, T., Hayashi, Y., Matsushima, Y. and Takamura, N. (1985). Dose-related enhancing effect of potassium bromate on renal tumorigenesis in rats initiated with N-ethyl-N-hydroxyethylnitrosamine. *Jpn. J. Cancer Res. (Gann)* **76,** 583-589.

Kurokawa, Y., Aoki, S., Matsushima, Y., Takamura, N., Imazawa, T. and Hayashi, Y. (1986a). Dose-response studies on the carcinogenicity of potassium bromate in F344 rats after long-term oral administration. *J. Natl. Cancer Inst.* **77,** 977-982.

Kurokawa, Y., Hayashi, Y., Maekawa, A., Takahashi, M. and Kokubo, T. (1982). Induction of renal cell tumors in F-344 rats by oral administration of potassium bromate, a food additive. *Gann* **73,** 335-338.

Kurokawa, Y., Hayashi, Y., Maekawa, A., Takahashi, M., Kokubo, t. and Odashima, S. (1983a). Carcinogenicity of potassium bromate administrated (sic) orally to F344 rats. *J. Natl. Cancer Inst.* **71,** 965-972.

Kurokawa, Y., Matsushima, Y., Takamura, M., Imazawa, T. and Hayashi, Y. (1987). Relationship between the duration of treatment and the incidence of renal cell tumors in male F344 rats administered potassium bromate. *Jpn. J. Cancer Res. (Gann)* **78,** 358-364.

Kurokawa, Y., Takahashi, M., Kokubo, T., Ohno, Y. and Hayashi, Y. (1983b). Enhancement by potassium bromate of renal tumorigenesis initiated by N-ethyl-N-hydroxyethylnitrosamine in F-344 rats. *Gann* **74,** 607-610.

Kurokawa, Y., Takayama, S., Konishi, Y., Hiasa, Y., Asahina, s., Takahashi, M., Maekawa, A. and Hayashi, Y. (1986b). Long-term in vivo carcinogenicity test of potassium bromate, sodium hypochlorite and sodium chlorite conducted in Japan. *Environ. Health Perspect.* **69,** 221-235.

Lee, Y., Choi, J., park, M., Choi, E., Kasai, H. and Chung, M. (1996). Induction of oh-8-Gua glycosylase in rat kidneys by potassium bromate (KBrO3) a renal oxidative carcinogen. *Mutation Research* **364,** 227-233.

Li, N. and Oberley, T. D. (1998). Modulation of antioxidant enzymes, reactive oxygen species, and glutathione levels in manganese superoxide dismutase-overexpressing NIH/3T3 fibroblasts during the cell cycle. *J. Cell Physiol.* **1771,** 148-60.

Mansur, C. P. (1998). The Regulation and Function of the p53 Tumor Suppressor. *Advances in Dermatology* **13,** 121-165.

Matsumoto, I. (1973). Clinical and experimental studies on ototoxicity of bromate (in Japanese). *Otol. Fukuoka* **19,** 220-236.

McLaren, J., Boulikas, T. and Vamvakas, S. (1994). Induction of poly(ADP-ribosyl)ation in the kidney after in vivo application of renal carcinogens. *Toxicology* **88,** 101-112.

Ohno, Y., Onodera, H., Takamura, N., Imazawa, T., Maekawa, A. and Kurokawa, Y. (1982). Carcinogenicity testing of potassium bromate in rats (in Japanese). *Bull. Natl. Inst. Hyg. Sci.* **100,** 93-100.

Oinuma, T. (1974). 8 cases of death by intoxication of potassium bromate (in Japanese). *Nichidaiishi* **33,** 759-766.

Onodera, H., Tanigawa, H., Matsushima, Y., Maekawa, A., Kurokawa, Y. and Hayashi, Y. (1985). Eosiniphilic bodies in the proximal renal tubules of rats given potassium bromate (in Japanese). *Bull. Natl. Inst. Hyg. Sci.* **103**.

Palmeira, C. M., Moreno, A. J. and Madeira, V. M. C. (1994). Metabolic alterations in hepatocytes promoted by the herbicides paraquat, dinoseb and 2,4-D. *Arch. Tox.* **68,** 24-31.

Polyak, K., Xia, Y., Zweier, J. L., Kinzler, K. W. and Vogelstein, B. (1997). A model for p53-induced apoptosis. *Nature* **389,** 300-305.

Rahman, I., Mulier, B. A., Lawson, M. F., Harrison, D. J., Macnee, W. and Smith, C. A. (1996). Transcriptional regulation of gamma-glutamylcysteine synthetase-heavy subunit by oxidants in human alveolar epithelial cells. *Biochem. Biophys. Res. Comm.* **229,** 832-837.

Sai, K., Umemura, T., Takagi, A., Hasegawa, R. and Kurokawa, Y. (1992). The Protective Role of Glutathione, Cysteine and Vitamin C against Oxidative DNA Damage Induced in Rat Kidney by Potassium Bromate. *Jpn. J. Cancer Res.* **83,** 45-51.

Shao, Z. M., dawson, M. I., Li, X. S., Rishi, A. K., Sheikh, M. S., Han, Q. X., Ordonez, J. V., Shroot, B. and Fontana, J. A. (1995). p53 independent G0/G1 arrest and apoptosis induced by a novel retinoid in human breast cancer cells. *Oncogene* **11,** 493-504.

Somogyi, R. and Sniegoski, C. A. (1996). Modelling the Complexity of Genetic Networks: Understanding Multigenic and Pleiotropic Regulation. In *Complexity*, pp. 45-63. New York, NY: J. Wiley & Sons, Inc.

Stein, G. and Weiss, J. (1948). Chemical effects of ionizing radiations. *Nature* **161,** 650.

Sun, Y. and Oberley, L. (1996). Redox Regulation of Transcriptional Activators. *Free Radical Biology & Medicine* **21,** 335-348.

Symonds, H., Krail, L. and Remington, L. (1994). p53-dependent apoptosis suppresses tumor growth and progression in vivo. *Cell* **78,** 703-711.

Takamura, N., Kurokawa, Y., Matsushima, Y., Imazawa, T., Onodera, H. and Hayashi, Y. (1985). Long-term oral administration of potassium bromate in male Syrian golden hamsters. *Sci. Rep. Res. Inst. Tohoku Univ., Ser. C* **32,** 43-46.

Taniguchi, N. (1989). Glutathione Centennial: Molecular Perspectives and Clinical Implications. New York: Academic Press Inc.

Tauber, A. I. and Babior, B. M. (1978). O(2)-. and host defence: the production and fate of O(2)-. in neutrophils. *Photochem. Photobiol.* **28,** 701-9.

Umemura, T., Sai, K., Takagi, A., Hasegawa, R. and Kurokawa, Y. (1993). A possible role for cell proliferation in potassium bromate (KBrO3) carcinogenesis. *Cancer Research Clinical Oncology* **119,** 463-469.

Umemura, T., Sai, K., Takagi, A., Hasegawa, R. and Kurokawa, Y. (1995). A possible role for oxidative stress in potassium bromate (KBrO3) carcinogenesis. *Carcinogenesis* **16,** 593-597.

Umemura, T., Takagi, A., Sai, K., Hasegawa, R. and Kurokawa, Y. (1998). Oxidative DNA damage and cell proliferation in kidneys of male and female rats during 13-weeks exposure to potassium bromate (KBrO3). *Arch. Toxicol.* **72,** 264-269.

Vos, T. A., Goor, H. v., Tuyt, L., Jager-Kridden, A. d., Leuvenink, R., Kuipers, F., Jansen, P. L. M. and Moshage, H. (1999). Expression of inducible nitric oxide synthase in

endotoxemic rat hepatocytes is dependent on the cellular glutathione status. *Hepatology* **29,** 421-426.

Wang, X. and Ohnishi, T. (1997). p-53-Dependent signal transduction induced by stress. *J. Radiation Res.* **38,** 179-194.

Wang, Y., Rea, T., Bian, J., Gray, S. and Sun, Y. (1999). Identification of the genes responsive to etoposide-induced apoptosis: application of DNA chip technology. *FEBS Lett.* **445,** 269-73.

Table 1. List of Selected mRNA's Significantly Up-regulated in $KBrO_3$ Treated Fred-Pe vs. Ctrl. ($p < 0.05$)

*Taqman confirmed expression changes.

	Ratio	
Transcription Factors	**4 h**	**12 h**
I-κB	1.4	2.1
*p21/waf1/cip1	10.0	17.6
c-myc	2.5	2.5
c-Jun	----	3.3
c-Fos	3.4	23.4
Jun-D	1.8	1.9
Jun-B	----	2.0
Signal Transduction/Growth Factors		
Sulfonylurea receptor	----	6.7
Nur77 early response protein; NGF-1 (nerve growth factor 1)	2.9	1.7
presenilin-2 (PS-2) homolog of Alzheimer's Disease susceptibility gene	9.6	----
presenilin-1 (PS-1) " "	3.9	----
signal transducer CD24 precursor	3.2	----
integrin beta 4 subunit precursor	2.5	----
CXC chemokine LIX	3.6	----
Transferrin receptor protein (p90)	----	2.3
Vegfr2; KDR/flk1 vascular endothelial growth factor tyrosine kinase receptor	----	2.0
Grb2; growth factor receptor-bound protein 2	----	2.2
Jnk1 stress-activated protein kinase	----	1.5
MAPKK1; MAP kinase kinase 1 (dual specificify) ERK activator kinase	----	1.5
Protein phosphatase 2A-beta catalytic subunit	----	1.3
Nuclear tyrosine phosphatase (PRL-1)	----	1.9

Adenosine A2b Receptor	----	----
Calcitonin receptor precursor	----	4.4
Metabotropic glutamate receptor 6 precursor	----	3.1
Glutamate receptor 2 precursor (GLUR-2)	----	2.4
Glutamate receptor 3 precursor (GLUR-3)	----	2.9
Glutamate receptor 4 precursor (GLUR-4)	----	2.0
Urokinase Receptor	----	5.8
β-Nerve Growth Factor Precursor	----	2.3
Growth factor (Arc)	----	18.3

Protein Synthesis and Degradation/Repair

Proteasome subunit R-iota	3.1	----
Proteasome activator rPA28 subunit alpha	2.5	----
Pancreatic secretory trypsin inhibitor 1 precursor	2.1	----
Mast cell protease 6 precursor (RMCP-6)	2.8	----
Serine protease RNK-MET1	3.6	1.5
Tissue-type plasminogen activator (t-PA)	2.9	1.3
chymotrypsinogen B precursor (EC 3.4.21.1)	----	2.2
Proteasome component R-Zeta	----	1.4
α-tubulin	3.1	2.2
ubiquitin	----	10.1
tissue inhibitor of metalloproteinase-1 (TIMP-1)	----	2.3
proteasome component C3	----	1.4
proteasome subunit RC7-1	----	1.7
metalloendopeptidase meprin β subunit	----	2.4
tissue carboxypeptidase inhibitor (TCI)	----	2.8

DNA Repair

HR6B ubiquitin-conjugating enzyme	----	2.0
msh2 DNA mismatch repair protein; MutS homolog 2	----	1.7
O-6 methylguanine DNA methyltransferase	----	2.2
Telomerase protein component 1 (TLP1)	----	1.6

*GADD 45	----	29.0
GADD 153	----	19.0
PCNA	----	1.7

Apoptosis

Fasl; Fas antigen ligand	----	7.8
TNFα (tumor necrosis factor α)	----	1.4
iNOS1 (inducible nitric oxide synthase)	----	1.9

Cell Cycle Control

cyclin G	----	3.4
p14ink4b;p15ink4b; cdk4 & cdk6 inhibitor	3.2	6.0
p27kip1; G1 cyclin-Cdk protein kinase inhibitor, p21 related	----	2.2
(this result confounded due to bleed from adjacent p21)		

Fatty Acid Biosynthesis and Repair

BiP steroidogenesis-activator polypeptide, IgG heavy chain binding protein	----	3.2
Fatty acid binding protein, epidermal (E-FABP)	----	3.3
Cytosolic phospholipase A2	----	1.6
Serine phospholipid-specific phospholipase A (PS PLA1 precursor)	----	1.4
Steryl-sulfatase precursor (steroid sulfatase)	----	5.1
Fatty acid binding protein, adipocyte (AFABP)	----	2.6
Sterol 26-hydroxylase mitochondrial precursor	2.0	----
20-Alpha-hydroxysteroid dehydrogenase (EC 1.1.1.149)	----	3.9
Bile-salt-activated lipase precursor (EC 3.1.1.3)(EC 3.1.1.3)	2.0	
Phospholipase A2 precursor (EC 3.1.1.4)	----	10.1

Oxidative Stress/Imbalance

Tpx thioredoxin peroxidase	----	2.0
GST pi class; preadipocyte growth factor	----	1.8

GST (theta type 1)	----	1.3
HSP 27 heat shock 27 kDa protein 1	----	6.2
HSP 60 heat shock 60 kDa protein 1 (chaperonin)	----	3.4
*HSP 70 heat shock 70 kDa protein	11.4	75.0
glyceraldehyde 3 phosphate dehydrogenase (GAPDH) 10.9	1.3	
P450 IA1; P450-C; 3-methylcholanthrene inducible	----	3.3

Cell Membrane Transport: Import/Export

mdr1; P-glycoprotein; multidrug resistance protein; efflux pump	----	57
Cardiac delayed rectifier potassium channel protein	2.1	----
Aquaporin (pancreas & liver, AQP 8)	2.3	----
CAT-1 (cationic amino acid transporter)	----	4.5
monocarboxylate transporter (MCT1)	----	4.8
sodium/bile acid cotransporter	----	2.3
glycine transporter	----	2.7
sodium dependent sulfate transporter	----	3.0
proton gated cation channel drasic	----	2.0
degenerin channel MDEG; amiloride-sensitive brain	2.6	----

Miscellaneous

E-Selectin Precursor (ELAM-1)	----	2.9
Protocadherin 4	----	2.5
Cadherin 6 precursor	----	2.2
Short-type PB cadherin	3.1	1.4
CD44 antigen precursor (Phagocytic glycoprotein 1)	----	2.3
amphiphysin II	----	5.0
Clusterin (testosterone-repressed prostate message 2)	----	3.6
Set β isoform + set α isoform	2.4	1.3
LRP; major vault protein (MVP)	5.6	3.0
B7.1	1.7	4.3
RET ligand 1 (RET 1)	2.4	----

Hormonal Activity

IRF-1 interferon regulatory factor 1	----	2.7
Somatoliberin Precursor (Growth Hormone-releasing Factor) (GRF)	----	2.7
Androgen binding protein	2.4	----
Follicle stimulating hormone beta subunit	2.1	----

Tumor Suppressor/Oncogene/Tumor Biomarker

APC (adenomatous polyposis coli protein)	----	1.8
ornithine decarboxylase (ODC)	----	2.3
34A transformation-associated protein; TAP-related	1.8	2.9
Von Hippel-Lindau tumor suppressor protein	----	1.5
c-Ets-1 (p54) protoo-oncogene protein	----	1.8
Pim-1 proto-oncogene	----	1.6

Clontech Rat Stress Array: Up-regulated mRNA's ($p < 0.05$)

	4 h	12 h
Signal Transduction/Growth Factors		
PKC zeta interacting protein	2.7	3.1
*p21; cip1; waf1	9.2	8.3
Growth-related c-myc-responsive protein; RCL	----	1.6
Protein Synthesis and Degradation/Repair		
Polyubiquitin	1.7	2.1
DNA Repair		
mdm2 protein; p53-associated protein+ mdm2-A + mdm2-C	5.9	1.4
*GADD45	8.4	12.5
GADD153	3.0	10.6
PCNA	----	1.7
Apoptosis		
Apoptosis regulator bcl-2	----	9.3
Fatty Acid Biosynthesis and Repair		
Phospholipase A2 precursor	2.1	2.3
Oxidative Stress/Imbalance		
Glutathione S-transferase P subunit; GST subunit 7 Pi	1.4	----
HSP27	1.7	4.6
HSP90	2.0	1.8
*HSP70	11.0	49.2

HSC73;HSC70 heat shock cognate 71 kDa protein	2.3	2.3
HSP70/HSP90-organizing protein (HOP); p60 protein	1.3	----
HSP10; chaperonin 10	1.5	1.7
*Heme oxygenase 1	40.3	78.7
*NAD(P)H dehydrogenase; quinone reductase	2.2	2.3

Table 2. List of mRNA's Significantly **Down-regulated** in 6 mM $KBrO_3$ Treated Fred-Pe Cells vs. Ctrl. ($p < 0.05$)

	4 h	12 h
Transcription Factors		
Jun-D; c-jun-related transcription factor	-1.8	-1.9
Id-1; DNA-binding protein inhibitor; HLH protein	-2.8	-2.4
Fibroblast growth factor	-4.6	----
Urokinase-type plasminogen activator precursor	-3.3	----
Fra-2 (fos-related antigen 2); Fosl 2	----	-3.3
NFκB p105; NF-kappa-B transcription factor p105 subunit	----	-1.5
Signal Transduction/Growth Factors		
Platelet-derived growth factor alpha receptor	-2.0	-5.2
Erk 1; MAPK1; extracellular signal-regulated kinase 1	-2.0	-2.2
RalGDSB; GTP/GDP dissociation stimulator for a ras	-1.9	-4.2
Glutamate receptor precursor (GLUR7)	-3.3	----
Adenosine A2b receptor	----	-8.0
Cak tyrosine-protein kinase; EDDR1	----	-2.8
Rac-beta serine/threonine protein kinase	----	-2.3
cAMP-dependent protein kinase catalytic subunit	----	-2.1
Jnk2 stress-activated protein kinase (SAPK-alpha); c-Jun N-terminal kinase	----	-2.1
MAP kinase p38; mitogen-activated protein kinase p38	----	-7.4
FAK; focal adhesion protein-tyrosine kinase	----	-3.3
PKN cell morphology-related protein kinase; homologous to PKC	----	-3.6
CAK beta; cell adhesion kinase beta; calcium dependent, FAK family	----	-3.3
PLC beta 3; phospholipase C beta 3	----	-4.9
PLC beta 1; phospholipase C beta 1	----	-2.3
PLC gamma-1; phospholipase C gamma 1	----	-2.0
PLC delta-1; phospholipase C delta 1	----	-3.3
Ral B; GTP-binding protein	----	-2.0
G12; G-alpha-12 guanine nucleotide regulatory protein	----	-2.4

Transducin beta-2 subunit; GTP-binding protein G(i)/G(s)/G(t) beta subunit	----	-2.2
M-ras protein, closely related to ras proto-oncogenes	----	-3.0
Rad (Ras associated with diabetes); Rad 1	----	-2.2
Adenylyl cyclase type VI; calcium-inhibitable	----	-2.7
rRAFT1; rapamycin and FKBP12 target 1 protein;	-2.7	-3.5
presenilin-2 (PS-2)	----	-2.1
SHPS-1 receptor like protein with SH2 binding site	----	-3.5
Transmembrane receptor UNC5H2	----	-2.5
Protein Synthesis and Degradation/Repair		
Stromelysin 3; matrix metalloproteinase-11	----	-2.3
Tissue carboxypeptidase inhibitor (TCI)	-2.4	----
Ribosomal protein S29	-3.0	-1.4
Matrix metalloproteinase-14 precursor (EC 3.4.24)	----	-3.0
Beta-actin + gamma-actin	----	-3.8
DNA Repair		
DNA Topoisomerase II (Top II alpha)	----	-1.9
Cell Cycle Control		
Cyclin C (G1-specific	-1.9	-3.4
Wee1/p87; cdc2 tyrosine 15-kinase	-1.8	-2.8
Cyclin B1 (G2/M specific)	----	-2.8
*Cyclin D1 (G1/S specific)	----	-4.9
Cyclin D2 (G1/S-specific); Vin-1 proto-oncogene	----	-2.5
Cyclin D3 (G1/S-specific)	----	-4.6
Cyclin E (G1/S-specific)	----	-1.9
Cdk4; cyclin-dependent kinase 4	----	-3.1
Cdk5; cyclin-dependent kinase 5; Tau protein kinase II	----	-2.7
Cdk1; cdc2 kinase homolog; cyclin-dependent kinase 1	----	-5.9
Cdk2; (alpha alt. Splice variant); cyclin-dependent kinase 2 alpha	----	-1.3

Cdc25b; cdc25M2; MP12 (M-phase inducer phosphatase 2)	----	-4.1
Apoptosis		
Interleukin-1 beta convertase precursor IL-1BC; caspase 1	----	-2.8
Bad; heterodimeric partner for Bcl-XL and Bcl-2	----	-2.1
Bax; Bcl-2 heterodimerization partner and homolog	----	-1.3
Bcl-X apoptosis regulator	----	-1.7
Oxidative Stress/Imbalance		
Glutathione S-transferase (microsomal)	----	-1.5
Cell Membrane Transport: Import/Export		
Water channel aquaporin 3 (AQP3)	----	-2.8
Protein kinase C-regulated chloride channel	-1.6	-2.2
Kidney glomeruli chloride channel (CIC-5)	-2.0	----
Voltage gated potassium channel; kv43	-2.1	----
Chloride channel RCL1	-3.0	-1.4
Beta-alanine sensitive neuronal GABA transporter	-6.4	----
Insulin-like growth factor binding protein 3 precursor	----	-1.4
Miscellaneous		
Cathepsin E		-4.5
Prothymosin alpha	----	-1.9
Calmodulin	----	-4.5
Beta-Arrestin 1	----	-3.9
Frizzled-1 (FZ-1); Drosophila tissue polarity gene homolog	----	-6.9
Hormonal Activity		
Growth hormone receptor	-2.4	----
Thyrotropin releasing hormone (TRH) precursor	-3.2	----

Presomatotropin	----	-3.2
Platelet activating factor receptor	----	-2.1
Prostaglandin F2 alpha receptor	----	-7.6
Testicular luteinizing hormone beta-subunit	----	-2.3

Tumor Suppressor/Oncogene/Tumor Biomarker

Ear-2; rCOUPg; v-erbA related proto-oncogene	-1.8	-3.8
Sky proto-oncogene; Tyro3; Rse; Dtk	-3.8	-3.3
Ornithine decarboxylase (ED 4.1.1.17; ODC)	-4.1	----
NF-2; merlin (moesin-ezrin-radixin-like protein); Shwannomin	----	-2.6
p130; Retinoblastoma gene product-related protein RB2/p130	----	-3.4
WT1; Wilms' tumor protein; tumor suppressor	----	-2.7
Mxi1; rMxi1; Myc-max-interacting tumor suppressor	----	-2.1
c-Raf proto-oncogene; Raf-1	----	-2.1
c-Met proto-oncogene (hepatocyte growth factor, HGF, receptor)	-2.7	
ErbB2 EGF receptor-related proto-oncogene	----	-3.3
c-Akt proto-oncogene; Rac-alpha; protein kinase B	----	-2.3

Clontech Rat Stress Array: Down-regulated mRNA's

Transcription Factors	4 h	12 h
Signal Transduction/Growth Factors		
Erk1 (MAPK1)	-1.3	-4.5
Erk2 (MAPK2)	----	-2.2
MAP kinase p38 (CSBP2)	-1.6	-13.8
MAP kinase kinase 2 (MAPKK2)	----	-4.5
SPS1/Ste20 homolog KHS1	----	-2.9
AIM-1	-1.5	-18.4
Nck, ash & phospholipase C gamma-binding protein	----	-3.3
DNA Synthesis/Repair		
DNA topoisomerase II alpha (TOP2A)	----	-2.2
DNA topoisomerase IIB (TOP2B)	----	-14.5
DNA-binding protein inhibitor ID-1	-2.5	-3.5
DNA-binding protein inhibitor ID-2	-3.5	----
DNA-binding protein inhibitor ID-3	-5.5	-12.5
Purine-rich single-stranded DNA-binding Protein alpha (PURA)	-1.9	-6.8
Heterogeneous nuclear ribonucleoprotein K (HNRNPK)	----	-2.0
Apurinic/appyridinic endonuclease (AP endonuclease)	----	-2.3
G/T mismatch-specific thymine DNA glycosylase (TDG)	-1.7	-3.3
Poly(ADP-ribose) polym. (PARP); NAD+ ADP-ribosyltransferase (ADPRT)	-1.4	-8.3
DNA excision repair protein ERCC1	----	-2.1
Replication protein A 32-kDa subunit (RPA)	----	-7.8
DNA polymerase delta catalytic subunit (POLD1)	----	-12.9
RecA-like protein HsRad51; DNA repair protein RAD51 homolog	----	-19.3
17 kDa ubiquitin-conjugating enzyme E2 (UBE2B)	----	-1.4
structure-specific recognition protein 1 (SSRP1) recomb. signal sequ.recog.	----	-3.7
high mobility group protein 2 (HMG2)	-2.2	-5.7
msh2 DNA mismatch repair protein	----	-19.0

Cell Cycle Control

M-phase inducer phosphatase 2 (MPI2); cell division control protein 25B (CDC25B)	-3.1	-20.6
cell division control protein 2 homolog (CDC2); cyclin dependent kinase 1 (CDK1)	-1.6	-23.4
cyclin-dependent kinase 2 alpha (CDK2-alpha) + cyclin-dep. kinase 2 beta (CDK2-beta)	----	-2.6
cyclin-dependent kinase 4 (CDK4); cell division protein kinase	----	-5.6
cyclin-dependent kinase 5 (CDK5); tau protein kinase II	----	-6.6
CDC-like kinase 3 (CLK3)	-1.6	-3.5
G2/M specific cyclin B1 (CCNB1)	----	-15.5
G1/S specific cyclin C (CCNC)	----	-14.5
*G1/S specific cyclin D1 (CCND1)	-1.9	-11.9
G1/S specific cyclin D2 (CCND2); vin-1 proto-oncogene	----	-4.6
G1/S Specific cyclin D3 (CCND3)	-1.9	-10.0
G1/S Specific cyclin E (CCNE)	-1.5	-4.9
p27/kip1	-3.8	-5.4
p55 CDC	-2.4	-21.4
galactosyltransferase-assoc. protein kinase (GTA); CDC-2 related	----	-3.8
replication protein A 32 kDa subunit	----	-7.8

Apoptosis

Apoptosis regulator bcl-x	----	-2.8
bcl-2-associated death promoter (BAD)	-1.4	-5.6
apoptosis regulator BAX-alpha	----	-3.3
bcl-2-related ovarian killer protein (BOK)	----	-3.1

Fatty Acid Biosynthesis and Repair

Long chain-specific acyl-CoA dehydrogenase precursor	----	-5.7

Oxidative Stress/Imbalance

HSP60 heat shock 60-kDa protein	----	-1.4
HSP47 heat shock 47-kDa protein	----	-2.2
HSP70/HSP90-organizing protein (HOP)	----	-1.3
HSC70-interacting protein (HIP)	----	-1.6
HSPB2	----	-5.1
Heme oxygenase 2	----	-2.1
94 kDa glucose-regulated protein (GRP94); endoplasmin precursor	----	-2.5
mitochondrial stress-70 protein precursor (MTHSP70)	----	-1.4
crystallin alpha B (CRYAB)	----	-2.6
calcium binding protein 2 (CABP2)	----	-2.4
150 kDa oxygen-regulated protein (ORP150)	----	-2.2
copper-zinc containing superoxide dismutase 1 (Cu/Zn SOD1)	----	-1.5
liver catalase (CAT)	----	-1.8
adrenodoxin precursor; adrenal ferredoxin (FDX1)	----	-12.5
glutathione reductase	----	-2.9
microsomal glutathione S-transferase (GST12)	----	-3.3
glutathione S-transferase Yb subunit (GSTM2)	----	-1.8
*cellular glutathione peroxidase 1 (GSHPX1; GPX1)	----	-7.2
bleomycin hydrolase (BLM hydrolase)	----	-4.5
membrane bound & soluble catechol-O-methyl transferase (MB-COMT + S-COMT)	1.40	-5.6
NADH-cytochrome b5 reductase: DIA1	1.43	-5.4

Cell Membrane Transport: Import/Export

multidrug resistance protein (MRP)	----	-5.9

Miscellaneous

Vimentin	1.4	-4.1
Prothymosin alpha	----	-2.7
Amphiphysin (AMPH1)	----	-8.0
Plectin	1.9	-5.1

Cytoplasmic beta-actin (ACTB)	1.9	-3.4
Myosin heavy chain 1 (MYR1)	----	-2.2
Hormonal Activity		
*prostaglandin G/H synthase 1 precursor; cyclooxygenase 1 (COX1)	-1.3	-5.9
Tumor Suppressor/Oncogene/Tumor Biomarker		
p53 nuclear oncoprotein	----	-3.2

Table 3. Comparisons of data derived from Clontech Rat Stress and Rat Atlas Arrays and TaqMan Real Time PCR For Control *versus* Treated After 12 Hours Exposure to Potassium Bromate

Gene	Stress Array Address	Stress Array Background Subtracted Intensity[a]		Fold Change on Stress Array	Atlas Array Address	Atlas Array Background Subtracted Intensity[a]		Fold Change on Atlas Array	TaqMan Cycle Threshold		Fold Change on TaqMan
		Control	Treated			Control	Treated		Control	Treated	
Mdr1	NA	NA	NA	NA	A7H	3	171	57	26.3	23.8	5.66
HSP70	5M	298[b]	14,700	49.2	A7G	60	3881	64.7	21.9	16.1	55.7
QR	8E	435	1,010	2.3	NA	NA	NA	NA	20.9	18.4	5.66
GADD45	14B	77	961	12.5	C2G	14	273	19.5	22.2	17.9	19.7
Cyclin D1	9K	870	73	-11.9	A5B	241	22	-11	19	21.1	-4.29
COX1	21E	551	94	-5.9	NA	NA	NA	NA	22.2	22.6	-1.32
Waf1/p21	10D	222	1830	8.3	A5M	39	529	13.6	21.7	17.4	19.7
HO-1	7E	29	2280	78.9	NA	NA	NA	NA	25.9	17.9	256
GPX1	18C	1570	218	-7.2	NA	NA	NA	NA	18.2	19.6	-2.64

[a]Normalized against all genes on respective comparison array

[b]All values rounded to 3 significant figures

NA Gene not included in the array

Table 4. Genes Changed in Both Rat Atlas & Stress Arrays (Fred-Pe Cells)

***confirmed by Taqman quantitative PCR Assay**

increased (+) or decreased (-)

NA = not on array

	Stress Array		Atlas Array	
	4 h	**12 h**	**4 h**	**12 h**
Signal Transduction/Growth Factors				
Erk1 MAPK1) (-)	√	√	√	√
MAP kinase p38 (CSBP2) (-)	√	√		√
MAPKK2 (MAP kinase kinase 2) (-)		√		√
Protein Synthesis and Degradation/Repair				
Ubiquitin (+)	√	√		√
Tubulin alpha 1 (+)	√	√	√	√
Beta-actin (-)	√	√		√
DNA Synthesis/Repair				
*GADD45 (+)	√	√		√
GADD153 (+)	√	√		√
PCNA (+)	√			√
Id-1; DNA-binding protein inhibitor; HLH protein (-)	√	√	√	√
DNA Topoisomerase II (TOP2A) (-)		√		√
Apoptosis				
bcl-2 (+)		√		
bad; heterodimeric partner for Bcl-XL and Bcl-2 (-)	√	√		√
bax; Bcl-2 heterodimerization partner and homolog (-)		√		√

	Stress Array		Atlas Array	
	4 h	**12 h**	**4 h**	**12 h**
bcl-X apoptosis regulator (-)		√		√
Cell Cycle Control				
*p21 $^{WAF1/CIP1}$ (+)	√	√	√	√
G2/M specific cyclin B1 (CCNB1) (+)		√		√
G1/S specific cyclin C (CCNC) (+)		√	√	√
*G1/S specific cyclin D1 (CCND1) (-)	√	√		√
G1/S specific cyclin D2 (CCND2); vin-1 proto-oncogene (+)		√		√
G1/S specific cyclin D3 (CCND3) (+)	√	√		√
G1/S specific cyclin E (CCNE) (+)	√	√		√
Fatty Acid Biosynthesis and Repair				
Bip steroidogenesis-activator polypeptide, IgG heavy chain binding prot. (+)	NA	NA		√
Phospholipase A2 precursor (+)	√	√		√
Oxidative Stress/Imbalance				
GST Pi class (+)	√			√
HSP27 (+)	√	√		√
*HSP70 (+)	√	√	√	√
GST (microsomal) (-)		√		√
Miscellaneous				
Prothymosin alpha (-)		√		√

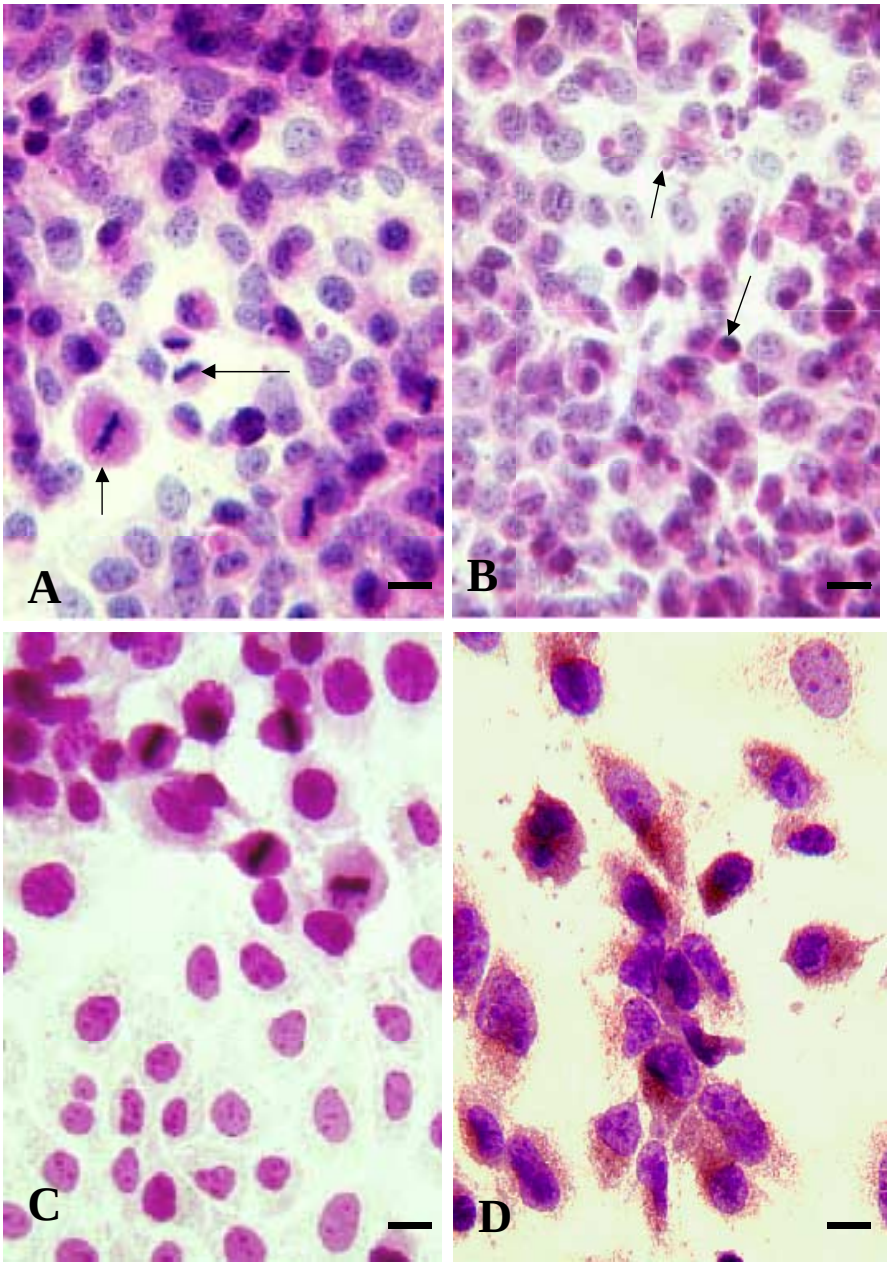

Fig. 1. H&E and Immunohistochemical Staining Using Antibody to Heme Oxygenase-1 in Fred-Pe Cells Treated with $KBrO_3$. A) H&E stain of control cells; small arrow – cell in metaphase, large arrow – cell in late telophase. B) H&E stain of cells exposed to 5 mM $KBrO_3$ for four h; small arrow – apoptotic body, large arrow – apoptotic cell. C) HO-1 immunostain of control cells. D) HO-1 immunostain of cells treated with 3 mM $KBrO_3$ for 24 h. Magnification: A) & B) bar represents 27 μm, C) & D) bar represents 20 μm.

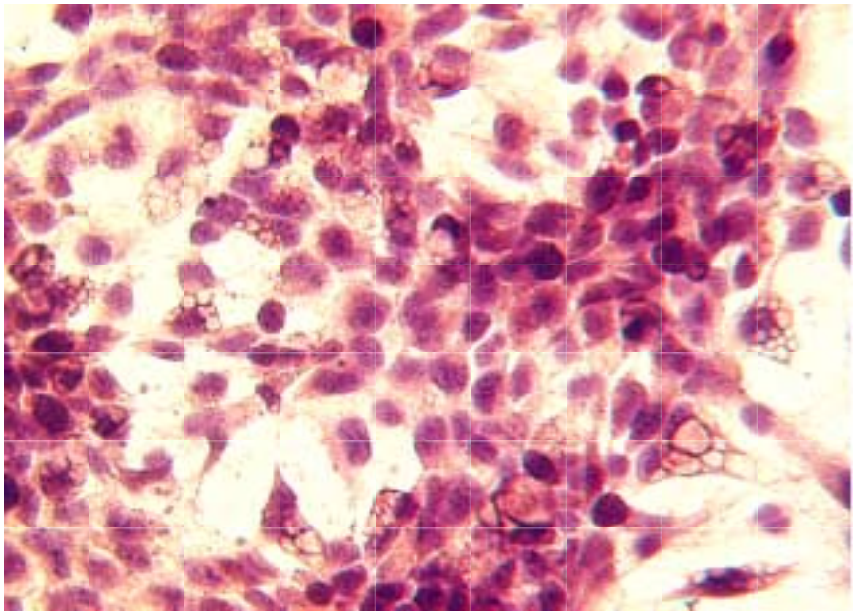

Fig. 2. Immunohistochemical staining of Fred-Pe cells using antibody to HO-1 demonstrates localization of HO-1 to "foamy" areas, highlighted by the staining. Magnification: bar represents 20 μm.

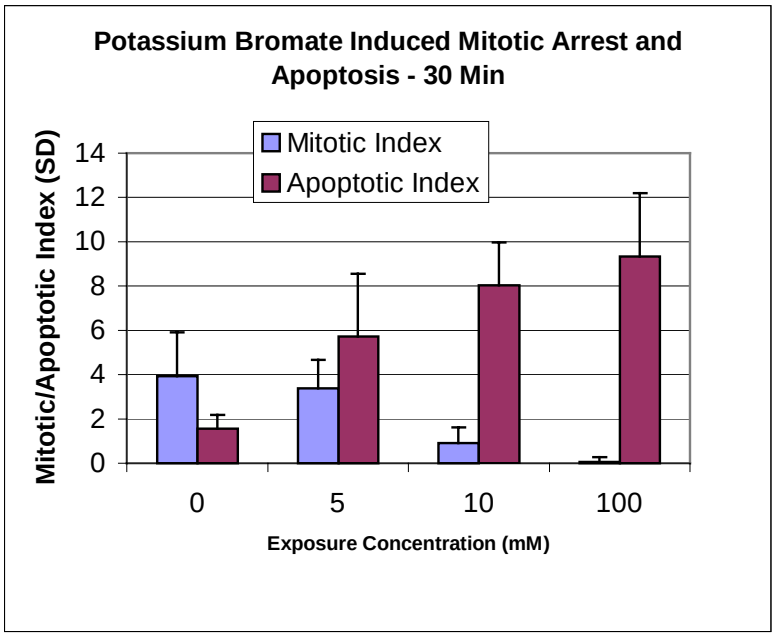

Fig. 3. $KBrO_3$ Induces Mitotic Arrest and Apoptosis in Fred-Pe Cells at 30 min. Error bars represent ± 1 std. dev. All exposure concentrations are significantly different than control ($p<0.01$ or lower).

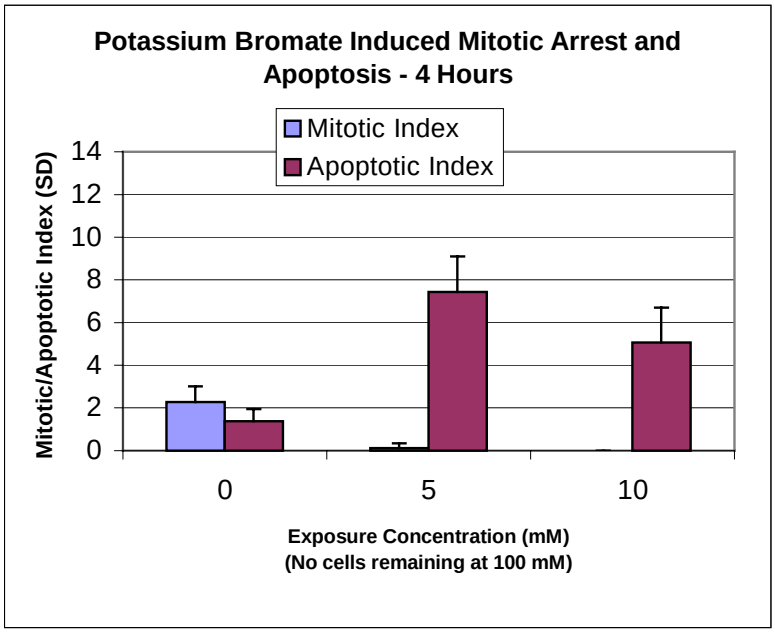

Fig. 4. $KBrO_3$ Induces Mitotic Arrest and Apoptosis in Mesothelial Cells at four hours. Error bars represent ± 1 std. deviation. (No cells remained on slide at 100 mM.) All samples are significantly different than control ($p<0.01$ or lower).

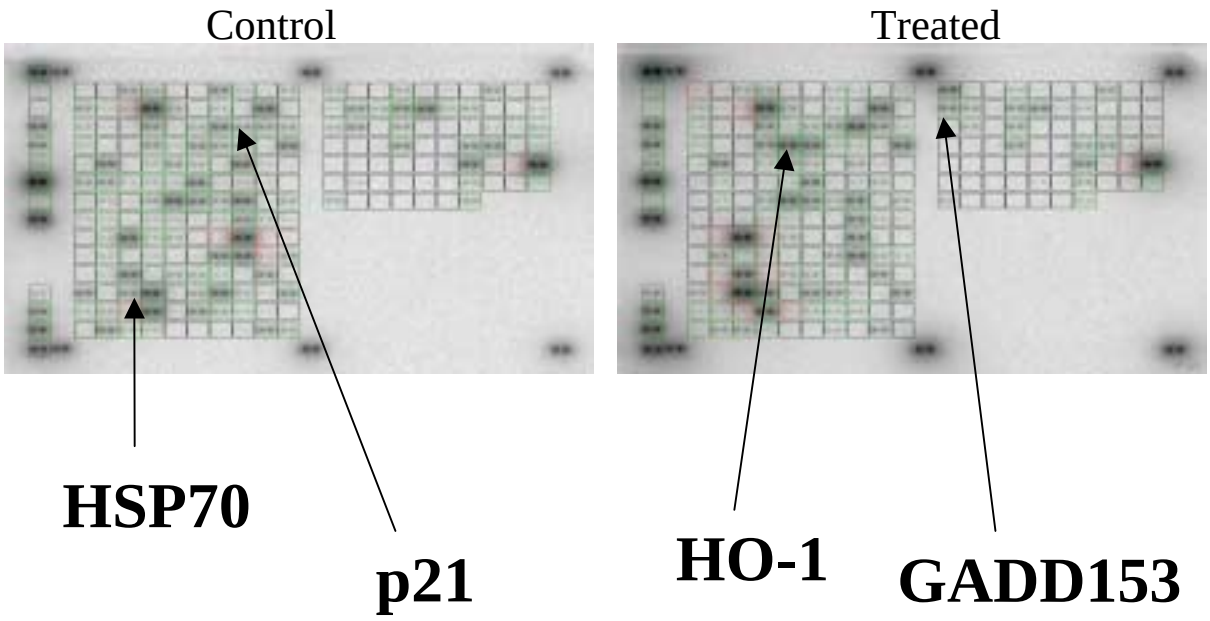

Fig. 5. Clontech Atlas™ Rat Stress/Toxicology Array showing differences in expression of HSP70, $p21^{waf1/cip1}$, HO-1 and GADD153 between treated and control samples.

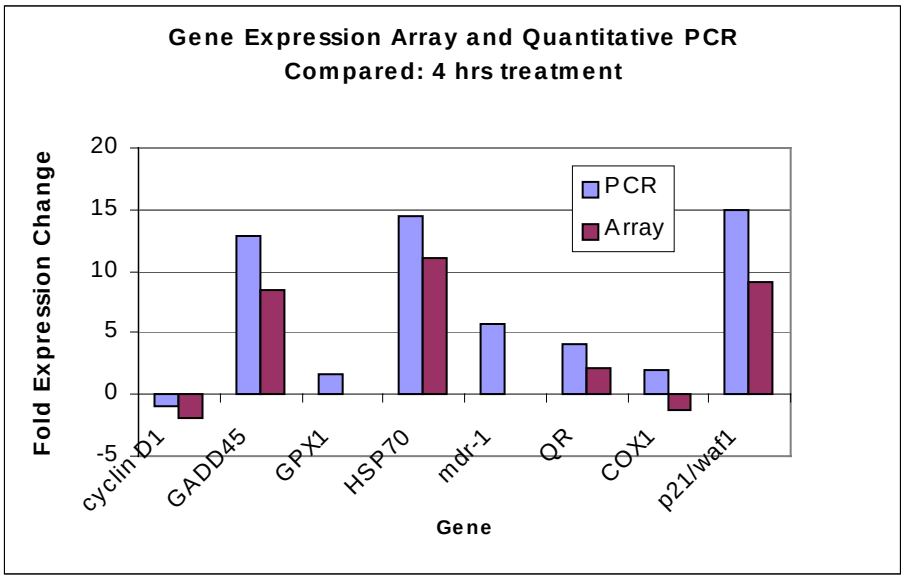

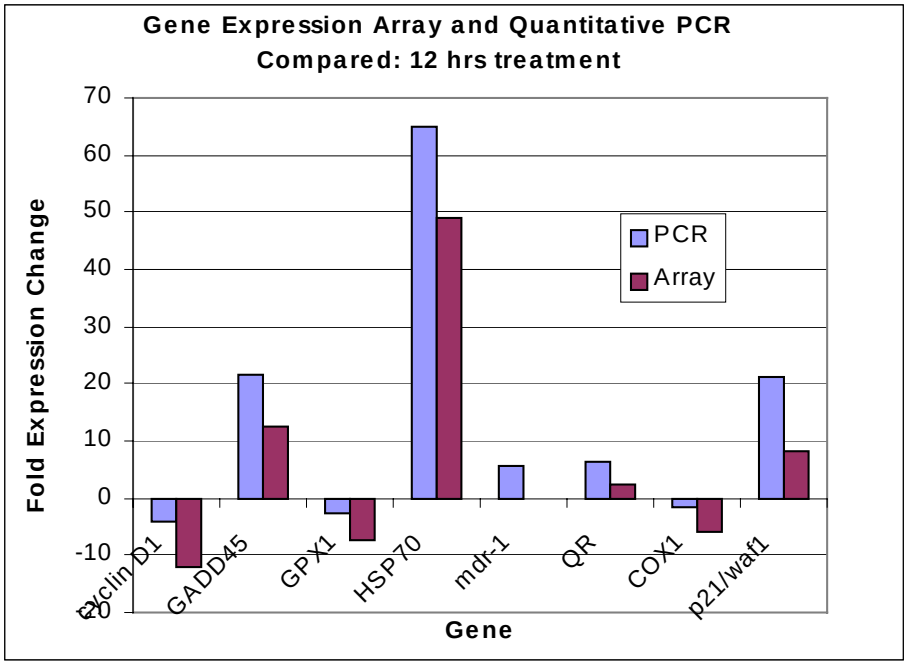

Fig. 6. Gene expression array and quantitative PCR results compared for mesothelial cells exposed to 6 mM $KBrO_3$ for four and 12 h. Note: mdr-1 array result omitted due to excessive bleed, HO-1 result omitted to allow appropriate scaling for remaining genes.

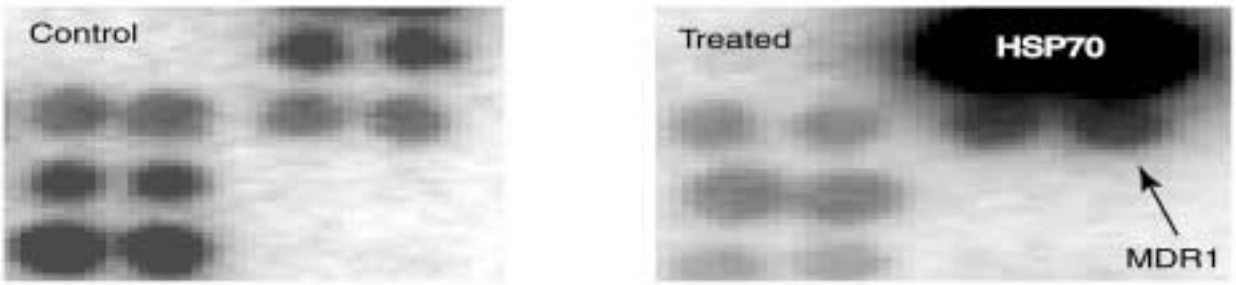

Fig. 7. mdr1 gene expression in control (left) and 6 mM $KBrO_3$-treated mesothelial cells: bleed from neighboring HSP70 signal (right) influences the mdr1 signal (result was 66.6-fold increase vs. Taqman™ quantitative PCR result of 5.8-fold increase, where bleed does not interfere).

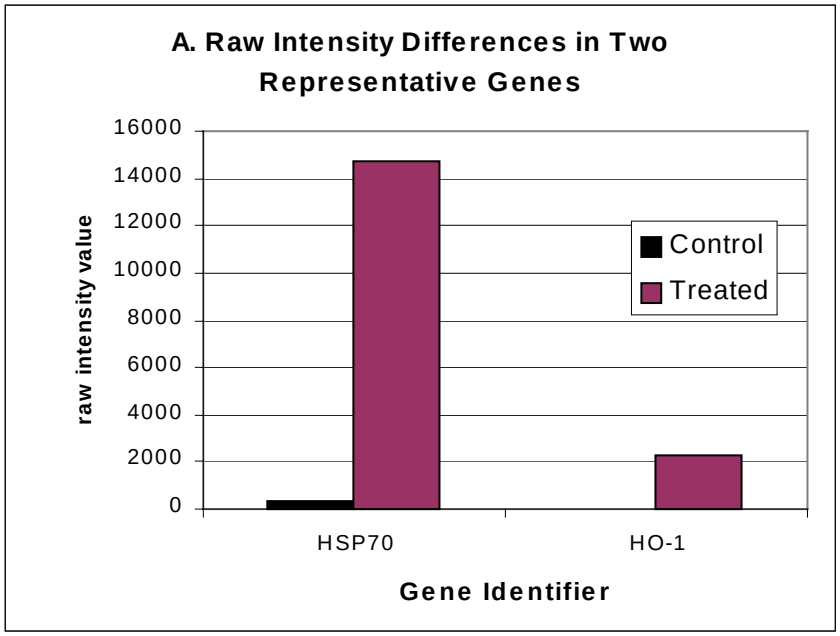

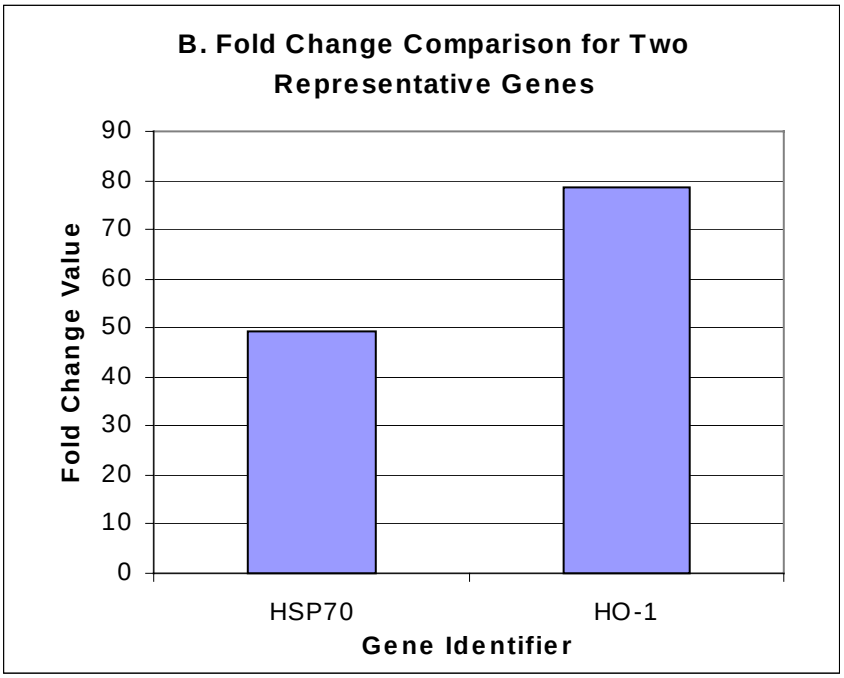

Fig. 8. Comparison of Gene Expression Changes for HO-1 and HSP70 Genes: What Raw Intensity Differences Reveal When Compared to Expression of Results as Fold Change

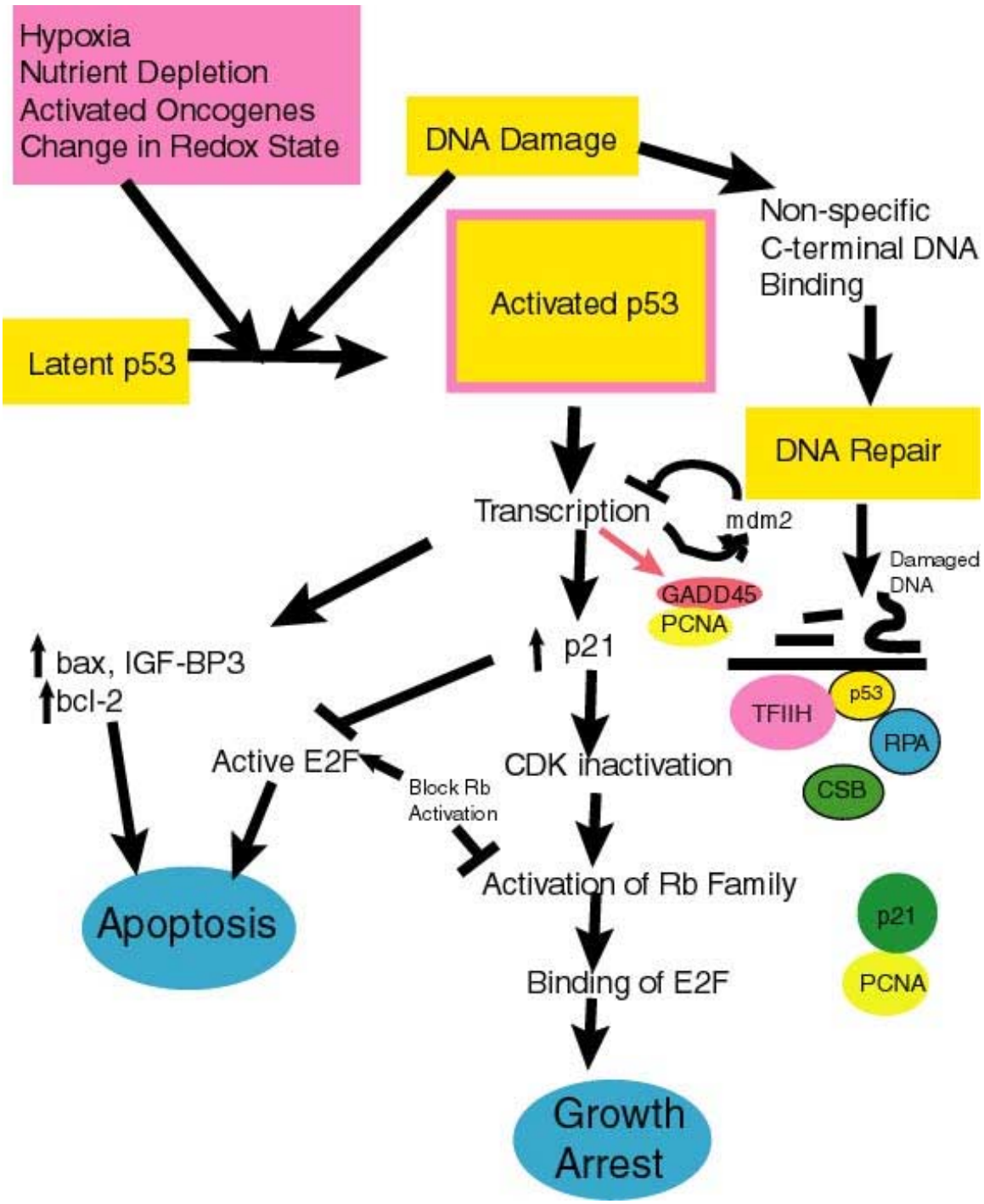

Fig. 9. Pathways leading to the activation of p53, reprinted from C.P. Mansur (1998). Abbreviations: IGF-BP3, insulin-like growth factor binding protein 3; CDK, cyclin-dependent kinase; GADD, growth arrest and DNA damage; PCNA, proliferating cell nuclear antigen; Rb, retinoblastoma; RP-A, replication protein A; TFIIA, transcription factor IIA; CSB, cockayne syndrome B.

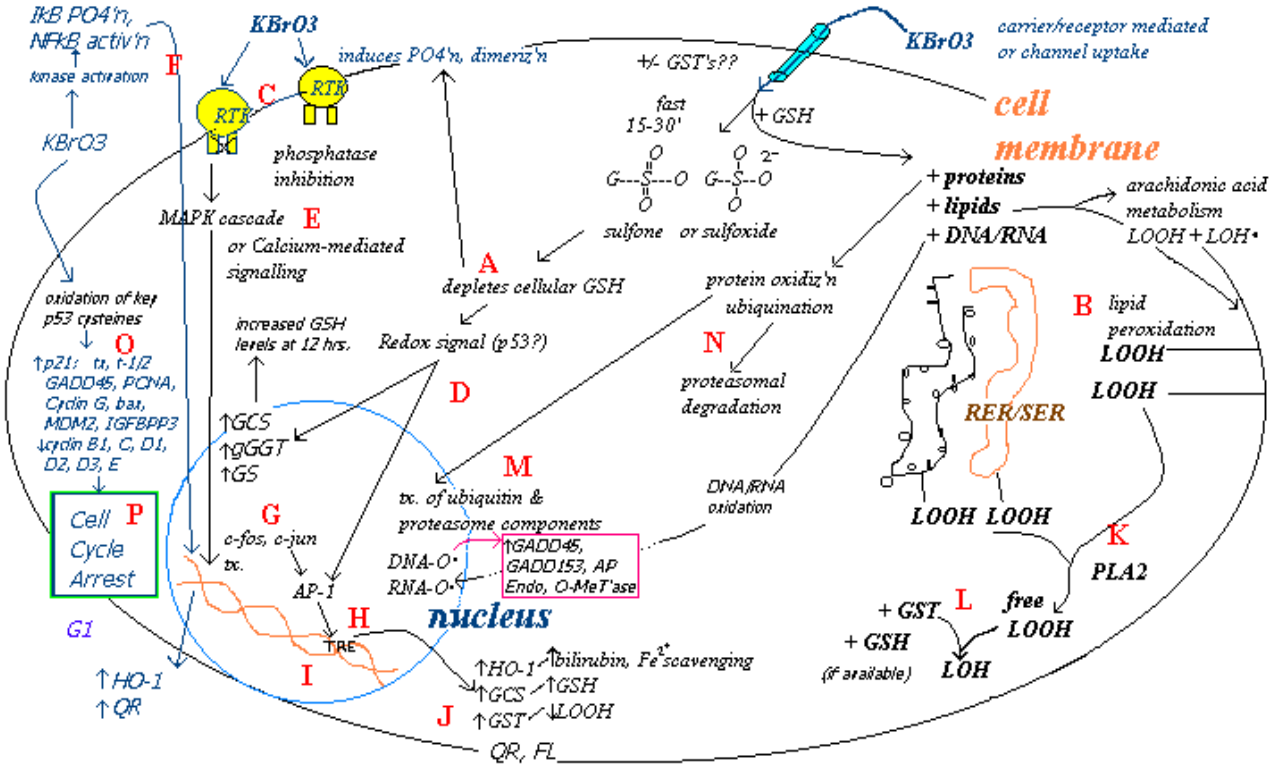

Fig. 10. Proposed mechanisms of $KBrO_3$ toxicity in the mesothelial cell. (See Discussion for detailed description.)

Chapter 5. Summary and Conclusions

The data presented herein support the conclusion that $KBrO_3$ induces mesothelioma in the male F344 rat, originating at specific locations on the mesothelium, (i.e., the tunica vaginalis testis mesorchium and the mesosplenium, or at an intermediate mesothelial location). The results of the tumor mapping study indicate that an identifiable pre-neoplastic lesion is present as early as 13 weeks in animals exposed to 0.4 g/L $KBrO_3$, and the incidence of this lesion increases linearly with respect to time, while malignancy follows the typical exponential increase over time. The requisite characteristics of the pre-neoplastic lesion are reactive mesothelial cells of >1 cell layer. The conclusion that mesothelioma most likely originates on the mesorchium was arrived at by mapping tumors from slides of every available animal necropsied and performing statistical analysis of the average distance of the tumor from the mesorchium. Finally, the correlation coefficient between occurrence of this type of tumor on the mesorchium and the mesosplenium was 0.98, a telling statistic which leads to the conclusion that occurrence of mesotheliomas in these two locations simultaneously is linked.

Biochemical studies comparing human hepatocellular carcinoma (HepG2) non-target cell cultures to mesothelial target cell cultures revealed that the average amount of GSH differed significantly between the two cell types. Importantly, pre-treatment with GSHoET protected mesothelial cells from $KBrO_3$-mediated toxicity under the conditions tested, while the same pre-treatment of HepG2 cells produced significantly less protection, such protection being at much higher GSHoET concentrations (see Table 3 and Fig. 3 of Chapter 3). Augmentation of GSH levels prior to $KBrO_3$ exposure thus was protective, while depletion exacerbated toxicity. A

protective role may also be inferred from strong intracellular peri-spindle GSH-specific staining with mercury orange. Also observed by fluorescent staining was the efficient depletion of GSH by $KBrO_3$, compared to depletion by either DEM or BSO. The timed depletion of GSH by $KBrO_3$ by four hours and Br^- ion selective electrode results showing GSH and $KBrO_3$ react together intracellularly indicate GSH is mechanistically related to $KBrO_3$ toxicity.

Gene expression analysis of the effects of $KBrO_3$ treatment at four and 12 hours, as well as immunohistochemical staining in mesothelial cells demonstrated the significant up-regulation of HO-1, the rate-limiting enzyme in heme catabolism, and a known oxidative-stress responsive gene. It is suggested that HO-1 can be used as a biomarker for oxidative stress as induced by $KBrO_3$, pending completion of *in vivo* type studies. Other oxidative stress-responsive genes (QR, GADD45, HSP70, $p21^{/waf1/cip1}$) were also highly expressed vs. controls at four hours, 12 hours or both. A real-time PCR study corroborated nine gene expression changes, including those just mentioned. Significantly increased apoptotic and decreased mitotic indices were observed morphologically; these changes were consistent with observed alterations in the expression levels of multiple cyclins, FasL, TNFα and iNOS1. It was also noted in that pro-apoptotic genes bax, bclX and bad were down-regulated by 12 hours, emphasizing the need for careful evaluation of data obtained and suggesting that multiple pro-apoptotic pathways exist within the cell which are capable of modulating the overall occurrence of apoptosis. Significant changes in gene expression patterns were discernible with the use of NLR software, which both normalizes and compares differences in treated and control samples. The utility of gene expression cDNA arrays to the elucidation of patterns of oxidative stress and possibly mechanisms of transformation was demonstrated, however a thorough exploration of the use of this technology will necessitate

dose-response titration down to the 'no observable change in expression level' (NOCEL). The choice of dose used in the gene expression studies was made based upon 1) the MTS cytotoxicity assay result (based upon cellular reducing capacity, largely NADPH/NADH pools, where six mM $KBrO_3$ was about 50% toxic to cells at 4 and 12 hours), 2) the GSH depletion experiment showing the 93% depletion of GSH by 5 mM $KBrO_3$ at four hours and partial recovery by 12 hours, and 3) the recovery to exponential growth after prolonged cell cycle arrest of mesothelial cells treated for five days with five mM $KBrO_3$. The goal of the gene expression study was to determine whether a change in gene expression could be observed upon exposure to $KBrO_3$ at the concentrations employed in *in vitro* experiments. Since it is unknown what concentration of $KBrO_3$ will transform cells *in vitro,* it could not have been known *a priori* what concentration to use in a gene expression experiment designed to measure changes that are known to result in cellular transformation. Only when a dose-response titration of transcriptional changes is employed for the investigation of $KBrO_3$-induced carcinogenesis will responses to toxic effects on the cell by the transcriptome be separable from effects associated with initiating events in the genesis of mesothelioma. Such a titration, while highly desirable, is beyond the scope of this work.

Many clues to the mechanisms of potassium bromate toxicity and carcinogenicity have been unearthed. GSH studies undertaken here suggest that depletion of GSH is prerequisite to the full expression of $KBrO_3$ toxicity, although in itself oxidation/conjugation of GSH would create a cellular redox imbalance with severe consequences to cell health. Gene expression studies suggest that the redox signal created by such an imbalance is capable of eliciting gene expression changes, which may significantly alter cell growth and differentiation. Activation of p53 may

participate in most of the observed transcriptional changes, according to the literature, suggesting that p53 inactivation may play a role in the reversion to proliferative status of cells that emerged from $KBrO_3$-induced cell cycle arrest. The results of the tumor mapping study intimate that anatomic/physiologic factors specific to the location of the mesorchium, mesosplenium, or intermediary mesothelium also contribute to the eventual development of cancerous lesions.

Appendices

TOXICOLOGIC PATHOLOGY, vol. 26, no. 6, pp. 724–729, 1998

Time- and Dose-Dependent Development of Potassium Bromate-Induced Tumors in Male Fischer 344 Rats*†

DOUGLAS C. WOLF,[1] LYNN M. CROSBY,[1] MICHAEL H. GEORGE,[1] STEVE R. KILBURN,[1] TANYA M. MOORE,[1] RICHARD T. MILLER,[2] AND ANTHONY B. DEANGELO[1]

[1]*Environmental Carcinogenesis Division, National Health and Environmental Effects Research Laboratory, U.S. Environmental Protection Agency, Research Triangle Park, North Carolina 27711, and*
[2]*Department of Microbiology, Pathology, and Parasitology, College of Veterinary Medicine, North Carolina State University, Raleigh, North Carolina 27606*

ABSTRACT

Potassium bromate ($KBrO_3$) is a rodent carcinogen and a nephro- and neurotoxicant in humans. $KBrO_3$ is used in cosmetics and food products and is a by-product of water disinfection by ozonization. $KBrO_3$ is carcinogenic in the rat kidney, thyroid, and mesothelium and is a renal carcinogen in the male mouse. The present study was designed to investigate the relationship of time and dose to bromate-induced tumors in male Fischer 344 (F344) rats and to provide some insight into the development of these tumors. $KBrO_3$ was dissolved in drinking water at nominal concentrations of 0, 0.02, 0.1, 0.2, and 0.4 g/L and administered to male F344 rats as the sole water source for 12, 26, 52, 78, or 100 wk. Renal cell tumors were present after 52 wk of treatment only in the high-dose group. Mesotheliomas developed after 52 wk of treatment on the tunica vaginalis. Mesotheliomas were present at sites other than the testicle after 78 wk of treatment, indicating that their origin was the testicular tunic. Thyroid follicular tumors were present as early as 26 wk in 1 rat each from the 0.1- and 0.2-g/L groups. The present study can be used as a basis for the determination of dose-time relationships of tumor development for a better understanding of $KBrO_3$-induced cancer.

Keywords. Disinfection by-products; kidney; mesothelioma; mesothelium; renal cell tumor; thyroid; urothelium; water

INTRODUCTION

Potassium bromate ($KBrO_3$) is a rodent carcinogen and a nephro- and neurotoxicant in humans (10, 17). Male and female Fischer 344 (F344) rats developed renal cell tumors and thyroid follicular tumors, and the male rats also had an increased incidence of abdominal mesotheliomas (6, 14, 16, 21). $KBrO_3$ has been used in cosmetics and food products; it is also a by-product of water disinfection by ozonization (1, 3, 10). We previously showed that $KBrO_3$ is carcinogenic in the rat kidney, thyroid, and mesothelium and that it is a renal carcinogen in the male mouse. $KBrO_3$ was carcinogenic in rats at water concentrations as low as 0.02 g/L (20 parts per million [ppm]) (6).

Male rats treated with 60, 125, 250, or 500 ppm $KBrO_3$ in drinking water for up to 2 yr had renal cell tumors in all dose groups, but there were statistically significant increases only at doses of ≥125 ppm. Of the 20 control rats that survived to 90 wk, none had renal cell tumors, and neither did the 16 that survived to 104 wk (14). Mesotheliomas were seen only in rats treated with ≥30 ppm bromate, with a significantly increased incidence only in the high-dose group (500 ppm). None of the control rats had mesotheliomas (14). Thyroid follicular tumors were present in all dose groups, but there were statistically significant increases only in the high-dose group (500 ppm). None of the 16 control thyroid glands examined at 104 wk had follicular tumors (14).

Male F344 rats treated with 500 ppm $KBrO_3$ for 13, 26, 39, 52, or 104 wk and then necropsied or those treated for that duration and then switched to plain water and necropsied at 104 wk developed renal cell tumors as early as 26 wk, but there were no statistically significant increases in incidence until 52 wk. All rats examined at 104 wk had statistically significant increases in renal cell tumors regardless of duration of $KBrO_3$ treatment. None of the control animals had renal cell tumors at any time (18). Thyroid follicular cell tumors were first identified after 26 wk of treatment, but there were no statistically significant increases until 104 wk. Rats treated for 26 or 52 wk and necropsied at 104 wk had statistically significant increases in numbers of thyroid follicular tumors (18). Mesotheliomas were first seen after 39 wk of treatment, but statistically significant increases were not seen until 104 wk. Rats treated for 13 wk or more and then examined at 104 wk had an increased incidence of mesothelioma, whereas none of the control rats had mesotheliomas (18). The present study was designed to investigate the relationship of time and dose to the development of bromate-induced tumors in male F344 rats by extending previous work to lower doses and a shorter duration of treatment.

MATERIALS AND METHODS

Complete study details were published previously (6). Briefly, $KBrO_3$ (99%; CAS 7758-01-2) dissolved in deionized water at nominal concentrations of 0, 0.02, 0.1,

* Address correspondence to: Dr. Douglas C. Wolf, U.S. EPA MD-68, 86 TW Alexander Drive, Research Triangle Park, North Carolina 27711; e-mail: wolf.doug@epamail.epa.gov.

† This manuscript has been reviewed and approved for publication by the Environmental Protection Agency and does not necessarily reflect the views of the agency. Mention of trade names or commercial products does not constitute endorsement or a recommendation for use.

0192-6233/98$3.00+$0.00

0.2, and 0.4 g/L was administered to male F344 rats as the sole water source for 12, 26, 52, 78, or 100 wk.

Three hundred seventy 28- to 30-day-old male F344 rats (Charles River Laboratories, Portage, MI) were acclimated to the environment for 1 wk and then randomly assigned to the treatment groups. The treatment rooms were maintained at 20–22°C and 40–60% humidity on a 12-hr light:dark cycle. Rats were housed 3 per cage on wood chips and provided Purina Rodent Laboratory Chow (St. Louis, MO) and water *ad libitum*. Animals were observed daily, and moribund animals were euthanatized and necropsied. Six animals from each group were euthanatized by CO_2 asphyxiation and necropsied after 12, 26, 52, and 78 wk of treatment; the remaining animals were euthanatized and necropsied after 100 wk of treatment. At necropsy, a blood sample was collected from each animal, and the serum was separated and frozen. The target tissues of kidneys, testes, thyroid gland, and gross lesions were removed, examined, and fixed in 10% neutral-buffered formalin. Fixed tissues were processed by routine methods for paraffin embedding, cut into 5-μm sections, stained with hematoxylin and eosin, and examined by light microscopy. Nephropathy scores were graded semiquantitatively on the basis of the percentage of the renal cortex involved. Grade 0 indicated no nephropathy; grade 1, 1–10% of renal cortex involved; grade 2, ~25% involved; grade 3, ~50% involved; grade 4, ~75% involved; and grade 5, >75% of the renal cortex involved and fibrosis and mineralization were present. The kidneys from rats treated with $KBrO_3$ for 12 wk were sectioned at 5 mm and stained with the Mallory-Heidenhain method to accentuate the droplets within the proximal tubules for qualitative analysis of droplet accumulation. The slides were scored on a 1–4 scale for mild, moderate, marked, and severe accumulations of large red droplets within the proximal tubule epithelium. Total serum, bound and unbound, triiodothyronine (T_3), and thyroxine (T_4) concentrations from animals euthanatized after 12 wk of study were determined by radioimmunoassay using a kit supplied by Diagnostic Products Corporation (Los Angeles, CA), according to the manufacturer's instructions. All aspects of these studies were conducted in facilities certified by the American Association for the Accreditation of Laboratory Animal Care in compliance with the guidelines of that association and those of the National Health and Environmental Effects Research Laboratory Animal Care and Use Committee.

Statistical analysis for histopathology included the Fisher exact test, and polynomial regression was used to determine dose- or time-related trends. Statistical analysis for T_3 and T_4 levels was performed using an ANOVA and a *t*-test. All values were determined to be significant when $p < 0.05$. In some instances, slightly higher values for p are noted when the change is deemed biologically significant but is >0.05.

Results

Mesotheliomas developed on the tunica vaginalis parietalis along the attachment between the testis and the epididymis (Table I and Fig. 1), as previously described (5). In addition to small mesotheliomas, there were also a few animals with hypertrophy and hyperplasia of the mesothelial cells along the parietal vaginal tunic (Table I and Fig. 2). Mesotheliomas of the tunica vaginalis testis were first seen after 52 wk of treatment. Mesotheliomas at sites other than the testicle were not present until after 78 wk of treatment, indicating that the origin of these tumors is likely the testicular serosa. The most common sites of secondary spread of the 52 rats with mesothelioma in this study were on the serosal surfaces of the spleen (56%) and gastrointestinal tract (56%), followed by the mesentery (46%), the pancreas (37%), the urinary bladder (27%), the liver (10%), and, rarely, the kidney (2%). None of the neoplasms invaded adjacent tissue or metastasized to other sites. None of the 52 rats diagnosed with mesothelioma had evidence of spread cranial to the diaphragm.

TABLE I.—Incidence of testicular mesotheliomas in male F344 rats treated with $KBrO_3$ in drinking water.

Group (g/L)	12 Wk	26 Wk	52 Wk	78 Wk	100 Wk
0	0	0	0	0	0
0.02	0	0	0	0	4/49
0.1	0	0	0	0	5/50*
0.2	0	0	1/6	0[a]	10/47**
0.4	0	0	0[a]	4/6*	27/43**[b]

[a] A single testicle from 1 animal had focal hypertrophy and hyperplasia of mesothelial cells on the tunica vaginalis testis.
[b] Trend over time and dose.
* $p < 0.06$ or ** $p < 0.001$ by Fisher exact test.

Renal cell tumors were seen after 52 and 78 wk of treatment only in the high-dose group (Table II). Although some of the renal tumors were large after 100 wk of treatment and were classified as carcinomas based on size, none of the renal tumors metastasized. The predominant cell type in these renal tumors was a markedly vacuolated cell of proximal tubule origin (Fig. 3). There was no increase in incidence or number of hyperplastic tubules with bromate treatment when compared with control animals (data not shown). In addition, the incidence and severity of nephropathy were not different between control and treated rats at any time (data not shown).

Proximal tubule epithelium had a treatment-related increase in eosinophilic droplets. In some cases, these droplets had a golden brown appearance consistent with lipofuscin granules, which are indicative of accumulation of undigested membranes. With decreasing dose at the early times, the eosinophilic droplets were similar in size and number to those of the control rats, and in the lower doses, they more closely resembled the α2u-globulin–containing hyaline droplets typical for this sex and strain of rat. Kidneys from rats treated for 12 wk had a dose-dependent increase in numbers of large red droplets within the proximal tubule epithelium (Table III).

The kidney had a treatment-related increase in mineralization of the inner medulla (data not shown). This mineralization was restricted to the renal papilla and became more severe with longer duration of treatment. The mineralized foci were scattered throughout the papillae and were associated with degeneration of the collecting ducts and expansion of the interstitial space with proteinaceous

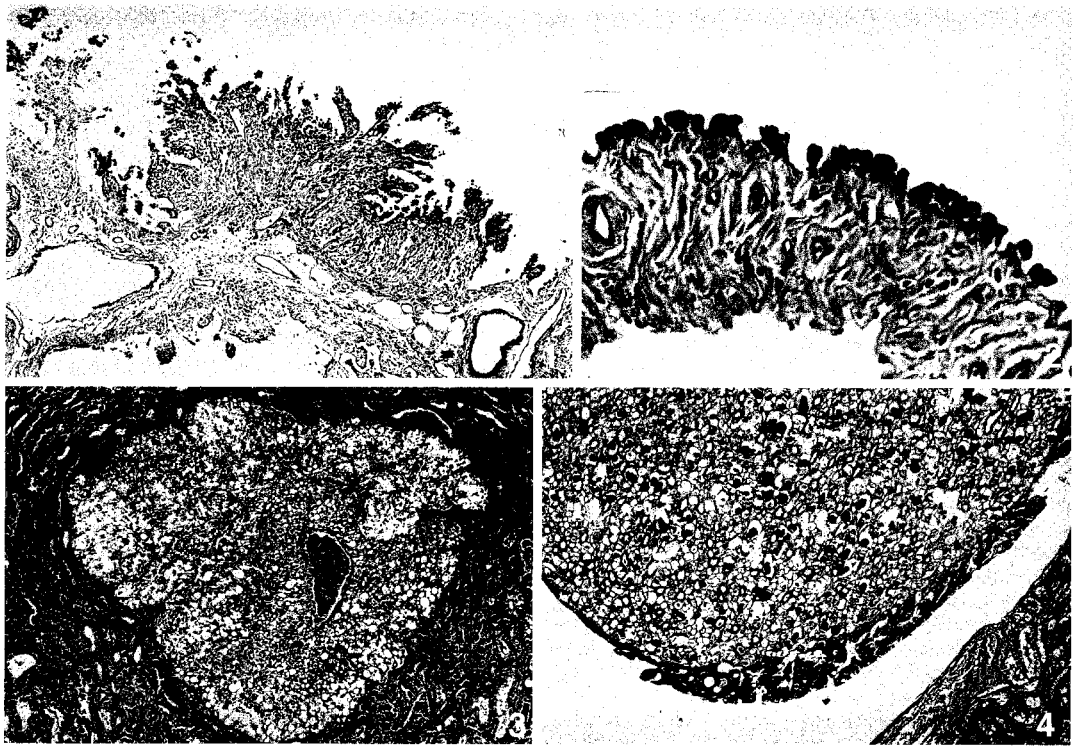

FIG. 1.—Mesothelioma on the tunica vaginalis testis from a male F344 rat treated with 0.4 g/L $KBrO_3$ for 78 wk. The serosal surface of the tunic has a focal proliferation of neoplastic mesothelial cells several layers thick resting on an extensive fibrous stroma. ×25.

FIG. 2.—Mesothelial hyperplasia on the tunica vaginalis testis from a male F344 rat treated with 0.4 g/L $KBrO_3$ for 52 wk. The serosal surface of the tunic has a focally extensive hypertrophy and hyperplasia of mesothelial cells 1 to 3 layers thick resting on the thin connective tissue stroma of the serosa. ×50.

FIG. 3.—Renal adenoma from a male F344 rat treated with 0.4 g/L $KBrO_3$ for 78 wk. This adenoma is characterized by an expansile mass of markedly vacuolated proliferating proximal tubule epithelial cells. The cells have pronounced cell membranes but thin wisps of cytoplasm between large cytoplasmic vacuoles. ×30.

FIG. 4.—Kidney from a male F344 rat treated with 0.4 g/L $KBrO_3$ for 78 wk. The renal papilla contains numerous foci of mineral, and the interstitium is prominent and expanded by a proteinaceous material, likely to be edema. The urothelium lining the renal papilla is markedly thickened by hyperplasia and projects into the pelvic lumen in numerous papillary fronds. ×30.

material (Fig. 4). This lesion was similar to what has been described as intermediate renal papillary necrosis with mineralization (2). In association with the mineralization of the renal papilla, there was moderate-to-marked urothelial hyperplasia that increased in incidence in a dose- and time-dependent manner in rats treated with ≥0.1 g/L (Table IV). The urothelium lining the papilla had increased thickness and projected into the urinary space of the renal pelvis in papillary fronds or sessile mats (Fig. 4). In the more severe cases, the entire pelvis was lined by hyperplastic epithelium, with projections into the lumen. None of the control rats or the rats treated with low-

TABLE II.—Incidence of renal cell tumors in male F344 rats treated with $KBrO_3$ in drinking water.

Group (g/L)	12 Wk	26 Wk	52 Wk	78 Wk	100 Wk
0	0	0	0	0	1/44
0.02	0	0	0	0	1/43
0.1	0	0	0	0	6/47
0.2	0	0	0	0	3/39
0.4	0	0	2/6	4/6*[a]	12/32**[b]

[a] Trend over dose.
[b] Trend over time and dose.
* $p < 0.06$ or ** $p < 0.001$ by Fisher exact test.

TABLE III.—Mean ± SD score of eosinophilic droplet accumulation within the renal proximal tubule epithelium in male F344 rats treated for 12 wk with $KBrO_3$ in their drinking water.

	Dose (g/L)				
	0	0.02	0.1	0.2	0.4
Score	1 ± 0	1.5 ± 0.6	1.7 ± 0.5	2.5 ± 0.6	4 ± 0

TABLE IV.—Incidence of urothelial hyperplasia of the renal pelvis in male F344 rats treated with $KBrO_3$ in drinking water.

Group (g/L)	12 Wk	26 Wk	52 Wk	78 Wk	100 Wk
0	0	0	0	0	7/44
0.02	0	0	0	0	6/41
0.1	0	0	0	0	25/47***
0.2	0	0	0	4/6*	32/39**[a]
0.4	0	0	1/6	6/6**[b]	30/32***[c]

[a] Trend over time.
[b] Trend over dose.
[c] Trend over dose and time.
* $p < 0.06$, ** $p < 0.05$, or *** $p < 0.001$ by Fisher Exact test.

dose $KBrO_3$ had renal papillary mineralization, and urothelial hyperplasia was only present in these groups after 100 wk (Table IV).

Thyroid follicular tumors were seen as early as 26 wk in 1 rat each from the 0.1- and 0.2-g/L groups (Table V). A few rats in the 0.2- and 0.4-g/L groups had follicular cell hyperplasia, but this was not a prominent finding (Table V). An apparent treatment-associated follicular cell degeneration was present in the rats treated with the high-dose of $KBrO_3$for 52 wk but was absent after a longer duration of treatment. The control animals did not develop any thyroid follicular tumors. Total serum concentrations (bound and unbound) of T_3 (but not T_4) were decreased in $KBrO_3$-treated rats (Fig. 5).

TABLE V.—Incidence of thyroid lesions in male F344 rats treated with $KBrO_3$ in drinking water.[a]

Group (g/L)	12 Wk	26 Wk	52 Wk	78 Wk	100 Wk
0	0	0	0	0	0
0.02	0	0	0	0	5/39* *1/39*
0.1	0	1/6	0	1/6 *1/6*	4/43 *2/43*
0.2	0	1/6	0	2/5 *2/6*	6/35**[b] *2/35*
0.4	0	0	1/6 *1/6*	4/6*[c] *1/6*	16/30***[d] *2/30*

[a] Top number is thyroid follicular tumor incidence; when present, bottom number in italics is incidence of follicular cell hyperplasia.
[b] Trend over time.
[c] Trend over dose.
[d] Trend over dose and time.
* $p < 0.06$, ** $p < 0.05$, or *** $p < 0.001$ by Fisher Exact test.

DISCUSSION

Chemically induced abdominal mesotheliomas have been seen almost exclusively in male F344 rats (8). Mesothelioma is preceded by mesothelial hyperplasia that is described as focal thickening or single papillary projections of mesothelial cells without stromal proliferation.

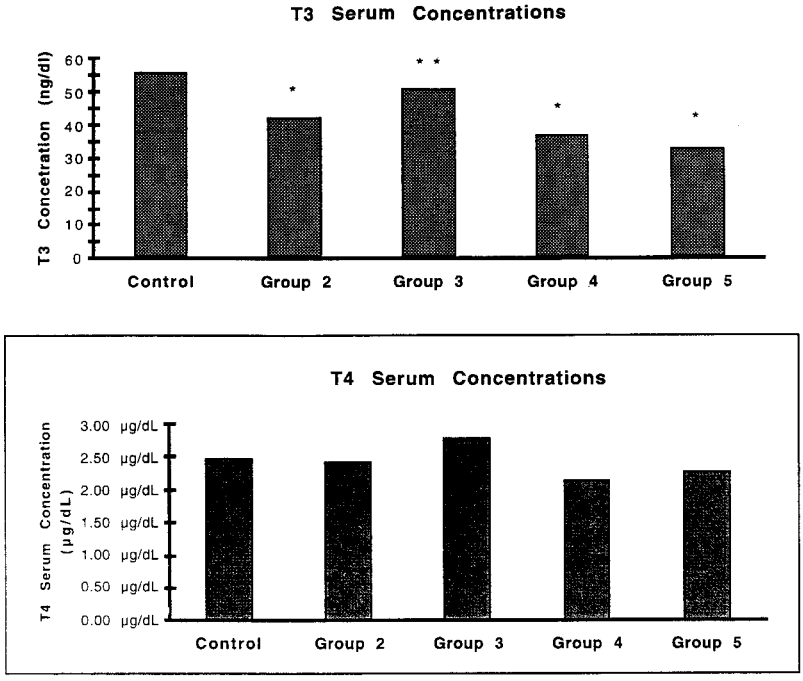

FIG. 5.—Serum concentrations of T_3 and T_4 in control and $KBrO_3$-treated male F344 rats after 12 wk of treatment. Serum T_3 concentrations were decreased in a treatment-dependent but not dose-dependent manner. T_4 concentrations were unaffected by $KBrO_3$ treatment. * $p < 0.05$; ** $p = 0.07$.

Mesothelioma is common on the tunica vaginalis and is found adhering to the epididymis or tunica albuginea of the testis of males, from which almost all spontaneous mesotheliomas are thought to originate. The earliest tumors are distinguished from hyperplasia by the presence of papillary growth with stratification and associated stromal proliferation. All mesotheliomas are considered malignant but appear to spread by direct extension or implantation throughout the peritoneum (8). Mesotheliomas were first seen after 39 wk of treatment of 500 ppm $KBrO_3$ and statistically significant increases were not seen until 104 wk (18). Rats treated for at least 13 wk and then examined at 104 wk had an increased incidence of mesotheliomas (18). In the present study all treatment groups had an increased incidence of mesotheliomas at 100 wk, with hyperplasia and small tumors first seen after 52 wk.

In previous work renal cell tumors were found in male rats given 500 ppm $KBrO_3$ that died after 14 wk of treatment (15). However, mean induction time for renal cell tumors ranged from 90 wk in rats given 500 ppm $KBrO_3$ to 111 wk in control male rats (15). Male F344 rats treated with 500 ppm $KBrO_3$ were found to have renal adenomas after 26 wk of treatment and statistically significant increases in numbers were seen after 52 wk (18). Renal tumor development was not reversible when treatment was stopped following continuous treatment for 13 wk or more. Lesions associated with nephropathy such as droplet accumulation were reversed and were not different from control animals after recovery treatment. It was suggested that because tumors arise after discontinued treatment that the mechanism of action is not related to the nephrotoxicity induced by bromate (18). This hypothesis is further supported by the finding from the present study that $KBrO_3$ did not enhance the development of nephropathy at any time.

Male, but not female, F344 rats treated for up to 13 wk with 500 ppm $KBrO_3$ in their drinking water had an increased accumulation of α2u-globulin–containing droplets in the proximal tubule epithelium (28). However, male and female F344 rats both had elevated 8-hydroxydeoxyguanosine levels in the kidney and increased S-phase labeling after up to 13 wk of treatment (28). These data, the present report, and previous work indicating that both male and female rats develop renal tumors suggest that α2u-globulin accumulation is not related to renal tumor development (12, 13, 28). The droplets that accumulate in association with bromate treatment are associated with bromate-induced oxidant damage and not α2u-globulin nephropathy.

$KBrO_3$ induced clear-cell renal tumors in the present and previous studies. This particular tumor type is common in humans with kidney cancer but is unusual in the rat (30). Specific molecular alterations have been associated with particular morphologic patterns of renal cell tumors in human patients (4, 7, 12, 30). Recently, molecular alterations of the *Tsc2* gene have been shown to be associated with chemically induced chromophilic renal cell carcinoma in rats (29). Human patients with nonpapillary clear-cell renal cancer most commonly have mutations in the *Vhl* gene (12). Bromate-induced renal cell tumors in rats are morphologically similar to human renal cell cancer of the clear-cell type. A molecular characterization of bromate-induced rat renal tumors has not been conducted.

Urothelial hyperplasia is commonly seen in the renal pelvis with severe nephropathy, which was not the case in this study. Treatment-related hyperplasia in the urothelium has also been associated with renal papillary necrosis, mineralization, and calculi formation (23). Advanced hyperplasia appears to form a continuum with papillomas of the renal pelvis (23). In the present study, urothelial hyperplasia developed in association with renal papillary mineralization and intermediate necrosis but did not progress to papilloma.

In the present study, thyroid gland follicular cell tumor numbers were increased after 78 wk of $KBrO_3$ treatment. Proliferation of thyroid gland follicular cells is thought to follow a progression from hyperplasia to neoplasia (9). Most chemically induced thyroid neoplasms appear to result from direct interference with the synthesis of thyroid hormones, resulting in a decreased circulating level of T_3 or T_4 with subsequent elevated thyroid stimulating hormone (TSH) secretion. Most agents that produce thyroid gland tumors do so by nongenotoxic mechanisms, rarely do chemicals induce tumors through mechanisms not involving TSH (27). However, a few chemicals do produce thyroid neoplasms without known interference with the pituitary-thyroid axis. These chemicals do not affect thyroid weight, but they induce neoplasms at other sites and they are genotoxic, suggesting that they may directly act on thyroid follicular cells (9). In a time-course study, thyroid follicular cell tumors were first identified after 26 wk of continuous treatment with $KBrO_3$, but statistically significant increases were not found until 104 wk (18). Rats treated for 26 or 52 wk with $KBrO_3$ and then necropsied at 104 wk also had statistically significant increased numbers of follicular tumors (18). The present study had a similar time course for thyroid follicular tumor development and a treatment-associated slight decrease in serum T_3 levels. Additional studies will examine the association between thyroid hormonal changes and $KBrO_3$-induced thyroid tumor development including measurement of serum TSH concentrations.

The specific mechanism by which $KBrO_3$ produces tumors is not known. $KBrO_3$ was mutagenic in the Ames test and caused chromosomal aberrations in Chinese hamster fibroblasts, but did not have initiating activity in the rat kidney and neither initiated nor promoted skin tumors (11, 13, 20, 22). Bromate is thought to produce its toxic response through oxidative damage that results from increased levels of lipid peroxide (19, 24–26). Bromate-induced carcinogenesis may result from lipid peroxidation and generation of oxygen radicals that induce DNA damage (17).

In summary, in the present study we found $KBrO_3$-induced tumors of the kidney, thyroid gland, and abdominal mesothelium. In addition, this study confirmed that $KBrO_3$-induced mesotheliomas originate on the tunica vaginalis at the attachment between the testicle and epididymis. The first tumors to develop from $KBrO_3$ treatment are thyroid gland follicular adenomas. We provided

additional support for the assertion that bromate-induced renal tumors develop unrelated to nephrotoxicity. This study provides a basis for the determination of dose-time relationships of tumor development for a better understanding of $KBrO_3$-induced cancer.

ACKNOWLEDGMENT

Portions of this work were carried out under EPA Contract 68-D03-0024 to Pathology Associates Inc., Frederick, MD.

REFERENCES

1. Anderson FA (1994). Final report on the safety assessment of sodium bromate and potassium bromate. *J. Am. Coll. Toxicol.* 13: 400–414.
2. Burry A (1978). Pathology of analgesic nephropathy: Australian experience. *Kidney Int.* 13: 34–40.
3. Cavanagh JE, Weinberg HS, Gold A, Sangalah R, Marbury D, Glase WH, Collette TW, Richardson SD, and Thruston AD (1992). Ozonation byproducts: Identification of bromohydrins from the ozonation of natural waters with enhanced bromide levels. *Environ. Sci. Technol.* 26: 1658–1662.
4. Corless CL, Kibel AS, Iliopoulos O, and Kaelin WG (1997). Immunostaining of the von Hippel-Lindau gene product in normal and neoplastic human tissues. *Hum. Pathol.* 28: 459–464.
5. Crosby LM, Morgan KT, and DeAngelo AB (1998). Potassium bromate-induced mesothelioma localizes to the mesorchium of the *tunica vaginalis testis* of the F344 rat. *Toxicol. Sci.* 42(suppl. 1): 72.
6. DeAngelo AB, George MH, Kilburn SR, Moore TM, and Wolf DC (1998). Carcinogenicity of potassium bromate administered in the drinking water to male $B6C3F_1$ mice and F344/N rats. *Toxicol. Pathol.* 26: 587–594.
7. Fleming S (1997). Genetics of renal tumours. *Cancer Metastasis Rev.* 16: 127–140.
8. Hall WC (1990). Peritoneum, retroperitoneum, mesentery, and abdominal cavity. In: *Pathology of the Fischer Rat,* GA Boorman, SL Eustis, MR Elwell, CA Montgomery, and WF MacKenzie (eds). Academic Press, Inc., San Diego, pp. 63–69.
9. Hardisty JF and Boorman GA (1990). Thyroid gland. In: *Pathology of the Fischer Rat,* GA Boorman, SL Eustis, MR Elwell, CA Montgomery, and WF MacKenzie (eds). Academic Press, Inc., San Diego, pp. 519–534.
10. International Agency for Research on Cancer (1986). Potassium bromate. *IARC Monogr. Eval. Carcinog. Risks Hum.* 40: 207–220.
11. Ishidate M, Sofuni T, Yoshikawa K, Hayashi M, Nohmi T, Sawada M, and Matsuoka A (1984). Primary mutagenicity screening of food additives currently used in Japan. *Food Chem. Toxicol.* 22: 623–636.
12. Kenck C, Whilhelm M, Bugert P, Staehler G, and Kovacs G (1996). Mutation of the VHL gene is associated exclusively with the development of non-papillary renal cell carcinomas. *J. Pathol.* 179: 157–161.
13. Kurata Y, Diwan BA, and Ward JM (1992). Lack of renal tumour-initiating activity of a single dose of potassium bromate, a genotoxic renal carcinogen in male F344/NCr rats. *Food. Chem. Toxicol.* 30: 251–259.
14. Kurokawa Y, Aoki S, Matsushima Y, Takamura N, Imazawa T, and Hayashi Y (1986). Dose-response studies on the carcinogenicity of potassium bromate in F344 rats after long-term oral administration. *J. Natl. Cancer Inst.* 77: 977–982.
15. Kurokawa Y, Hayashi Y, Maekawa A, Takahashi M, and Kokubo T (1982). Induction of renal cell tumors in F-344 rats by oral administration of potassium bromate, a food additive. *Gann* 73: 335–338.
16. Kurokawa Y, Hayashi Y, Maekawa A, Takahashi M, Kokubo T, and Odashima S (1983). Carcinogenicity of potassium bromate administered orally to F344 rats. *J. Natl. Cancer Inst.* 71: 965–972.
17. Kurokawa Y, Maekawa A, Takahashi M, and Hayashi Y (1990). Toxicity and carcinogenicity of potassium bromate—a new renal carcinogen. *Environ. Health Perspect.* 87: 309–335.
18. Kurokawa Y, Matsushima Y, Takamure N, Imazawa T, and Hayashi Y (1987). Relationship between the duration of treatment and the incidence of renal cell tumors in male F344 rats administered potassium bromate. *Jpn. J. Cancer Res.* 78: 358–364.
19. Kurokawa Y, Takamura N, Matsuoka C, Imazawa T, Matsushima Y, Onodera H, and Hayashi Y (1987). Comparative studies on lipid peroxidation in the kidney of rats, mice, and hamsters and on the effect of cysteine, glutathione, and diethyl maleate treatment on mortality and nephrotoxicity after administration of potassium bromate. *J. Am. Coll. Toxicol.* 6: 489–501.
20. Kurokawa Y, Takamura N, Matsushima Y, Imazawa T, and Hayashi Y (1984). Studies on the promoting and complete carcinogenic activities of some oxidizing chemicals in skin carcinogenesis. *Cancer Lett.* 24: 299–304.
21. Kurokawa Y, Takayama S, Konishi Y, Hiasa Y, Asahina S, Takahashi M, Maekawa A, and Hayashi Y (1986). Long-term *in vivo* carcinogenicity tests of potassium bromate, sodium hypochlorite, and sodium chlorite conducted in Japan. *Environ. Health Perspect.* 69: 221–235.
22. Matsushima Y, Takamura N, Imazawa T, Kurokawa Y, and Hayashi Y (1986). Lack of carcinogenicity of potassium bromate after subcutaneous injection of newborn mice and newborn rats. *Sci. Rep. Res. Inst. Tohoku Univ.* 33: 22–26.
23. Montgomery CA and Seely JC (1990). Kidney. In: *Pathology of the Fischer Rat,* GA Boorman, SL Eustis, MR Elwell, CA Montgomery, and WF MacKenzie (eds). Academic Press, Inc., San Diego, pp. 140–142.
24. Sai K, Takagi A, Umemura T, Hasegawa R, and Kurokawa Y (1991). Relation of 8-hydroxydeoxyguanosine formation in rat kidney to lipid peroxidation, glutathione level and relative organ weight after a single administration of potassium bromate. *Jpn. J. Cancer Res.* 82: 165–169.
25. Sai K, Uchiyama S, Ohno Y, Hasegawa R, and Kurokawa Y (1992). Generation of active oxygen species *in vitro* by the interaction of potassium bromate with rat kidney cell. *Carcinogenesis* 13: 333–339.
26. Sai K, Umemura T, Takagi A, Hasegawa R, and Kurokawa Y (1992). The protective role of glutathione, cysteine and vitamin C against oxidative DNA damage induced in rat kidney by potassium bromate. *Jpn. J. Cancer Res.* 83: 45–51.
27. Thomas GA and Williams D (1994). Changes in structure and function of the thyroid follicular cell. In: *Patholobiology of the Aging Rat,* Vol. 2, U Mohr, DL Dungworth, CC Capen (eds). ILSI Press, Washington, D.C., pp. 277–280.
28. Umemura T, Takagi A, Sai K, Hasegawa R, and Kurokawa Y (1998). Oxidative DNA damage and cell proliferation in kidneys of male and female rats during 13-weeks exposure to potassium bromate (KBrO3). *Arch. Toxicol.* 72: 264–269.
29. Urakami S, Tokuzen R, Tsuda H, Igawa M, and Hino O (1997). Somatic mutation of the tuberous sclerosis (Tsc2) tumor suppressor gene in chemically induced rat renal carcinoma cell. *J. Urol.* 158: 275–278.
30. Walker C (1998). Molecular genetics of renal carcinogenesis. *Toxicol. Pathol.* 26: 113–120.

Normalization and analysis of DNA microarrays by self-consistency and local regression

Thomas B. Kepler, Biomathematics Graduate Program
Department of Statistics
North Carolina State University
Raleigh NC

Lynn Crosby
Department of Toxicology
North Carolina State University
and Strategic Toxicological Sciences
GlaxoWellcome
Research Triangle Park NC

Kevin Morgan
Strategic Toxicological Sciences
GlaxoWellcome
Research Triangle Park NC

September 7, 1999

Abstract

With the advent of DNA hybridization microarrays comes the remarkable ability, in principle, to simultaneously monitor the expression levels of large numbers of genes (up to tens of thousands at present). The quantitative comparison of 2 or more assays can reveal, for example, the differing patterns of gene regulation among different cellular phenotypes or the transcriptional response to various external conditions. Normalization of the measured intensities is an essential component in such comparisons, yet has not been systematically studied. We show that the common methods for normalization, which rest on the implicit assumption of linear response between true expression level and output intensity, perform poorly in practice. We have developed a robust semi-parametric normalization technique based upon the assumption that the large majority of genes will not have their relative expression levels changed from one treatment group to the next and on the assumption that departures of the response from linearity are small and slowly-varying. We use local regression to estimate the normalized expression levels as well as the expression level-dependent error. We illustrate

the use of this technique in a comparison of the expression profiles of cultured human pleural mesotheliomas (Met5a) and hepatocellular carcinomas (HepG2).

1 Introduction

Among the most fascinating open questions in biology today are those that surround the issue of global regulation of gene expression, itself the basis for the unfolding of the developmental program, the response of cells to changing environments and many other phenomena. The answers to some of these questions have been moved a few steps closer to realization with the advent of DNA hybridization microarrays. These tools allow the simultaneous monitoring of the expression levels of many genes from tens to tens of thousands in number. One such microarray, for example, assays the expression level of all of the expressed genes in the yeast *Saccharomyces cerevisiae*.

Microarrays are fabricated in a variety of ways but all operate on the same basic principle. DNA probes, consisting either of synthesized oligonucleotides or known cDNAs, are anchored to a solid substrate at identifiable locations forming an array. Each of these array spots selectively hybridizes to a specific solution-phase mRNA. A solution containing a set of tagged mRNAs at unknown relative abundances is incubated with the array. The hybridized array is then imaged and the intensity at each of the array locations is quantitated, thus giving a measure of the quantity of specific mRNA present in the target solution.

In order to compare the mRNA levels in two or more target solutions, it is necessary to normalize the measured intensities. This requires knowledge of the response curve, or how the measured intensity of the spots on the array relate to the target concentrations in the solution, including the distribution of the inherent variability of the system. One approach is to assume a particular functional form for this relationship and fit the data based on the chosen model. The techniques commonly used at this time fall into this category and all implicitly assume a linear relationship between the mRNA concentrations and the spot intensities. Under these conditions, normalization amounts to the estimation of a single multiplicative constant for each array. This can be implemented by whole-array methods, using the median or mean of the spot intensities or by the inclusion of control mRNA.

We have found that in a variety of different hybridization systems the response curve is neither sufficiently linear, nor consistent among replicate assays. The problems are not obviated by the use of "housekeeping" genes as controls. First, their quantitative stability is not *a priori* assured nor has such stability been demonstrated empirically, and second, even if such genes were found, the non-linearity of the response is Neither can extrinsic controls (such as bacterial mRNA spiked into human targets) ensure adequate normalization since the relative concentration of control to target mRNA cannot be made accurately enough. Even simultaneous two-color probes on the same microarray do not obviate the problems of normalization since the relative activity of

the two dyes used varies.

One possible approach to the normalization problem would be to obtain detailed quantitative understanding of each step in the process in order to develop a mechanistic model for the response curve. Alternatively, one may use the vast quantity of data generated and the assumption of self-consistency to semi-parametrically estimate the response curve.

We have pursued the latter path. Our approach does not rely on the consistency of an extrinsic marker or the stability of expression for any given set of genes or on the correctness of an *a priori* model for the response. Instead, it relies upon the assumption that the majority of genes in any given comparison will be expressed at constant relative levels; that only a minority of genes will have their expression levels affected. Thus, we normalize pairs or groups of assays relative to each other by maximizing the consistency of relative expression levels among them.

2 Modeling and Estimation

We concentrate here on the experimental design in which we have two treatment groups and two or more replicate arrays per group. Generalization to more than two groups is straightforward. Comparisons made without replicate arrays are also be possible, and much of the methodology discussed here can be applied in that case as well, but the lack of true replicates introduces unique non-trivial problems that will not be discussed here.

Basic Model.

Although we have found that the normalization function is not constant, we start with a model that assumes such a constant normalization. This affords us a concise description of the self-consistency condition. Subsequently, we relax this condition to discuss non-constant normalization.

Let Y_{ijk} denote the logarithm of the measured intensity of the kth spot in the jth replicate assay of the ith treatment group. The logarithmic transformation homogenizes the variances to a large extent (but see below) and converts a multiplicative normalization constant to an additive normalization constant, so we write

$$y_{ijk} = \alpha_{ij} + \xi_k + \delta_{ik} + \epsilon_{ijk} \tag{1}$$

where α_{ij} is the normalization constant, ξ_k, is the (logarithm of the) mean mRNA abundance of the kth gene (or more accurately, of the mRNA that hybridizes to the kth spot, since we cannot distinguish between specific and non-specific hybridization), δ_{ik} is the difference between the log abundance in group i and the overall mean ξ_k. This difference δ_{ik} is the quantity of most direct interest for comparing expression profiles. Finally, ϵ_{ijk} is the unmodeled variability (noise), which we take to be mutually independent.

This model is not uniquely specified, since there are a number of operations that change the individual parameters, but leave their sum invariant (*e.g.*, add a constant to α_{ij} and subtract it from ξ_k). We need an additional set of conditions to uniquely specify the parameters. We take $\sum_k \xi_k = 0$ and $\sum_i \delta_{ik} = 0$ as two, conventional conditions. The first step in estimating the parameters is accomplished using ordinary least squares, yielding (where Roman characters are used to indicate estimators of the corresponding (greek-charactered) parameters.

$$\begin{aligned} x_k &= \bar{y}_{\cdot\cdot k} - \bar{y}_{\cdots} && (2) \\ a_{ij} &= \bar{y}_{ij\cdot} - \bar{d}_{i\cdot} && (3) \\ d_{ik} - \bar{d}_{i\cdot} &= \bar{y}_{i\cdot k} - \bar{y}_{\cdot\cdot k} - \bar{y}_{i\cdot\cdot} + \bar{y}_{\cdots} && (4) \end{aligned}$$

where overbars and subscript dots indicate the average over the replaced index.

Self-consistency.

An additional condition is required to complete the estimation. This last condition is not simply conventional but is of real consequence to subsequent inference. It is in this conditions that the assumption of self-consistenecy enters.

We want to assume that the δ are small in some sense. The motivation for this is the assumption that the majority of genes will not have their expression levels changed appreciably from one treatment to the next. Clearly, there may be some treatment pairs for which this is not a reasonable assumption, but we argue that as long as the cell is alive, the basic mechanism of cell maintenance must continue; the relevant gene products must appear relatively stable. This approach can be viewed as a generalization of the method of using "housekeeping" genes to normalize the array. Rather than assume that any given gene is stable, we assume that the overall background pattern of activity is stable, that there is a transcriptional "core". In fact this core may differ from treatment to treatment, but as long as there is significant overlap, our technique will work well.

One particularly convenient implementation of this idea is to minimize $\sum_{ik} \delta_{ik}^2$ over $\bar{\delta}_{1\cdot\cdot}$. The result is simply

$$\bar{d}_{1\cdot} = 0 \qquad (5)$$

which can be substituted back into Eq.(4) to complete the estimation procedure. For later notational convenience we will write the relationship between d and y as a matrix equation,

$$d_{ik} = (DY)_{ik} \qquad (6)$$

where Y is a 3-dimensional matrix with components y_{ijk} and D is given by Eqs.(4,5).

Although simple, this procedure may penalizes too harshly the few large deviations that we might reasonably expect to see. A more attractive procedure from this perspective is to minimize the sum of *absolute* errors, rather than squared errors, as is routinely done in robust regression. Fortunately, we find that in the analysis of real data, the two procedures lead to nearly identical inferences.

Bias removal by local regression.
The basic model above assumes that the normalization "constants" are indeed independent of the abundance, and consequently of the observed intensities. While this is sometimes a fair approximation, we have found that in all arrays from the platforms we have tested, there is a non-negligible deviation from constancy of the normalization. Figure 1 provides an illustration of this phenomenon. In all cases, the normalization factor appears to be a slowly-varying function of the mean log intensity, and so can be estimated using local regression on x, the estimator for the log abundance.

The new model can then be written

$$y_{ijk} = \beta_{ij}(\xi_k) + \delta_{ik} + \epsilon_{ijk} \tag{7}$$

where the funciton β_{ij} represents the normalization factor, now defined as everything that is slowly varying with respect to the underlying mean abundances ξ, including ξ itself.

Estimation is carried out by using the estimate x for ξ as given by Eq.(4), and using this variable as the predictor in a local regression to estimate β. Local regression is a generalization of the intuitive idea of smoothing by using a moving average in which one estimates, not just the average of a set of measured points, but all of the coefficients in a regression in which the regression coefficients themselves are slowly varying functions of the predictor variable. The availability of inexpensive powerful computing has sparked renewed interest in local regression techniques and its theoretical underpinnings have been extensively elucidated[].

The local regression estimate b of β is given by

$$b_{ij}(x_k) = (L_0(x_k)Y)_{ij} \tag{8}$$

where $L_0(x)$ is the linear operator giving the intercept of the local regression centered at x. Now *delta* can be estimated as

$$d_{ik} = (D(I - L_0(x))Y)_{ik} \tag{9}$$

where I is the identity operator. The residuals are then given by

$$e_{ijk} = ((I - L_0(x))(I - D)Y)_{ijk}. \tag{10}$$

The linearity of the regression means that all of the necessary error estimates can be and have been obtained in a straightforward manner[], allowing us to compute familiar test statistics and proceed to test the significance of individual differences in the usual manner.

Heteroscedasticity and Error estimation

In addition to local bends in the response curve, we also find that the data are heteroscedastic: the magnitude of the error depends on the mean. The logarithmic

transformation removes a substantial part of this dependence, but it does not flatten it out altogether. We also use local regression to estimate this non-constant variance. For this assuming that local heteroscedasticity. The noise level will depend on the expression level itself. Again, one might try an *a priori* accounting of the sources of error and therby provide a parametric model for it. Instead, we estimate local variance by again using local regression. The technique involves computing the local likelihood and the effective residual degrees of freedom (Loader, 199?). The ratio is a smooth estimate of the local variance.

3 Example: differential expression patterns in cultured hepatocytes and mesothelial cells

We illustrate the use of these methods by applying them to data generated in an experiment on human cell cultures.

Materials and Methods

Complete details of the experimental protocols can be found in Crosby et al. (in preparation). A brief description is given here.

Recently sub-cultured MeT-5A (human SV-40 transformed mesothelioma cell line) and HepG2 (human hepatocellular carcinoma cell line) cells were separately plated and grown until confluent. After confluence, dishes were treated with 3 mL media for 4, 12 or 24 hours, in triplicate. Subsequently, all media was removed by aspiration, cells were rinsed and lysed. The TRIZOL total RNA extraction protocol was followed for extraction of nucleic acid. RNA was quantitated by spectrophotometry.

A priming reaction was carried out at 70C for 10 minutes (containing total RNA and oligo dT), followed by an elongation reaction for 90 minutes at 37C (containing buffer, DTT, dNTP mix, RT, and 33P dCTP). The labeled product was purified by passage through a spin column. One microliter was added to scintillation fluid and the incorporated counts quantified. The remaining probe was denatured by boiling for three minutes and added directly to the pre-hybridization solution. Research Genetics ???-cDNA GF211 filters were prepared according to Research Genetics protocol[]. Membranes were hybridized overnight at 42C. The washed membranes were then mounted on Whatman paper, wrapped in plastic wrap and applied to a rare earth screen for 24 hours. The screen raw intensities were read by a phosphoimager (Cyclone) and Pathways (Research Genetics) software was used to quantify the intensities.

Software for the implementation of the statistical estimation and testing procedures was written in FORTRAN and run on desktop PCs. Additional computations were performed using Splus 4.5 (MathSoft, Inc.).

3.1 Results

Figure ?? shows a comparison between the standardized differences resulting from use of the first-stage (unsmoothed) data (but using local error estimation) and of fully normalized data. It is clear that the full normalization produces more significant differences by the identification of what had been treated as a component of the variance in the unsmoothed data with nonlinearities in the response curve. The comparison also reveals a subtle but easily perceived curvature in the standardized differences (unsmoothed data) that seems difficult to explain biologically and is removed by the local regression.

Biological validation.

Research Genetics gene expression array platform GF211, in combination with statistical analysis revealed a number of clear differences between the mesothelial (Met5a) and the hepatocellular carcinoma (HepG2) cells which were consistent with their cell types of origin. For instance, vimentin is an established marker protein used to identify mesothelial cells in culture, and is was more highly expressed in the Met5a cells used for these studies (Crosby, Morgan and DeAngelo, 1999). In contrast, Hepsin is known to be highly expressed in liver cells (Qinguy, et al., 1998) while these cells are also known to secrete alpha-fetoprotein and albumin into the blood; all of the latter genes were more highly expressed in the HepG2 cells. The well documented ability of the liver to metabolise xenobiotics was reflected by the higher expression levels of both phase I (cytochrome p450) and phase II (UDP glucuronosyltransferase) genes. The fact that HepG2 cells are cancerous was consistent with the high expression of carcinoembryonic antigen. Much less is known about mesothelim than about the liver. Gene expression studies of this type, when combined with appropriate experimental design and statistical analysis, followed by confirmatory studies such as Northern analysis or immunocytochemistry, may throw light on the normal physiology of this cell type. For instance, there was marked expression of collagens of type alpha-1 and 2, which may relate to the nature of peritoneal fluid or the role of mesothelial basement membrane in this physically and biochemically challenged region of the body.

Simulation studies.

TO COME.

4 Conclusions

DNA hybridization microarrays promise to provide new insights into many areas of cell biology, but statistical methods will be essential for making sense of the vast datasets. Comparisons between datasets, in particular, will require more sophisticated normalization procedures than has hitherto been appreciated.

We have presented a method for normalizing microarray data that relies upon the statistical consistency of relative expression levels among a core set of genes that is not

identified in advance, but inferred from the data itself. The normalization and variance estimation are both performed using local regression. We are then able to perform standard comparison tests. This technique reveals biologically plausible expression-level differences between HepG2 and Met5a cell lines; simulation studies how that the technique performs as expected theoretically.

...?

References

[1] Cleveland, W.S. & Devlin, S.J. (1988) Locally weighted regression: An approach to regression analysis by local fitting. *J. Amer. Statist. Assoc.* **83**: 596–610.

[2] Loader, C.R. (1996) Local likelihood density estimation. *Ann. Statist.* **24**: 1602–1618.

[3] Cleveland, W.S. & Grosse, E.H. (1991) Computational methods for local regression. *Statist. Comput.* **1**: 47–62.

[4] M. Marton *et al.* (1998) Drug target validation and identification of secondary drug target effects using DNA microarrays. *Nat. Med.* **4**: 1293–1301.

[5] Hacia, G. H., Brody, L. C., Chee, M. S., Fodor, S.P.A. & Collins, F. S. (1996) Detection of heterozygous mutations in *BRCA1* using high density oligonucleotide arrays and two-colour fluorescence analysis. *Nat. Gen.* **14**: 441–447.

[6] DeRisi, J. *et al.* (1996) Use of a cDNA microarray to analyze gene expression patterns in human cancer. *Nat. Gen* **14**: 457–460.

[7] Schena, M., Shalon, D., Davis, R.W. & Brown, P.O. (1995) Quantitative monitoring of gene expression patterns with a complementary DNA microarray. *Science* **270**: 467–70.

[8] Spellman et al., (1998). Comprehensive Identification of Cell Cycle-regulated Genes of the Yeast Saccharomyces cerevisiae by Microarray Hybridization. it Mol. Biol. Cell **9**: 3273–3297.

[9] Ermolaeva, O. et al. (1998) Data management and analysis for gene expression arrays. *Nat. Gen* **20**: 19–23.

[10] Fodor, S.P. et al. (1993) Multiplexed biochemical assays with biological chips. *Nature* **364**: 555–6 .

[11] Velculescu, V.E., Zhang, L., Vogelstein, B. & Kinzler, K.W. (1995) Serial analysis of gene expression. *Science* **270**: 484-7 .

[12] DeRisi, J.L., Iyer, V.R. & Brown, P.O. (1997) Exploring the metabolic and genetic control of gene expression on a genomic scale. *Science* **278**: 680-6 .

[13] Wodicka, L., Dong, H., Mittmann, M., Ho, M.H. & Lockhart, D.J. (1997) Genome-wide expression monitoring in *Saccharomyces cerevisiae*. *Nat. Biotech.* **15** 1359–67.

[14] Lockhart, D.J. et al. (1996) Expression monitoring by hybridization to high-density oligonucleotide arrays. *Nat. Biotech.* **14**: 1675-1680.

[15] de Saizieu, A. et al. Bacterial transcript imaging by hybridization of total RNA to oligonucleotide arrays. *Nat. Biotech.* **16**: 45-8 (1998).

[16] Chen, Y., Dougherty, E.R. & Bittner, M.L. (1997) Ratio-based Decisions and the Quantitative Analysis of cDNA Microarray Images. *Biomed. Opt.* **2** 364–374.